NASA CR-72286
NBS REPORT 9705

FINAL REPORT

THERMODYNAMIC DEPRESSIONS WITHIN CAVITIES AND CAVITATION INCEPTION IN LIQUID HYDROGEN AND LIQUID NITROGEN

by J. Hord, D. K. Edmonds, and D. R. Millhiser

Prepared for
NATIONAL AERONAUTICS AND SPACE ADMINISTRATION
CONTRACT No. C-35560-A
March, 1968

Technical Management
NASA Lewis Research Center
Cleveland, Ohio
Liquid Rocket Technology Branch
Werner R. Britsch

NBS - U. S. Department of Commerce, Boulder, Colorado

FOREWORD

This report was prepared by the National Bureau of Standards, Institute for Basic Standards, United States Department of Commerce under Contract C-35560-A. The contract was administered by the Lewis Research Center of the National Aeronautics and Space Administration, Cleveland, Ohio. The work summarized in this report was performed during the period 15 July 1964 to 15 December 1967. The NASA project manager for the Contract was Mr. Werner R. Britsch. Mess'rs. R. S. Ruggeri, T. F. Gelder, and R. D. Moore of the Fluid Systems Components Division at NASA Lewis Research Center---under the direction of M. J. Hartmann---served as research consultants and technical advisers during the course of this program.

TABLE OF CONTENTS

LIST OF ILLUSTRATIONS

Page

LIST OF TABLES

Page

THERMODYNAMIC DEPRESSIONS WITHIN CAVITIES AND CAVITATION INCEPTION IN LIQUID HYDROGEN AND LIQUID NITROGEN

J. Hord, D. K. Edmonds, and D. R. Millhiser

ABSTRACT

Cavitation characteristics of liquid hydrogen and liquid nitrogen in a transparent plastic venturi have been determined. The experimental data are presented in tabular and graphical form. Conventional cavitation-inception-parameter and head-velocity curves are given over the range of experimental temperatures (36.5 to 41°R for hydrogen and 140 to 170°R for nitrogen) and inlet velocities (70 to 185 ft/sec for hydrogen and 20 to 70 ft/sec for nitrogen). Minimum local wall pressure at incipience was calculated[1] to be less than bulkstream vapor pressure by as much as 328 feet of hydrogen head and 63 feet of nitrogen head in some inception tests.

Thermodynamic data, consisting of pressure and temperature measurements within fully developed cavities, are also given. Minimum measured[1] cavity pressure was less than bulkstream vapor pressure by as much as 651 feet of hydrogen head and 44 feet of nitrogen head; measured temperatures and pressures within the cavities were generally not in thermodynamic equilibrium. At constant bulkstream temperature, cavity pressure depressions increased with increasing velocities and cavity length. For fixed velocities, cavity pressure depressions increased with increasing fluid temperature and cavity length. Existing theory is used to obtain equations which correlate the experimental data for developed cavitation in liquid hydrogen and liquid nitrogen.

---

1 - Variations in test conditions preclude direct comparison of minimum calculated (at incipience) and minimum measured pressure depressions.

1. Introduction

Cavitation is usually defined as the formation, caused by a reduction in pressure, of a vapor phase within a flowing liquid or at the interface between a liquid and a solid. Since the formation and collapse of vapor cavities alters flow patterns, cavitation may reduce the efficiency of pumping machinery [1], and reduce the precision of flow measuring devices. Collapse of these vapor cavities can also cause serious erosion damage [2] to fluid-handling equipment. While the noncavitating performance of hydraulic equipment may be predicted from established similarity laws, cavitating performance can seldom be predicted from fluid-to-fluid. The effects of fluid properties on cavitation performance are well recognized [3-12] and require more understanding to develop improved similarity relations [13] for equipment design.

NASA has undertaken a program [1] to determine various cavitation characteristics and the thermodynamic behavior of different fluids in an effort to obtain improved design criteria to aid in the prediction of cavitating pump performance. The experimental study described herein was conducted in support of this program.

Liquid hydrogen and liquid nitrogen were chosen as test fluids for this study for the following reasons: (1) the ultimate goal of this program is to acquire sufficient knowledge to permit intelligent design of pumps for near-boiling liquids and (2) predictive analyses indicated [1] that the physical properties of hydrogen and nitrogen make them particularly desirable test fluids. The objective of this study was to determine the flow and thermodynamic conditions required to induce incipient and developed cavitation on the walls of a transparent plastic venturi using liquid hydrogen and liquid nitrogen. The shape of the venturi was chosen to duplicate the test section used by NASA [13-17]. In the inception studies, the test section inlet velocity was varied from 70 to 185 ft/sec with hydrogen and from 20 to 70 ft/sec with nitrogen. Inlet temperatures were varied from 36.5 to 41°R with hydrogen and from 140 to 170°R with nitrogen, in order to determine the effects of temperature upon cavitation inception. Both incipient and desinent cavitation data were acquired with no noticeable hysteresis; i.e., the flow conditions corresponding to vapor inception are identical whether the data point is approached from non-cavitating or fully developed cavitating flow. In this paper, incipience refers to the appearance of barely visible cavities, whether they be due to incipient or desinent cavitation.

Pressure and temperature profiles within fully developed cavities were measured and are referred to herein as thermodynamic data. Nominal cavity lengths studied were 1.25, 2, and 3.25 inches with liquid hydrogen and 3.25 inches with liquid nitrogen. Venturi inlet velocities were varied from 110 to 200 ft/sec in hydrogen and from 35 to 75 ft/sec in nitrogen. Inlet temperatures ranged from 36.5 to 42.5°R in hydrogen and from 140 to 160°R in nitrogen. Since the bulkstream vapor pressure exceeds the measured cavity pressure and the saturation pressure corresponding to the measured cavity temperature, the measured pressure and temperature depressions within the cavity are appropriately called "thermodynamic depressions." A similarity equation has been suggested [13] for correlating cavitation data for a particular test item from fluid to fluid; this correlation is also useful in extending the velocity and temperature range of data for any given fluid. The experimental data from this study have been used to evaluate the exponents on various terms in this correlating equation.

All data reported here are intended to supplement that given in references [13-17] for a geometrically similar, but 1.414 times as large, test section.

2. Apparatus

The facility used for this study consisted of a blow-down system with the test section located between the supply and receiver dewars; see figure 2.1. Dewars and piping were vacuum shielded to minimize heat transfer to the test fluid. Flow control was attained by regulating the supply and receiver dewar pressures. Pressure and volume capacities of the supply and receiver vessels are indicated on figure 2.1. The receiver dewar pressure control valving limited the inlet velocity, V_o, to around 200 ft/sec in hydrogen, while the supply dewar pressure rating limited the inlet velocity to about 70 ft/sec in nitrogen.

Valves located on each side of the test section permit flow stoppage in the event of venturi failure while testing with liquid hydrogen. A plenum chamber was installed upstream of the test section to assure uniform non-cavitating flow at the test section inlet. The supply dewar was equipped with a 5 kW heater which was used to heat the test fluid.

2.1 Test Section

A photograph of the test section as viewed through one of the windows in the vacuum jacket is shown in figure 2.2. The transparent plastic venturi was flanged into the apparatus using high compression elastomeric "O" rings. Test section details are given in figures 2.3 and 2.4.

Referring to figure 2.3, static pressure tap No. 1 was the only instrument port drilled and used in the liquid hydrogen inception tests. Some liquid nitrogen data were acquired with all of the pressure and temperature sensing ports instrumented, figure 2.2. Since incipient cavitation involves very small cavities at or near the minimum pressure point--see figures 2.4 and 2.5--the presence or absence of the additional sensing ports has no effect on the inception data reported. All of the sensing ports were used during the thermodynamic tests to determine the temperature and pressure depressions within the cavities. Cavity length was determined from scribe marks on the plastic venturi; see figure 2.2. The theoretical and as-built venturi contours are shown on figure 2.4. The test section dimensions were checked by using the plastic venturi as a mold for a dental plaster plug. The plug was then removed and measured. Pressure distribution for non-cavitating flow across the quarter-round contour [14, 18] is shown in figure 2.5. This pressure profile has been confirmed using several test fluids [14-16] and data from this study, and applies when $(Re)_{D_o} \geq 4 \times 10^5$.

2.2 Instrumentation

Location of the essential instrumentation is shown on figures 2.1 and 2.3.

Liquid level in the supply dewar was sensed with a ten-point carbon resistor rake. Test fluid temperature in the supply dewar was determined by two platinum resistance thermometers, see figure 2.1. Fluid temperature at the flowmeter and test section inlet were also measured with platinum resistance thermometers. These platinum thermometers were calibrated to provide temperature readings accurate within $\pm$ 0.04°R. The thermometers were powered with a current source which did not vary more than 0.01 percent. Voltage drop across the thermometers was recorded on a 5 digit electronic voltmeter data acquisition system. The overall accuracy of the platinum thermometer temperature measurement is estimated to be within ±0.09°R. Chromel-constantan thermocouples were used to determine the temperature profile within the cavities during the thermodynamic tests. The reference thermocouple was placed in the plenum chamber beside the platinum thermometer used to determine bulkstream temperature at the test section inlet. The thermocouples had exposed, welded junctions, and were constructed from one mil wire to ensure rapid response. The thermocouple leads extending from the reference to cavity thermocouples were thermally lagged to the cold pipe. The signal leads which penetrated the vacuum barrier were also tempered to the cold pipe to minimize heat transfer to the thermocouples. Details of the thermocouple installation are shown on figures 2.6 and 2.7. The thermocouple circuit was calibrated, over the range of experimental velocities and temperatures, from tests involving non-cavitating flow through the venturi. Accuracy of the cavity temperature measurements is estimated at ± 1°R for hydrogen and ±0.4°R for nitrogen.

System gage and differential pressure measurements were obtained with pressure transducers mounted in a temperature stabilized box near the test section. Differential pressure measurements were used where possible to provide maximum resolution. The pressure transducers were calibrated via laboratory test gages at frequent intervals during the test series. These transducers have a repeatability of better than ± 0.25 percent and their output was recorded on a continuous trace oscillograph with approximately one percent resolution. The overall accuracy of the pressure measurement, including calibration and read-out errors is estimated to be within ± 2.0 percent. Bourdon gages were used to monitor the various tests.

Volumetric and mass flow rates were determined via Herschel venturi flow meter designed to ASME Standards [19]. The internal contour of this meter was verified in the same manner as the test venturi. An error analysis of this flow device and associated pressure and temperature measurements indicates an accuracy in mass flow of about one percent.

An electronic pulsing circuit provided a common time base for correlating data between oscillograph, digital voltmeter, and movie film. The data were reduced by first viewing film of the test event. A solenoid-actuated counter, installed adjacent to the test section was energized by the electronic pulser and appears on the film, figure 2.2. Thus, the data are reduced at the desired instant of time by simply matching the number of voltage pulses which have elapsed.

An acoustic cavitation detection device was developed and successfully used to determine cavitation inception. This device was found to be more sensitive than the human eye, i.e., cavitation inception could be detected with the acoustic transducer before it was visible to the unaided eye. Visible incipience is frequently used as the criterion for cavitation inception and is normally reported in the literature since the sensitivity [20-22] of various acoustic detectors can vary appreciably. Although the inception data presented here are based upon visible incipience, a full description of the acoustic transducer is given for reference in Appendix A of this paper.

2.3 Visual and Photographic Aids

Use of a plastic test section, liquid hydrogen, and relatively high pressures precluded direct visual observation; therefore, closed-circuit television was used to observe the tests.

Movies of cavitation tests were taken at approximately 20 frames per second on 16 mm film. The variable speed camera was equipped with a 75 mm lens and synchronized with a high intensity stroboscope, providing a 3 μsec exposure. The stroboscope was situated directly opposite the camera lens and illuminated the test section through a plastic diffuser mask; this technique provided bright field illumination or a back-lighting effect and excellent contrast between vapor and liquid phases in the test section.

3. Test Procedure

The following procedure refers to figure 2.1. The supply dewar was filled with test liquid and then some of the liquid extracted through valves A and B to cool the test section and piping. Approximately two hours was required to cool the plastic test section without breakage. Cooldown was monitored via platinum resistance thermometers in the plenum chamber. Upon completion of cooldown, the contents of the supply dewar was transferred through the test section into the receiver dewar, and then back into the supply dewar again. This operation cooled the entire flow system in preparation for a test. The test section and connecting piping were kept full of liquid (at near-ambient pressure) during preparatory and calibration periods between tests; therefore, the plastic venturi was generally colder than the test liquid. Next, the liquid in the supply dewar was heated to the desired temperature. Supply and receiver dewars were then pressurized to appropriate levels and flow started by opening valve C. In the case of non-cavitating flow, inception was induced by lowering the receiver dewar pressure and thus increasing the flow velocity until vapor appeared. To obtain desinent cavitation from fully developed cavitating flow, the receiver dewar pressure was increased until the vapor cavity was barely visible. For thermodynamic tests, the receiver dewar pressure was adjusted to obtain the desired cavity length. Receiver dewar pressure was remotely controlled by means of a pneumatic transmitter, differential controller, and vent valve arrangement, figure 2.1. It was necessary to increase test section back-pressure by means of throttle valve D for some of the liquid nitrogen tests. Flow was terminated by closing valve C. The supply dewar was then vented and the test liquid transferred back into the supply dewar for another test. As previously mentioned, the entire test event was recorded on movie film which was subsequently used to determine incipience, desinence, and desired cavity lengths.

4. Data Analysis and Discussion

4.1 Inception Data

All of the useable experimental inception data are given in tables 4.1 and 4.2. The same data points were mathematically temperature-compensated and presented in table 4.3. Derivation of these compensated data is described in Appendix B of this paper.

The conventional cavitation parameter, K_{iv}, for liquid hydrogen is shown on figure 4.1. Little temperature dependency is evident in this plot of experimental data and prompted the presentation of calculated data given on figures 4.2 and 4.3. The calculated data used in the preparation of figures 4.2 and 4.3 are derived as explained in Appendix B and are presented in table 4.4. The liquid nitrogen data were handled in a similar manner and plotted on figures 4.4 and 4.5 from the data of table 4.5. Photographs of cavitation inception are shown for both test fluids on figures 4.6 and 4.7.

4.1.1 Inception Data Analysis

Computed values of K_{iv} were plotted as a function of V_o for both hydrogen and nitrogen. However, inspection of the plots showed no readily discernible temperature dependence of K_{iv} (see figure 4.1; nitrogen is similar and is not shown).

The temperature dependence of K_{iv} is complicated by the fact that errors in the measured variable h_o are magnified in the calculation of K_{iv} as follows:

$$K_{iv} = 2g_c \left[\frac{h_o - h_v}{V_o^2}\right] ; \qquad [4.1\text{-}1a]$$

differentiating [4.1-1a] at constant temperature and velocity there results,

$$d\,K_{iv} = \frac{2g_c}{V_o^2}\, dh_o . \qquad [4.1\text{-}1b]$$

The fractional change in K_{iv} due to a change dh_o is obtained by dividing [4.1-1b] by [4.1-1a] ,

$$\frac{d\,K_{iv}}{K_{iv}} = \frac{dh_o}{h_o - h_v} . \qquad [4.1\text{-}2]$$

The fractional change in h_o due to a change in dh_o is by definition

$$\frac{dh_o}{h_o} .$$

The ratio of the fractional change in K_{iv} to the fractional change in h_o is obtained by dividing [4.1-2] by dh_o/h_o ,

$$\frac{d\,K_{iv}/K_{iv}}{dh_o/h_o} = \frac{h_o}{h_o - h_v} . \qquad [4.1\text{-}3]$$

Therefore any scatter which may occur in measuring h_o will be amplified by the term $\frac{h_o}{h_o - h_v}$, which has values as large as six for both hydrogen and nitrogen data given in this report.

Plots were also made of h_o as a function of V_o using the experimental data from this study. Both hydrogen and nitrogen data showed a distinct temperature dependence; however, there was sufficient experimental variation about each desired nominal liquid temperature to cause concern in constructing the individual isotherms. A nominal temperature or nominal isotherm is defined as that temperature which is selected to represent a specific group of data points with little temperature variation.

A technique was devised to evaluate the effect of temperature on the data and is detailed in Appendix B of this report.

4.2 Thermodynamic Data

Selected thermodynamic data are given in table 4.6 for liquid hydrogen and table 4.7 for liquid nitrogen. Profiles of pressure depression are given on figures 4.8 to 4.22 for liquid hydrogen and figures 4.23 to 4.34 for liquid nitrogen.

Photographs of fully developed cavities in liquid hydrogen and liquid nitrogen are shown in figures 4.35 and 4.36. Inlet velocity and temperature were observed to have very little effect on the appearance of cavitating hydrogen and a pronounced effect on the appearance of nitrogen cavities.

4.2.1 Thermodynamic Data Analysis

The pressure depression in the cavitated region is determined by subtracting the measured cavity pressure in one case and the saturation pressure associated with the measured cavity temperature in the other case, from the vapor pressure of the liquid entering the test section.

The calculation of feet of head from psi requires evaluation of the liquid density at the point of measurement. Measured pressures and temperatures at the test section inlet were used to obtain head data for the inception tests; however, the liquid density is not so easily obtained from the thermodynamic data. Figures 4.8 to 4.34 indicate that the measured pressures and temperatures, within the cavities, are generally not in equilibrium. Also, due to the thermal expansivity of liquid hydrogen, the bulkstream temperature changes appreciably as the liquid flows through the venturi. The following methods were used to calculate feet of head from the thermodynamic measurements: (1) Head (h_n) was calculated from measured cavity pressure by using the saturation density at the measured pressure. (2) Head ($h_{n,T}$) was calculated from measured cavity temperature by using the saturation density at the measured temperature. Both values of head are given in tables 4.6 and 4.7 for the two test fluids.

The cavitation parameter for fully developed cavitation, K_v, was calculated and tabulated for each run.

The similarity equation [13] (used for correlation of thermodynamic cavitation data in similar test items) was fitted with exponents for both hydrogen and nitrogen, using data from this experiment. The purpose [1] of this equation is to predict the cavitating performance of a test item from fluid-to-fluid and from one temperature to another when limited data from a single fluid are available. The similarity equation in its basic form is given [13] as

$$B = (B)_{ref}\left[\left(\frac{\alpha_{ref}}{\alpha}\right)\left(\frac{x_{ref}}{x}\right)\left(\frac{V_o}{V_{o,ref}}\right)\right]^{0.5}\left(\frac{t_v}{t_{v,ref}}\right); \qquad [4.2\text{-}1]$$

the symbols are identified in the nomenclature of this paper. Gelder, et. al. [13] equate the cavity thickness term in [4.2-1] to unity and individually evaluate the exponents on the various terms in [4.2-1] to account for differences in theory and experiment; the modified expression may be written

$$B = (B)_{ref}\left(\frac{\alpha_{ref}}{\alpha}\right)^{m}\left(\frac{x_{ref}}{x}\right)^{n}\left(\frac{V_o}{V_{o,ref}}\right)^{p}, \qquad [4.2\text{-}2]$$

where the exponents m, n, and p are evaluated from the experimental data and theoretical data [13] for B---see following discussion. Any single experiment may be chosen to provide the reference data in this equation. In this study the exponents were obtained from a least squares fitting technique and a digital computer; the results of the computer program are given in tables 4.8 and 4.9 for liquid hydrogen and liquid nitrogen, respectively. The exponents obtained by Gelder, et al., [13] from Freon 114 data are included in these tables for comparison. In equation [4.2-2] the physical properties are evaluated at P_o and T_o and B_{ref} is obtained from theory [13] using $(P_v - P_2)_{ref}$ and $T_{o,ref}$. Choosing values for m, n, and p, the B factor may be computed from [4.2-2]. To evaluate the standard deviation in tables 4.8 and 4.9, B_t for each data point is obtained from theory in the same manner as B_{ref}. The standard deviation in B factor is minimized in the computer program when one or more of the exponents is selected by the computer; the absolute minimum standard deviation is obtained when all three exponents are selected by the computer. The standard deviation is simply computed in those cases where the exponents are not selected by the computer.

4.3 Discussion of Data

4.3.1 Discussion of Inception Data

It was pointed out earlier that no temperature dependence could be determined from the K_{iv} versus V_o plots when the uncompensated experimental data were used, figure 4.1. However, once the nominal h_o versus V_o isotherms were established by mathematical temperature compensation, the K_{iv} versus V_o nominal isotherms may be computed from the basic definition of K_{iv}.

Data on figures 4.2 and 4.4 represent the final "best-fit" of the experimental data points, "transferred" by means of equations [10-3] and [10-4] to the nominal isotherms shown. This method of presenting the h_o versus V_o data eliminates the scatter due to experimental temperature variation. Good agreement was obtained with NASA data [18] for liquid nitrogen at 140°R; see figure 4.4. Since the NASA test section was 1.414 times as large as the plastic venturi described herein, negligible scale effects are indicated.

Minimum local wall pressure at incipient cavitation was calculated to be less than bulkstream vapor pressure by as much as 328 feet of hydrogen head and 63 feet of nitrogen head. These data are obtained by subtracting $\check{h}$ from h_v in tables 4.1 and 4.2.

Figures 4.3 and 4.5 are presented as a matter of interest, but it is to be noted that these K_{iv} curves depend entirely on the shape of the h_o versus V_o curves, and that errors in h_o are amplified in K_{iv} (as was shown earlier). Little variation in the shape of the h_o versus V_o curves is required to eliminate the inflection points in the corresponding K_{iv} versus V_o curves. The K_{iv} curves indicate the usual trends, i.e., K_{iv} increases with increasing velocities and decreasing temperatures. Figure 4.3 shows the isotherms for hydrogen intersecting at an inlet velocity of about 140 ft/sec. While this intersection may be tenable, it could also be attributed to experimental data scatter. Reference to figure 4.1 indicates little separation between isotherms, and suggests that K_{iv} may be invariant at inlet velocities greater than 140 ft/sec. Both hydrogen and nitrogen K_{iv} curves exhibit little temperature or velocity dependence at the higher velocities.

4.3.2 Discussion of Thermodynamic Data

In figures 4.8 to 4.34, the data points representing cavity pressure measurements have been connected to facilitate comparison with the data points obtained from the cavity temperature measurements. The pressure depressions obtained from the cavity temperature measurements are, for the most part, greater than those derived from the measured cavity pressures. Some of the hydrogen data indicate that the cavity pressures and temperatures are nearly in equilibrium at axial positions near the leading and trailing edges of the cavity; this is particularly true near the leading edge where vaporization occurs. The nitrogen data are more erratic near the leading edge of the cavity; it is believed that this is due to the fact that the nitrogen cavities sometimes resemble vapor streams, while the hydrogen cavities always present a complete annulus of vapor. Therefore, the pressure and temperature sensing ports are continuously covered with vapor during a hydrogen experiment, but may be intermittently covered with first vapor and then liquid in a nitrogen test. The characteristics of the nitrogen cavities vary with inlet temperatures and velocities as shown in figure 4.36. Minimum measured cavity pressure was less than bulk-stream vapor pressure by as much as 651 feet of hydrogen head and 44 feet of nitrogen head. These pressure depressions are obtained by subtracting h_2 from h_v in tables 4.6 and 4.7.

The data given on figures 4.8 to 4.34 indicates[2] that some of the cavities were shorter than their nominal (as observed on film) length. Apparently, the actual length of the cavity and the observed length differ somewhat, perhaps due to the irregular trailing edges of the cavity. The cavity length was observed (on film) to be within ± one-fourth inch of the nominal length of all the data reported.

A similarity equation, used to correlate cavitation performance of various flow devices from fluid-to-fluid, was fitted with numerical exponents derived from the experimental data of this study. The similarity equation and exponent data for Freon 114 were obtained from the literature; the numerical exponents for Freon 114 were then compared in tables 4.8 and 4.9 with those deduced from this experiment, using liquid hydrogen and liquid nitrogen. The exponents given in tables 4.8 and 4.9 were obtained from a least-squares fitting technique and a digital computer. The suitability of the various exponents to the experimental data of this study is indicated by the standard deviation in these tables. The data given in tables 4.8 and 4.9 points up the difference between theory and experiment. The data given on figures 4.8 to 4.22 were used to estimate the cavity length (the data were extrapolated to zero pressure-depression) and little improvement in data fit was realized, see results in table 4.8.

5. Summary

5.1 Summary of Cavitation Inception Experiments

Cavitation inception parameters have been experimentally measured for liquid hydrogen and liquid nitrogen flowing in a clear plastic

2 - The pressure depression should be zero at the trailing edge of the cavity.

venturi. The experimental data points are given in table 4.1 for liquid hydrogen and table 4.2 for liquid nitrogen.

Temperature compensated values of inlet head, h_o, versus inlet velocity, V_o, are presented on a background of mathematically derived isotherms; liquid hydrogen data are shown on figures 4.2 and liquid nitrogen data appear on figure 4.4. The 140°R isotherm constructed from the liquid nitrogen data is coincident with data furnished by Ruggeri [18]. The venturi used in that experiment [15] was larger by a factor of 1.414:1; therefore, negligible scale effects are indicated. The mathematical technique used to temperature-compensate the experimental data is outlined in Appendix B of this paper.

Figure 4.1 shows experimental K_{iv} data points for liquid hydrogen; these data have not been temperature compensated and show no particular temperature trends. Temperature compensated values of the conventional cavitation parameter, K_{iv}, are also shown on figure 4.3 for liquid hydrogen and on figure 4.5 for liquid nitrogen: These curves have been derived from the smooth isotherms on the h_o versus V_o plots (figures 4.2 and 4.4). The data shows that K_{iv} increases with increasing velocities and decreases with increasing temperatures. At the high velocities, the K_{iv} curves indicate very little temperature or velocity dependence. The data used to construct figures 4.3 and 4.5 are given in tables 4.4 and 4.5.

The experiments showed that both liquid hydrogen and liquid nitrogen can sustain relatively large magnitudes of thermodynamic metastability; i.e., minimum local wall pressure was calculated to be considerably less than bulkstream vapor pressure. The magnitude of metastability for the various experiments is obtained by subtracting $\check{h}$ from h_v in tables 4.1 and 4.2.

5.2 Summary of Thermodynamic Depression Experiments

Pressure and temperature profiles were measured within fully developed cavities of 1.25, 2, and 3.25 inch nominal lengths in liquid hydrogen and 3.25 inch nominal length in liquid nitrogen. The results of these experiments are given as thermodynamic depressions on figures 4.8 thru 4.34. In general, the measured pressure and temperature depressions were not in thermodynamic equilibrium; the pressure depressions obtained from the cavity temperature measurements are usually greater than those derived from the measured cavity pressures. Some of the hydrogen experiments indicate that the cavity vapor is almost in thermodynamic equilibrium near the leading and trailing edges of the cavity; considerable thermodynamic metastability occurs in the mid-region of the cavity in all of the hydrogen data. This behavior may be due to lag in the thermal-response of the liquid, to rapidly varying pressure, as a particle of liquid traverses the test section contour. The nitrogen thermodynamic data are considerably more erratic than the data for hydrogen, particularly near the leading edge of the cavity: This feature of the nitrogen thermodynamic data is attributed to the porous, non-uniform character of the cavities; while the cavities in hydrogen were uniformly developed and well defined, the nitrogen cavities were quite irregular and definition varied considerably with flow conditions, see figures 4.35 and 4.36.

The experimental data of the study were used to fit a similarity equation with numerical exponents, see tables 4.8 and 4.9. The equation is used to correlate the cavitation performance of liquid pumps from fluid to fluid.

6. Acknowledgements

A considerable number of people have been associated with this project at various times and their individual efforts are respectfully acknowledged. Mess'rs. Thomas T. Nagamoto, Dale R. Nielsen, Raymond V. Smith, and W. Harry Probert assisted in the early phases of apparatus assembly and experimentation. Mr. Peter Pemberton participated in some design modifications and Ajit Rapial was very helpful in the reduction and analysis of data. The photographic instrumentation and techniques used in this study are attributed to Thomas T. Theotokatos.

7. Nomenclature

A_o = test section inlet flow area [≡ 0.008063 ft^2 at 36°R]

B = ratio of vapor to liquid volume associated with the formation and sustenance of a fixed cavity in a liquid

C_n = (n = 1, 2---): constants appearing in equation [10-1] which are evaluated from best-fit curves through h_o vs V_o data points

C'_n = (n = 1, 2): modified values of C_n

C_p = pressure coefficient [$\equiv (h_x - h_o)/(V_o^2/2g_c)$]

$\check{C}_p$ = minimum pressure coefficient [$\equiv (\check{h} - h_o)/(V_o^2/2g_c)$]

D_o = test section inlet diameter

g_c = conversion factor in Newton's law of motion, given in engineering units as g_c = 32.2 (ft) (pounds mass)/(sec^2)(pounds force)

h_n = (n = 2, 4, 5, 7 or 9): head corresponding to cavity pressure measured at a particular instrument port in wall of plastic venturi, ft

$h_{n,T}$ = (n = 2, 6, or 8): head corresponding to the saturation pressure at the cavity temperature measured at a particular instrument port in wall of plastic venturi, ft

h_o = test section inlet head corresponding to absolute inlet pressure, ft

$h_{o,1}$ = value of inlet head corresponding to a data point before it is "transferred" to a new position, ft

$h_{o,2}$ = value of inlet head corresponding to a data point after it has been "transferred" to a new position, ft

h_v = head corresponding to saturation or vapor pressure at the test section inlet temperature, ft

h_x = head corresponding to absolute pressure measured at wall of plastic venturi at distance x, downstream of the minimum pressure point, ft

$\check{h}$ = head corresponding to the minimum absolute pressure on quarter-round contour of plastic venturi, computed from expression for $\check{C}_p$, ft

K_{iv} = incipient cavitation parameter $[\equiv (h_o - h_v)/(V_o^2/2g_c)]$

K_v = fully developed cavitation parameter $[\equiv (h_o - h_v)/(V_o^2/2g_c)]$

$\dot{m}$ = mass flow rate, e.g., (pounds mass)/sec

P_n = (n = 2, 4, 5, 7, or 9): absolute cavity pressure measured at a particular station or instrument port in wall of plastic venturi

$P_{n,T}$ = (n = 2, 6, or 8): saturation pressure corresponding to the measured cavity temperature at a particular station or instrument port in wall of plastic venturi

P_o = test section absolute inlet pressure

P_v = saturation or vapor pressure at test section inlet temperature

$(Re)_{D_o}$ = Reynolds number, based on test section inlet diameter

t_v = thickness of vapor-filled cavity

T_n = (n = 2, 6, or 8): measured cavity temperature at a particular station or instrument port in wall of plastic venturi

T_o = bulkstream temperature in degrees Rankine, of liquid entering the test section

$T_{o,1}$ = the inlet temperature from which a data point is to be "transferred"

$T_{o,2}$ = the inlet temperature to which a data point is being "transferred"

$T_{o,B}$ = the nominal temperature chosen for construction of a "base" isotherm due to the availability of sufficient h_o vs V_o data at or near that temperature

T_o' = a nominal isotherm on a h_o vs V_o plot

T_o'' = a nominal isotherm, different from T_o', on a h_o vs V_o plot

V_o = velocity of test liquid at inlet to test section, ft/sec

x = distance measured from minimum pressure point on quarter-round contour along axis of plastic venturi

Greek

α = thermal diffusivity of liquid

Subscripts

ref = reference test, or set of test conditions, to which a computation is being referenced when attempting to correlate cavitation performance via the similarity equation [4.2-1]

t = denotes derivation from theory

Superscripts

m = exponent on thermal diffusivity ratio in equation [4.2-2]

n = exponent on cavity length ratio in equation [4.2-2]

p = exponent on test section inlet velocity ratio in equation [4.2-2]

8. References

1. Pinkel, I., M. J. Hartmann, C. H. Hauser, M. J. Miller, R. S. Ruggeri, and R. F. Soltis, Pump Technology, Chap. VI, p. 81-101, taken from Conference on Selected Technology for the Petroleum Industry, NASA SP-5053 (1966).

2. Erosion by Cavitation or Impingement, STP-408, 288 pages (1967), available from ASTM, 1916 Race St., Phila., Pa., 19103.

3. Hord, J., R. B. Jacobs, C. C. Robinson, and L. L. Sparks, Nucleation Characteristics of Static Liquid Nitrogen and Liquid Hydrogen, ASME Journ. of Engr. for Power, p. 485-494, (Oct. 1964).

4. Brand, R. S., The Motion of a Plane Evaporation Front in a Superheated Liquid, Univ. of Conn., Tech. Rept. No. 2 (April 1963).

5. Clark, J. A., The Thermodynamics of Bubbles, Mass. Inst. of Tech., Tech. Rept. No. 7 (Jan. 1956).

6. Holl, J. W., and G. F. Wislicenus, Scale Effects on Cavitation, ASME Journ. of Basic Engrg., p. 385-398, (Sept. 1961).

7. Huppert, M. C., W. S. King, and L. B. Stripling, Some Cavitation Problems in Rocket Propellant Pumps, Rocketdyne Rept., Canoga Park, Calif.

8. Karelin, V. Ya., Cavitation Phenomena in Centrifugal and Axial Pumps, Available from NASA, STIF, Call No. n66-14532 (consists of 128 pages) (1963).

9. Spraker, W. A., The Effects of Fluid Properties on Cavitation in Centrifugal Pumps, ASME Journ. of Engr. for Power, Vol. 87, p. 309-318 (July 1965).

10. Stepanoff, A. J., Cavitation Properties of Liquids, ASME Journ. of Engrg. for Power, Vol. 86, p. 195-200, (April 1964).

11. Wilcox, W. W., P. R. Meng, and R. L. Davis, Performance of an Inducer-Impeller Combination at or Near Boiling Conditions for Liquid Hydrogen, Adv. in Cryogenic Engrg., Vol. 8, p. 446-455, Plenum Press, Inc., (1963).

12. Hollander, A., Thermodynamic Aspects of Cavitation in Centrifugal Pumps, ARS Journ., Vol. 32, p. 1594-1595, (Oct. 1962).

13. Gelder, T. F., R. S. Ruggeri, and R. D. Moore, Cavitation Similarity Considerations Based on Measured Pressure and Temperature Depressions in Cavitated Regions of Freon 114, NASA TN D-3509 (July 1966).

14. Ruggeri, R. S. and T. F. Gelder, Effects of Air Content and Water Purity on Liquid Tension at Incipient Cavitation in Venturi Flow, NASA TN D-1459, (1963).

15. Ruggeri, R. S. and T. F. Gelder, Cavitation and Effective Liquid Tension of Nitrogen in a Tunnel Venturi, NASA TN-2088, (1964).

16. Gelder, T. F., R. D. Moore, and R. S. Ruggeri, Incipient Cavitation of Freon -114 in a Tunnel Venturi, NASA TN D-2662, (1965).

17. Ruggeri, R. S., R. D. Moore, and T. F. Gelder, Incipient Cavitation of Ethylene Glycol in a Tunnel Venturi, NASA TN D-2772, (1965).

18. Ruggeri, R. S., Private communication.

19. Flow Measurement, Chap. 4, Part 5 - Measurement of quantity of materials, p. 17, PTC, 19.5; 4-1959, the American Society of Mechanical Engineers, 29 West 39th St., New York 18, N. Y.

20. Kittredge, C. P., Detection and Location of Cavitation, Plasma Physics Lab, Princeton Univ., Princeton, N. J., Report MATT-142 (Aug. 1962). Available from O. T. S., U. S. Dept. of Commerce, Washington, 25, D. C.

21. Lehman, A. F. and J. O. Young, Experimental Investigations of Incipient and Desinent Cavitation, ASME Paper No. 63-AHGT-20 (Mar. 1963).

22. Holl, J. W., Discussions of Symposium on Cavitation Research Facilities and Techniques, Presented at Fluids Engr'g. Div. Confer., Phila., Pa., May 18-20, 1964, Available from ASME, United Engineering Center, 345 East 47th St., New York 17, New York.

9. Appendix A---Acoustic Detector

A detailed drawing of the acoustic transducer is given on figure 9.1 and a schematic of the instrument hook-up is given on figure 9.2.

The transducer consists of a barium-titanate piezoelectric crystal sandwiched between the body of the transducer and a machine screw, figure 9.1. The mechanical coupling or initial compression level in the crystal could be varied by means of the machine screw. Thus, the sensitivity of the crystal to mechanical vibration could be adjusted somewhat. Electrical leads were attached to the adjustment screw and to the body of the transducer. Coaxial electrical wire was used to connect the transducer to a cathode-follower-amplifier, see figure 9.2. The signal was then filtered through a variable band-pass filter and displayed on an oscilloscope. The band-pass filter was set to admit signal frequencies of 3 to 200 kHz for most tests.

The acoustic transducer was screw-mounted in the downstream flange of the plastic venturi via pipe threads. Most of the system vibration and noise appeared to be of low frequency and was easily eliminated with the band-pass filter.

Cavitation was readily discernible on the oscilloscope and was characterized by large-amplitude, high-frequency signals.

10. Appendix B---Method Used to Compensate the Experimental Inception Data for Temperature Deviation about the Nominal Isotherms

(1) It was assumed that a change in inlet temperature, dT_o, will produce a change in inlet head, dh_o, along a constant velocity path, which will be a function of the velocity and temperature only; it is also assumed that this function may be approximated by a few terms of a polynomial. Justification of these assumptions is evidenced by the good results which were obtained for both hydrogen and nitrogen (see figures 4.2 and 4.4) by using the following equation:

$$dh_o = [C_1 T_o^2 + C_2 T_o + C_3 V_o^2 + C_4 V_o + C_5]\, dT_o. \qquad [10\text{-}1]$$

Holding V_o constant and integrating from $h_{o,1}$ to $h_{o,2}$ and from $T_{o,1}$ to $T_{o,2}$ there results:

$$\left[h_{o,2} - h_{o,1}\right]_{V_o} = C_1'[(T_{o,2})^3 - (T_{o,1})^3] + C_2'[(T_{o,2})^2 - (T_{o,1})^2] + (T_{o,2} - T_{0,1})(C_3 V_o^2 + C_4 V_o + C_5), \qquad [10\text{-}2]$$

where the subscript "1" refers to the position of a data point before it is transferred to a new position identified by the subscript "2".

For each of the following steps (two through seven) there is a corresponding graphical illustration on Figure 10.1.

(2) h_o vs V_o experimental data were plotted, a separate graph being used for each test fluid. The data points were identified with their individual temperatures so that "best-fit" curves could be drawn through each group of data points having a common nominal temperature. A nominal temperature is defined as that temperature which is selected to

represent a specific group of data points having little temperature variation. These first-approximation isotherms are shown as dashed lines on step two of figure 10.1.

One of the nominal isotherms is chosen, on the basis of availability of sufficient experimental h_o vs V_o data at or near that temperature, as a reference or "base" isotherm for succeeding computations. This isotherm is designated $T_{o,B}$ in figure 10.1 while the other isotherms are designated T_o' and T_o''.

(3) The constants in equation [10-2] are evaluated by selecting pairs of values of h_o and T_o from the nominal isotherms at identical velocities as follows: on figure 10.1 the tail of each arrow indicates a value of $h_{o,1}$ and $T_{o,1}$ while the arrow head points to $h_{o,2}$ and $T_{o,2}$. The coordinate points from each arrow are then used in equation [10-2]. Note that each arrow provides one equation, hence five arrows are needed to evaluate the constants in [10-2]. The arrows always follow a constant velocity path and must be strategically placed in order for the five equations to be independent. The actual data points are not shown since they are not used in this step. The equation derived from this step will "transfer" data from one temperature to another within the confines of the bounding isotherms.

(4) In step four of the illustration, arrows are used to indicate the "transferral" of experimental data points to a new location near the base isotherm. $h_{o,1}$ and $T_{o,1}$ are known from the experimental data, while $T_{o,2}$ is simply the base nominal temperature, $T_{o,B}$; values of $h_{o,2}$ can then be determined, by using equation [10-2], and plotted near the base temperature, $T_{o,B}$. Note that the data transfer always follows a constant velocity path.

(5) A new "best fit" isotherm can then be drawn through all of the "transferred" data points at $T_{o,B}$. This new curve is shown as a solid line in figure 10.1; the first approximation isotherms, drawn as dashed lines, are no longer needed and are omitted in the illustration of this step. The curve obtained from this step represents an improved reference isotherm.

(6) The new reference isotherm and equation [10-2] may now be used to reconstruct the other nominal isotherms. T_o' and T_o'' may be reconstructed by using equation [10-2] and $h_{o,1}$ values from the new base isotherm. Note that $T_{o,B}$ now becomes $T_{o,1}$ and T_o' and T_o'' take their respective turns as $T_{o,2}$. Values of $h_{o,2}$ are then computed in order to plot the two new isotherms shown in the illustration of this step on figure 10.1.

(7) The original experimental data points were then transferred to their nearest nominal temperature by means of equation [10-2]. Those points having a nominal temperature of $T_{o,B}$ were relocated in their final position in step four. This process brings the data points near their respective isotherms, as shown by the arrows in the illustration of step seven. Note that $h_{o,2}$ is again the only unknown in equation [10-2].

(8) The agreement between the new nominal isotherms and the transferred experimental data points was then observed: If the fit was not satisfactory, "best-fit" curves were drawn through the "transferred" data points and the entire computational procedure---steps (3) through (7)--- was repeated. Several iterations were necessary to obtain suitable mathematical expressions for liquid hydrogen and liquid nitrogen: tables 4.3, 4.4, and 4.5 as well as figures 4.2 and 4.4 were prepared by using the following equations.

Hydrogen:

$$\left[h_{o,2} - h_{o,1}\right]_{V_o} \approx 5.86\,[(T_{o,2})^2 - (T_{o,1})^2]$$

$$+ (T_{o,2} - T_{o,1})(0.41\,V_o - 400.35). \qquad [10\text{-}3]$$

Nitrogen:

$$\left[h_{o,2} - h_{o,1}\right]_{V_o} \approx 0.000835\,[(T_{o,2})^3 - (T_{o,1})^3]$$

$$-0.2729\,[(T_{o,2})^2 - (T_{o,1})^2] + 30.152\,(T_{o,2} - T_{o,1}). \qquad [10\text{-}4]$$

It should be noted that some of the terms in equation [10-2] become negligible and consequently are not included in [10-3] and [10-4]. It is observed that equation [10-3] for hydrogen is velocity dependent, while equation [10-4] for nitrogen is not. It is not recommended that equations [10-3] and [10-4] be used outside the general area of the data points given.

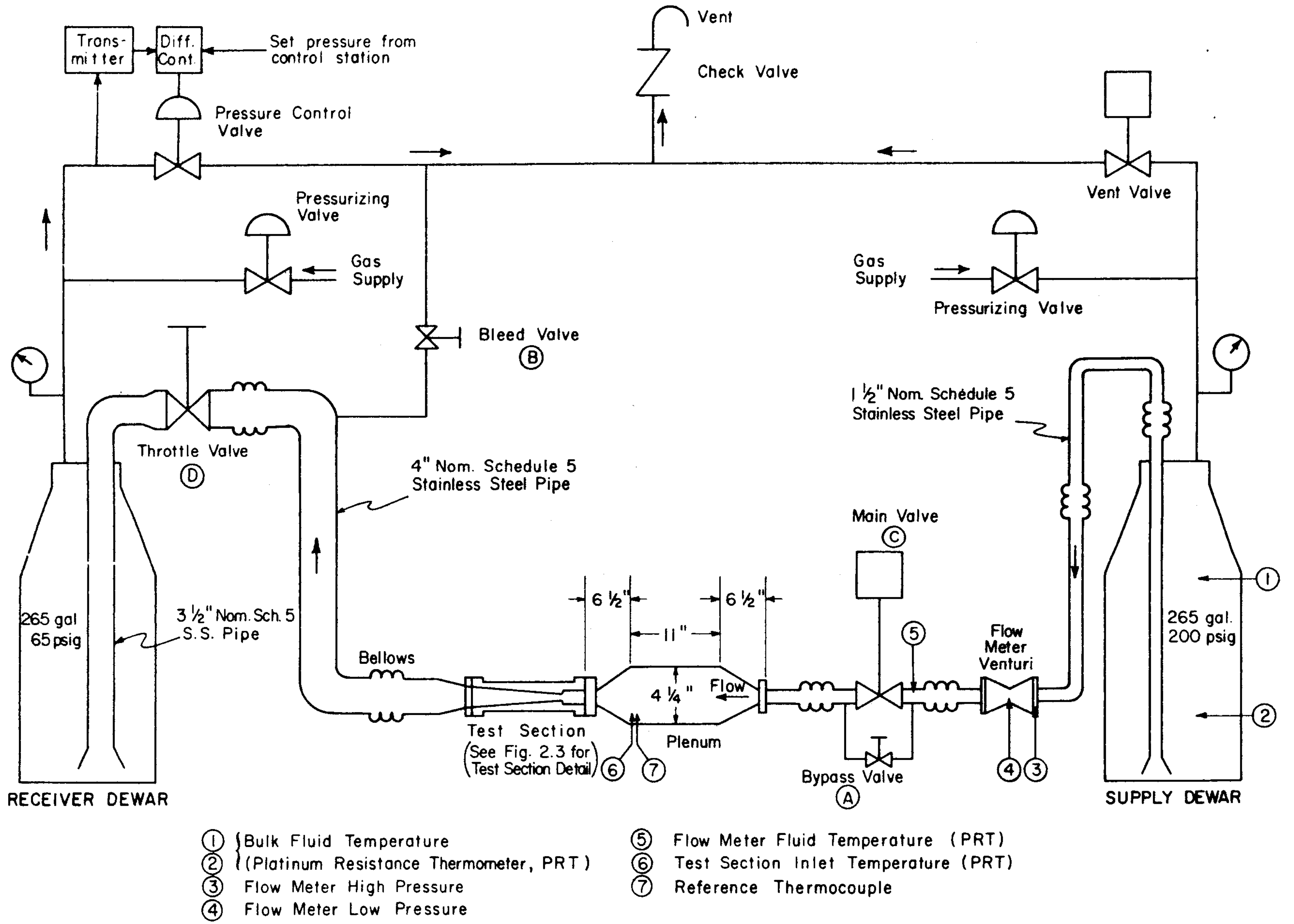

Figure 2.1 Schematic of Cavitation Flow Apparatus.

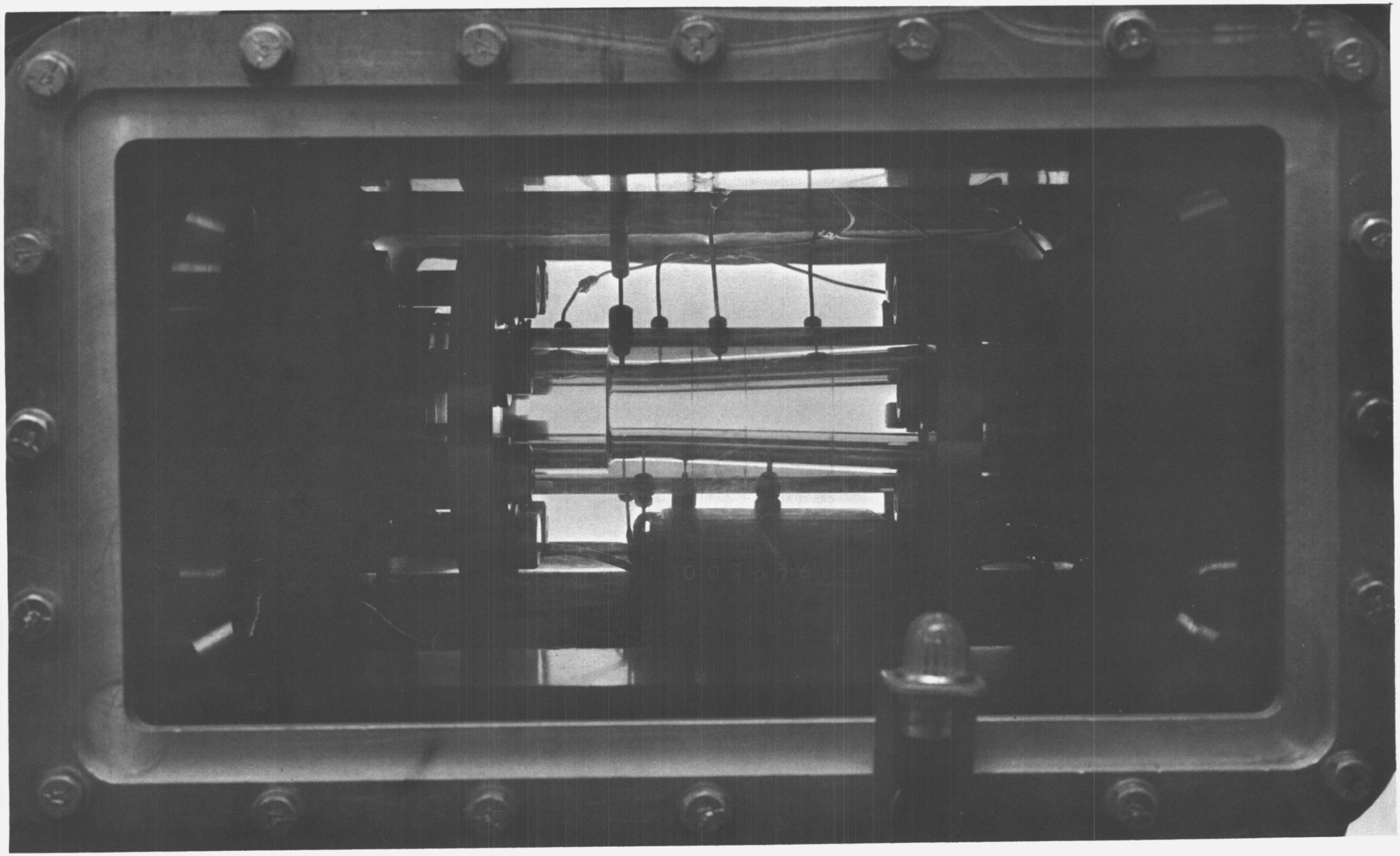

Figure 2.2 Photograph of Plastic Venturi Test Section Installed in System. Note Counter -- Used to Correlate Flow Data with Film Event.

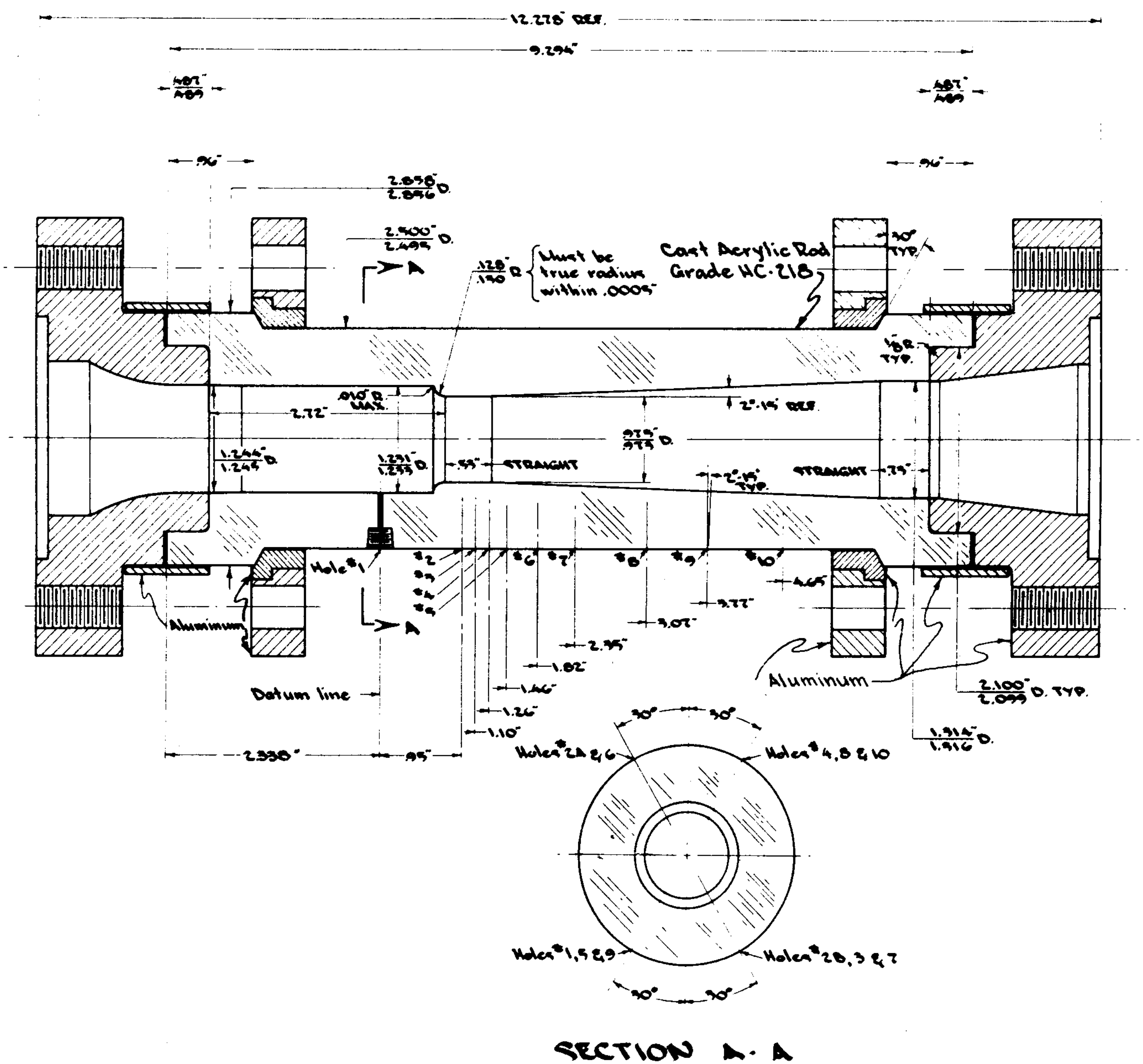

Figure 2.3 Sketch of Plastic Venturi Section Showing Dimensions and Location of Pressure and Temperature Instrumentation.

69875

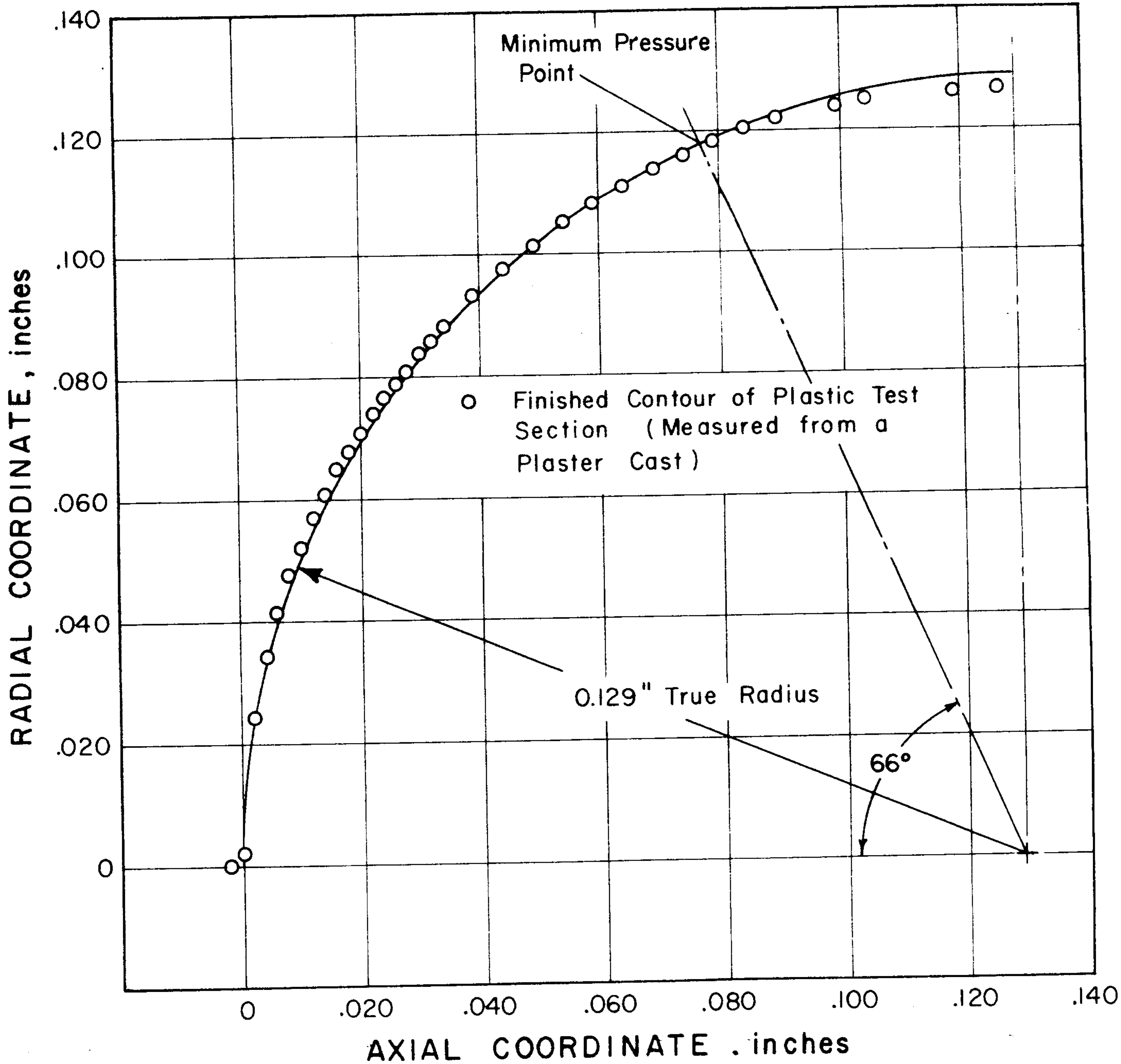

Figure 2.4 Quarter-Round Contour of Convergent Region of Plastic Test Section.

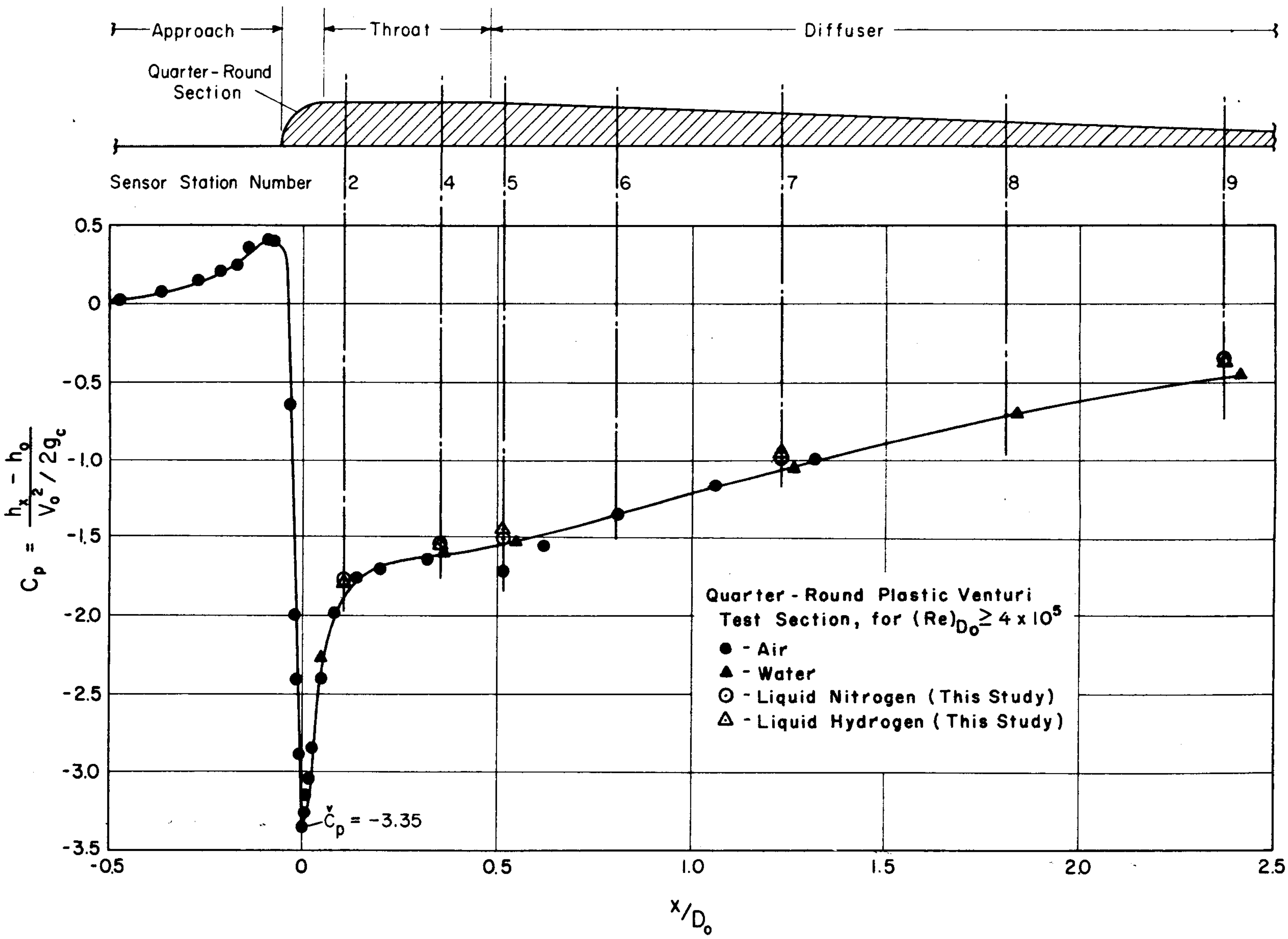

Figure 2.5 Pressure Distribution Through Test Section for Non-Cavitating Flow.

B-70178

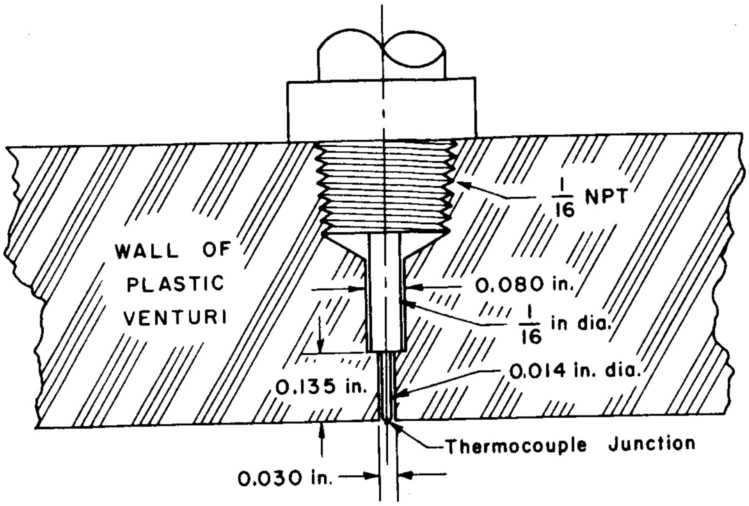

(.1): Detail of thermocouple instrument port

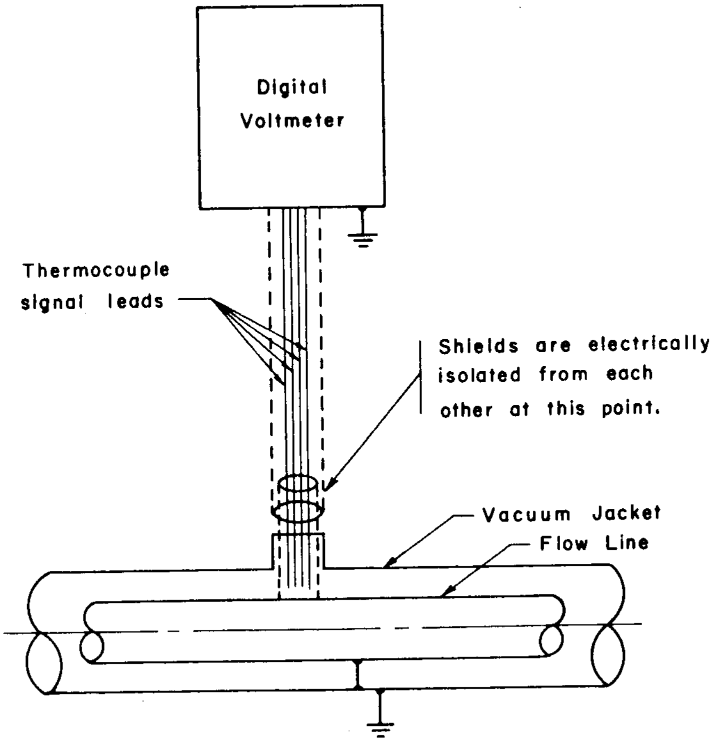

(.2): Schematic of thermocouple recording circuit

Figure 2.6 Installation and wiring details of thermocouples used to measure cavity temperatures

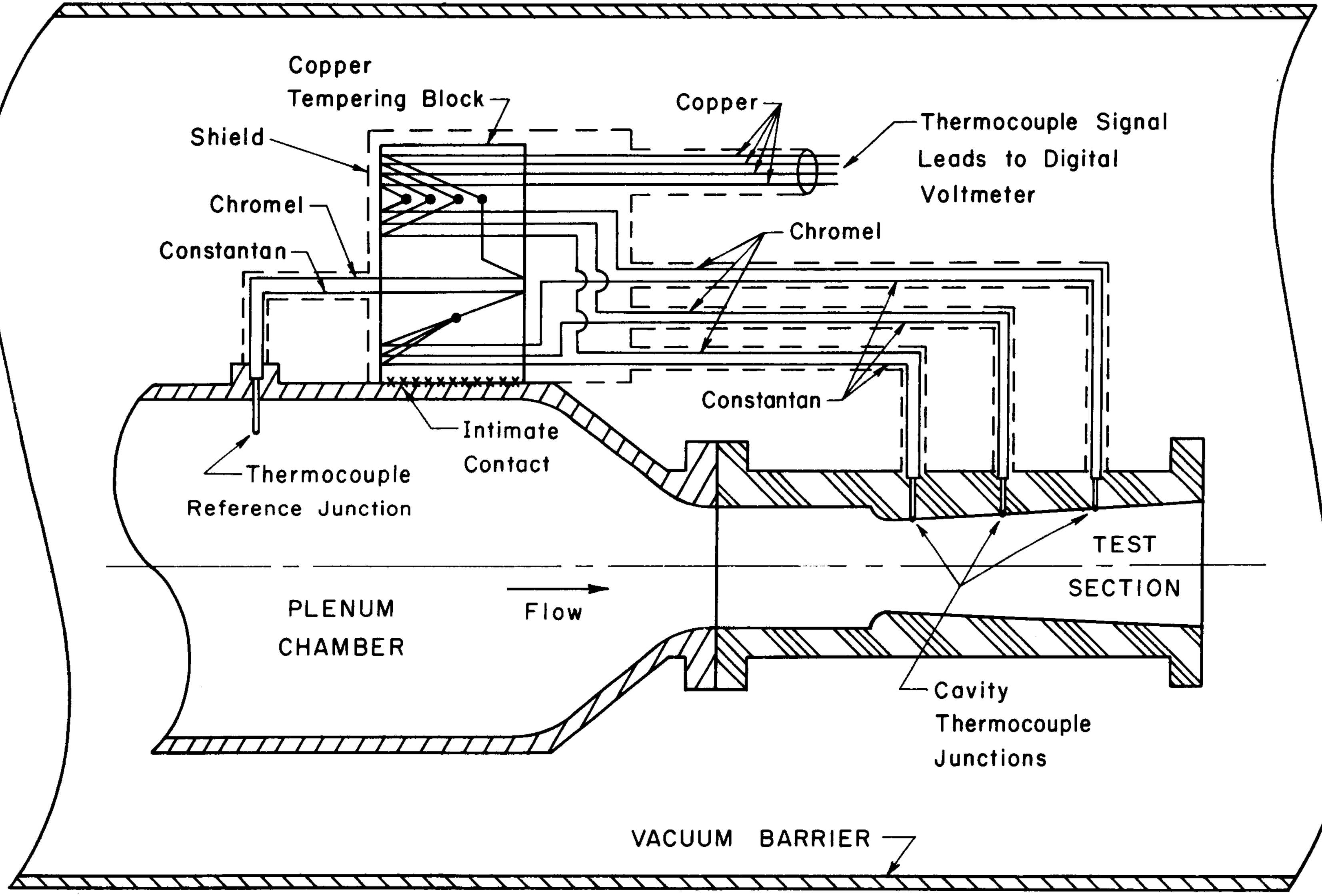

Figure 2.7 Schematic diagram of thermocouple measuring circuit, showing physical location and electrical connections for the thermocouples

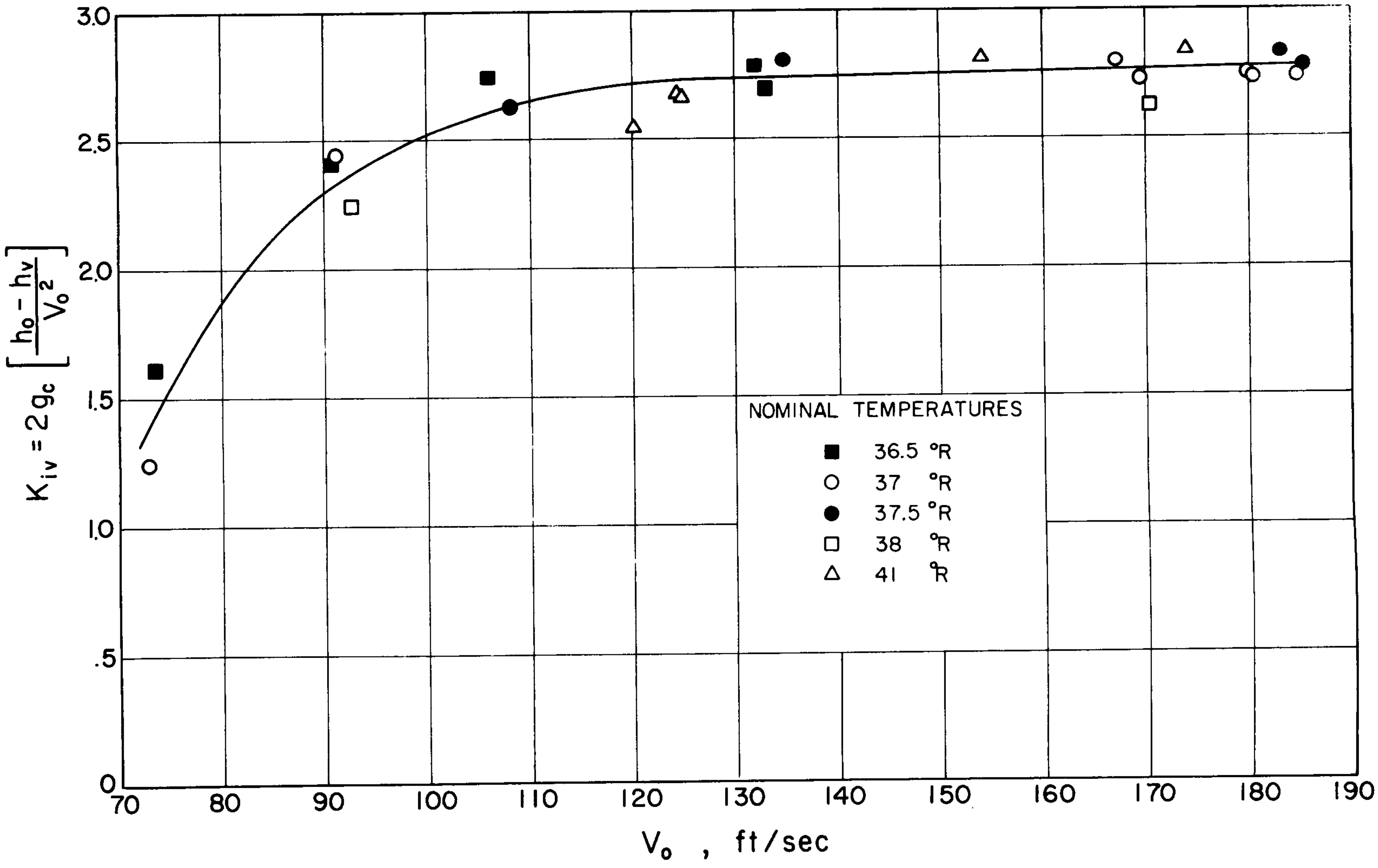

Figure 4.1 Cavitation Parameter for Liquid Hydrogen as Function of Test Section Inlet Velocity.

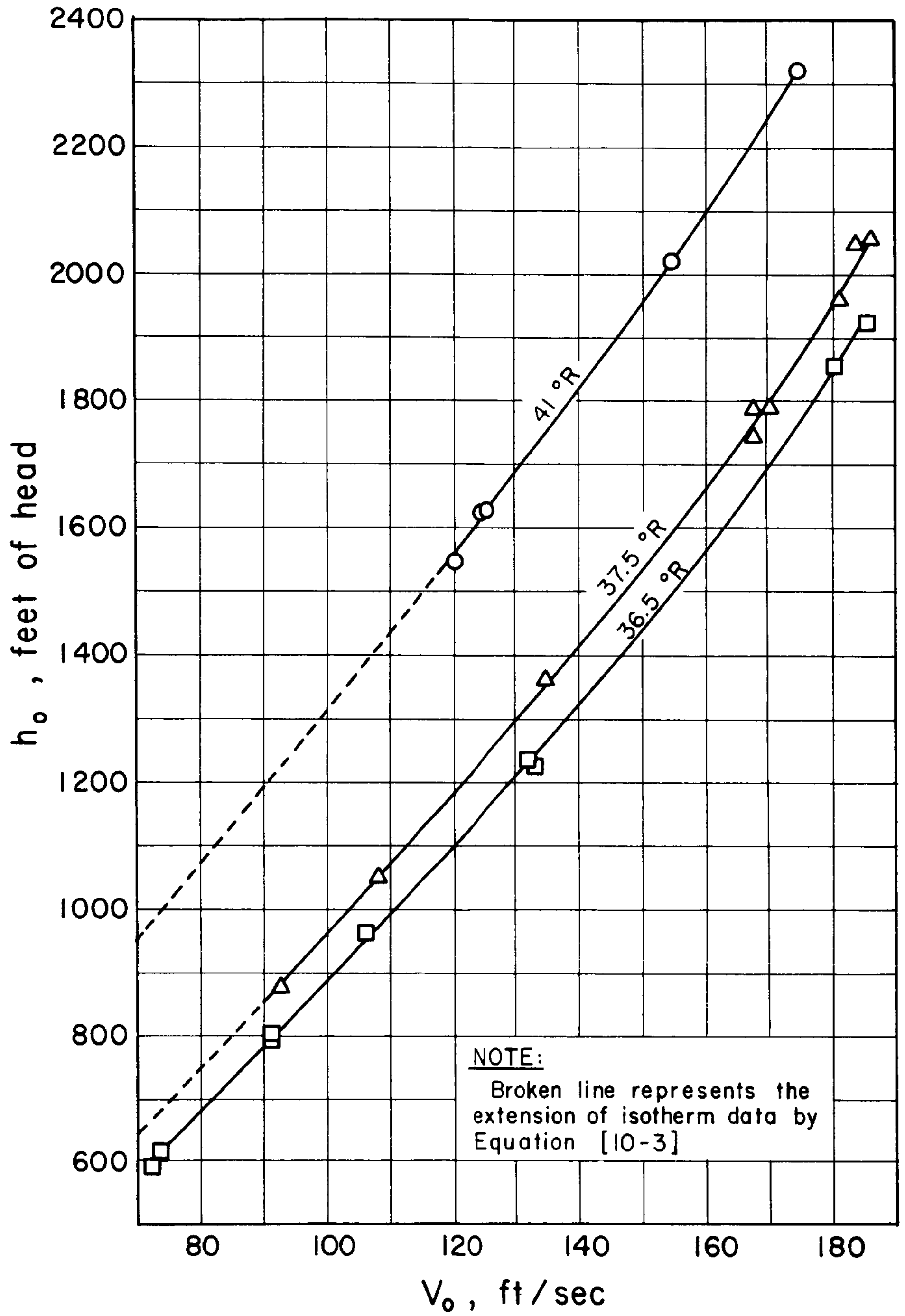

Figure 4.2 Effect of Test Section Inlet Velocity and Liquid Temperature on Required Inlet Head for Cavitation Inception in Liquid Hydrogen

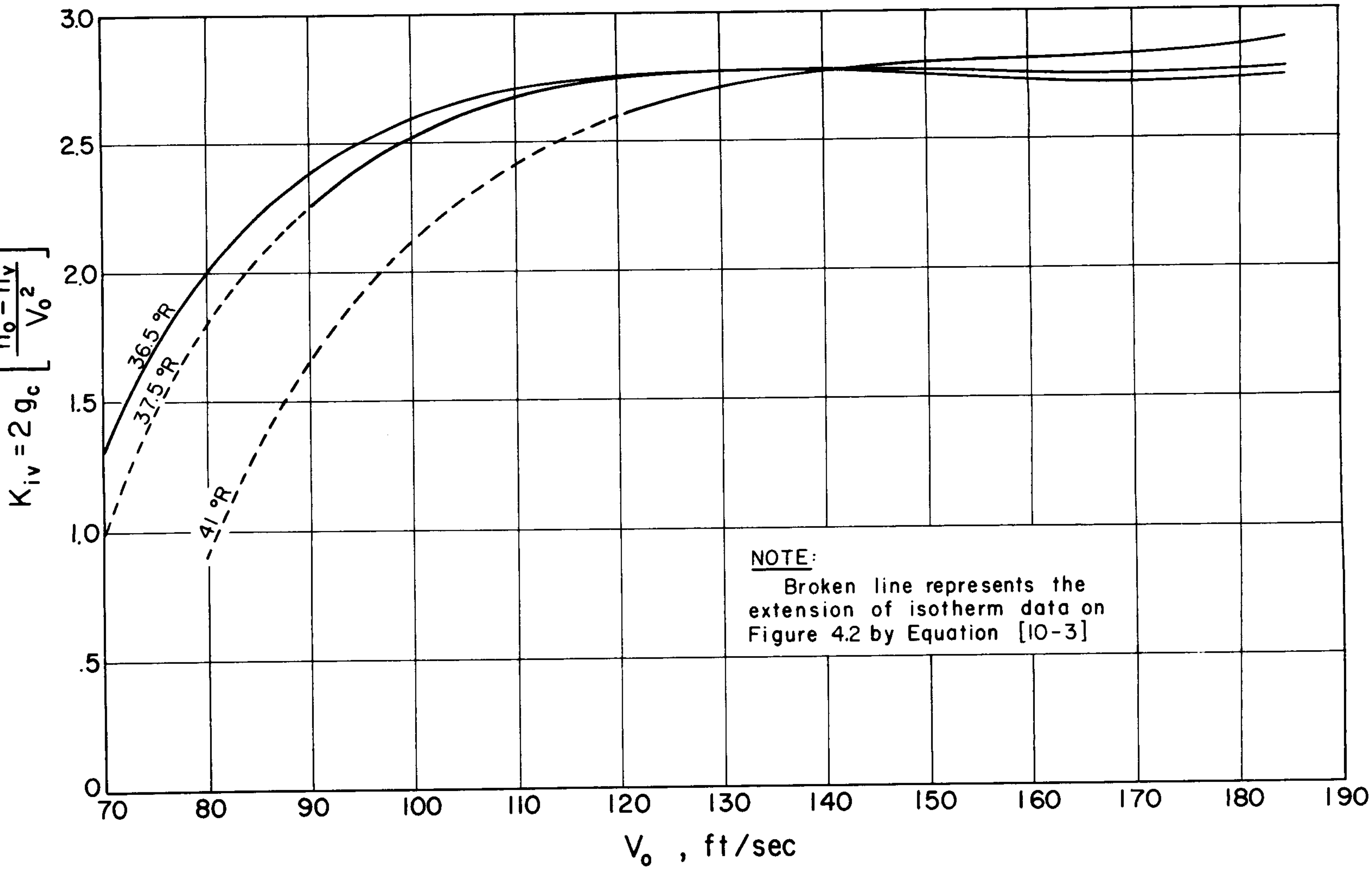

Figure 4.3 Cavitation Parameter for Liquid Hydrogen as a function of Test Section Inlet Velocity and Liquid Temperature.

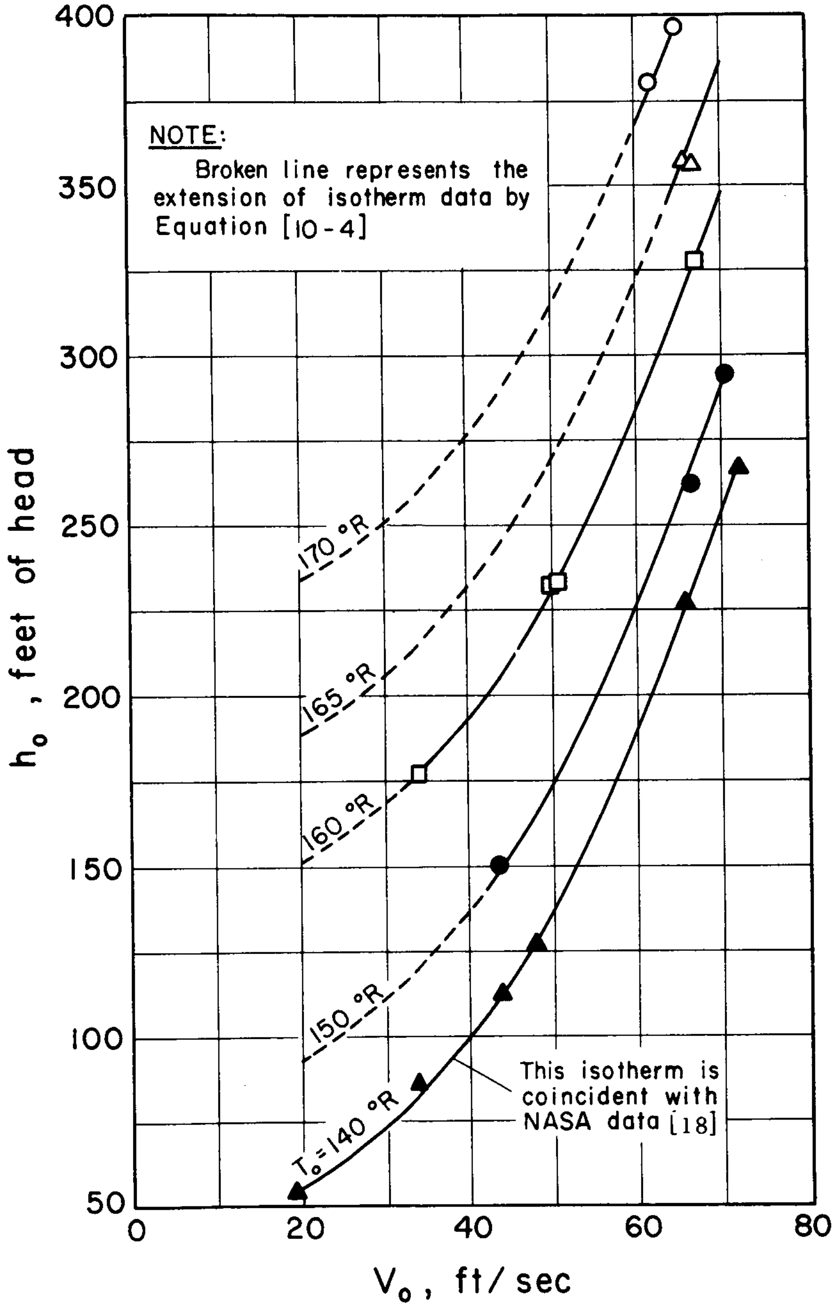

Figure 4.4 Effect of Test Section Inlet Velocity and Liquid Temperature on Required Inlet Head for Cavitation Inception in Liquid Nitrogen.

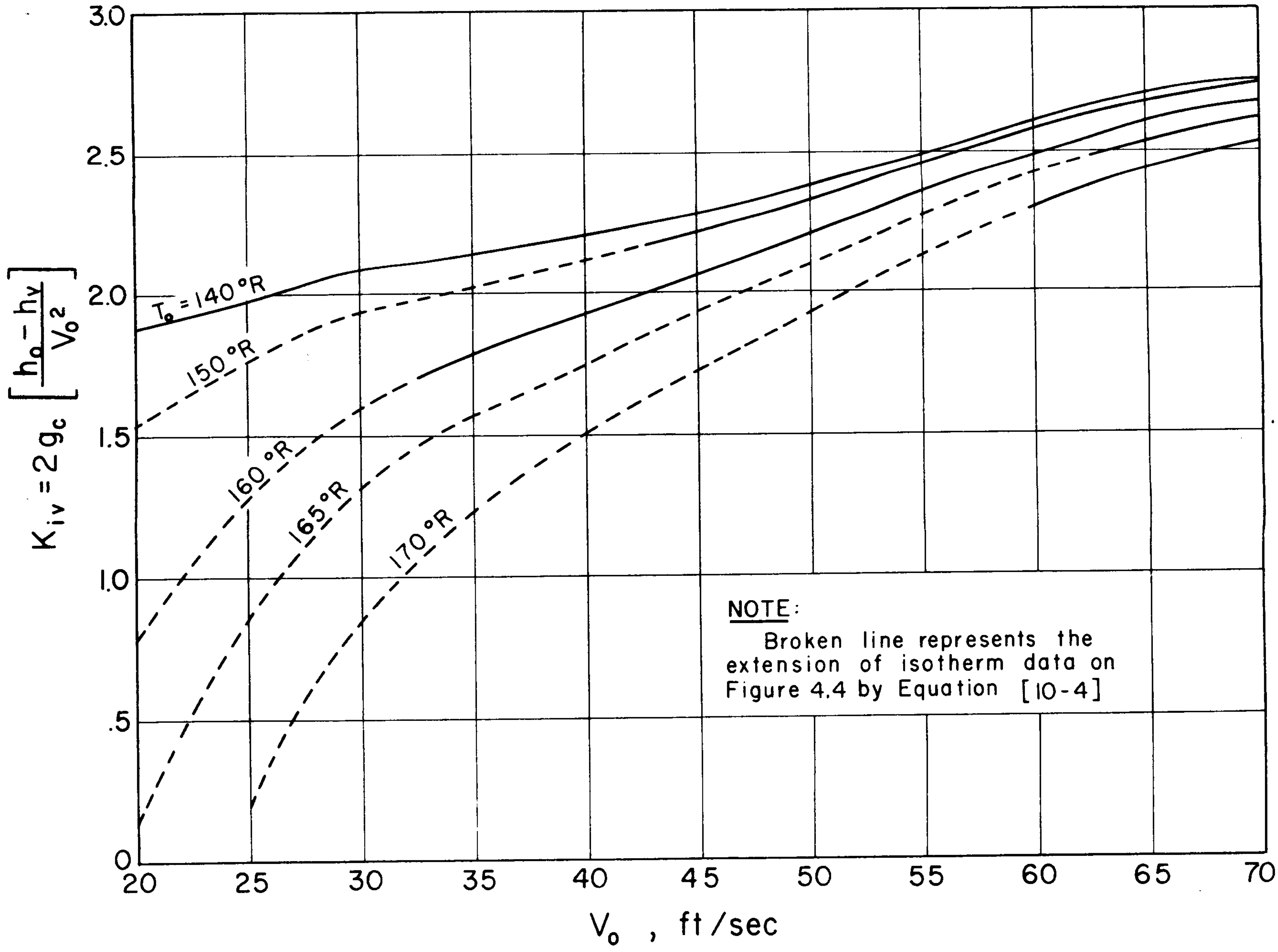

Figure 4. 5 Cavitation Parameter for Liquid Nitrogen as Function of Test Section Inlet Velocity and Liquid Temperature.

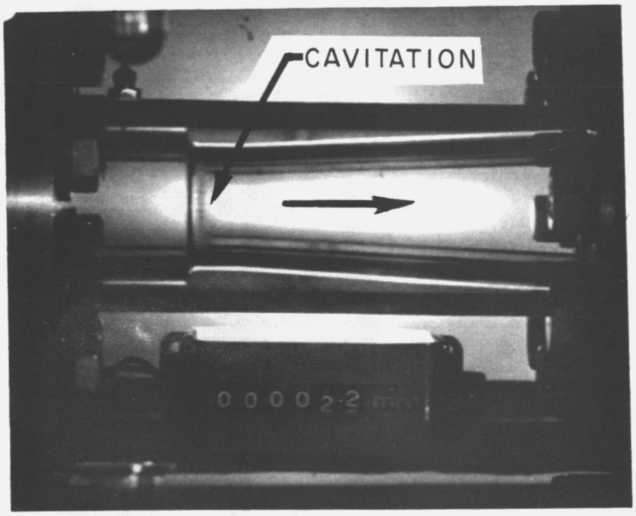

Figure 4.6 Photograph Showing Typical Cavitation Inception in Liquid Hydrogen

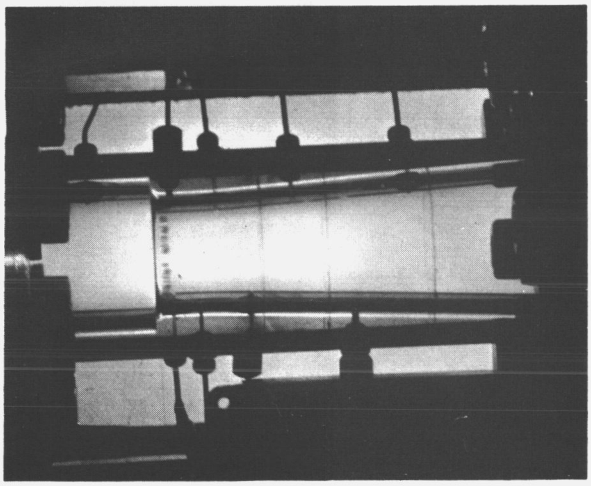

Figure 4.7 Photograph Showing Typical Cavitation Inception in Liquid Nitrogen

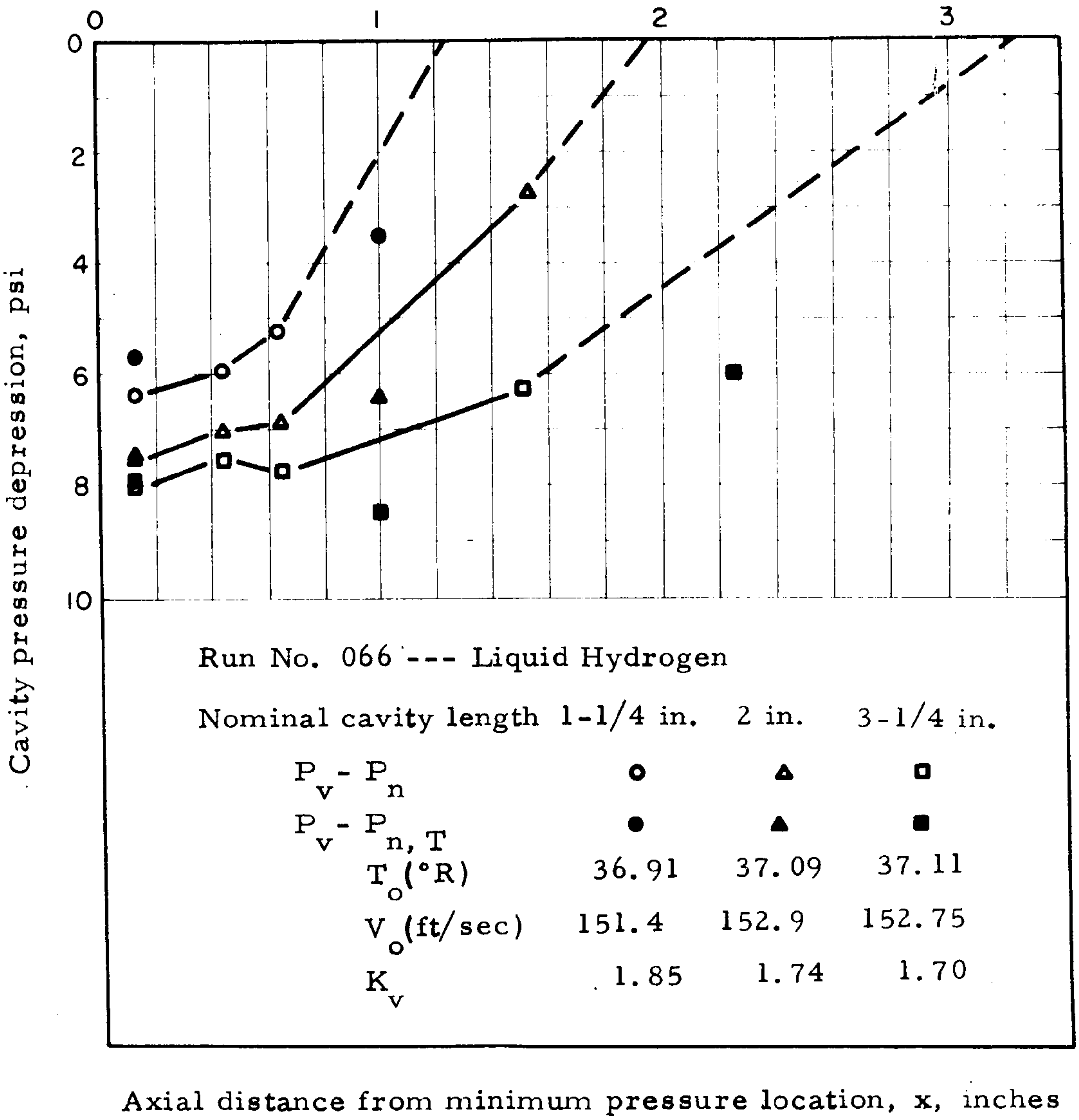

Figure 4.8 Pressure and temperature depressions within cavity in liquid hydrogen.

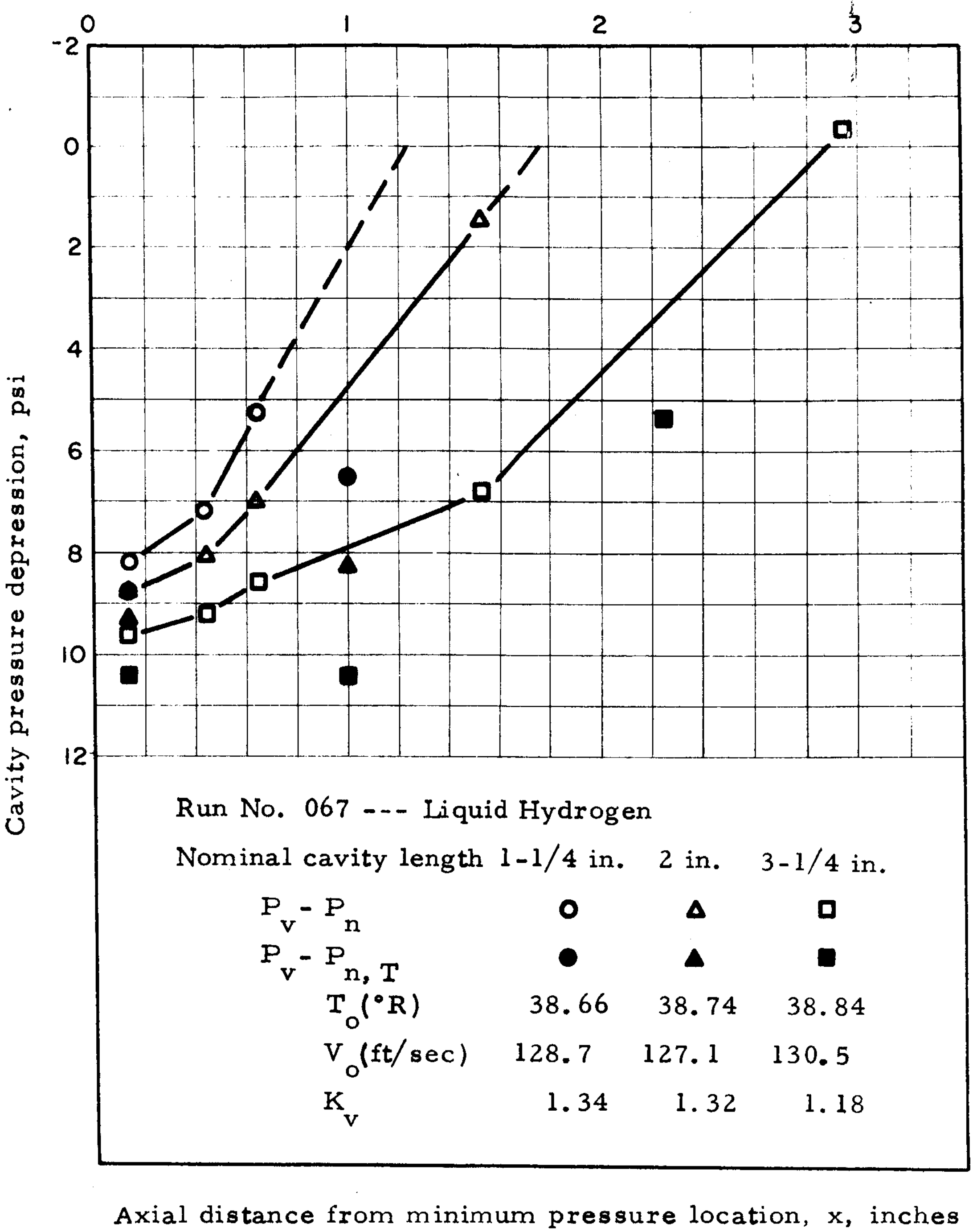

Figure 4.9 Pressure and temperature depressions within cavity in liquid hydrogen.

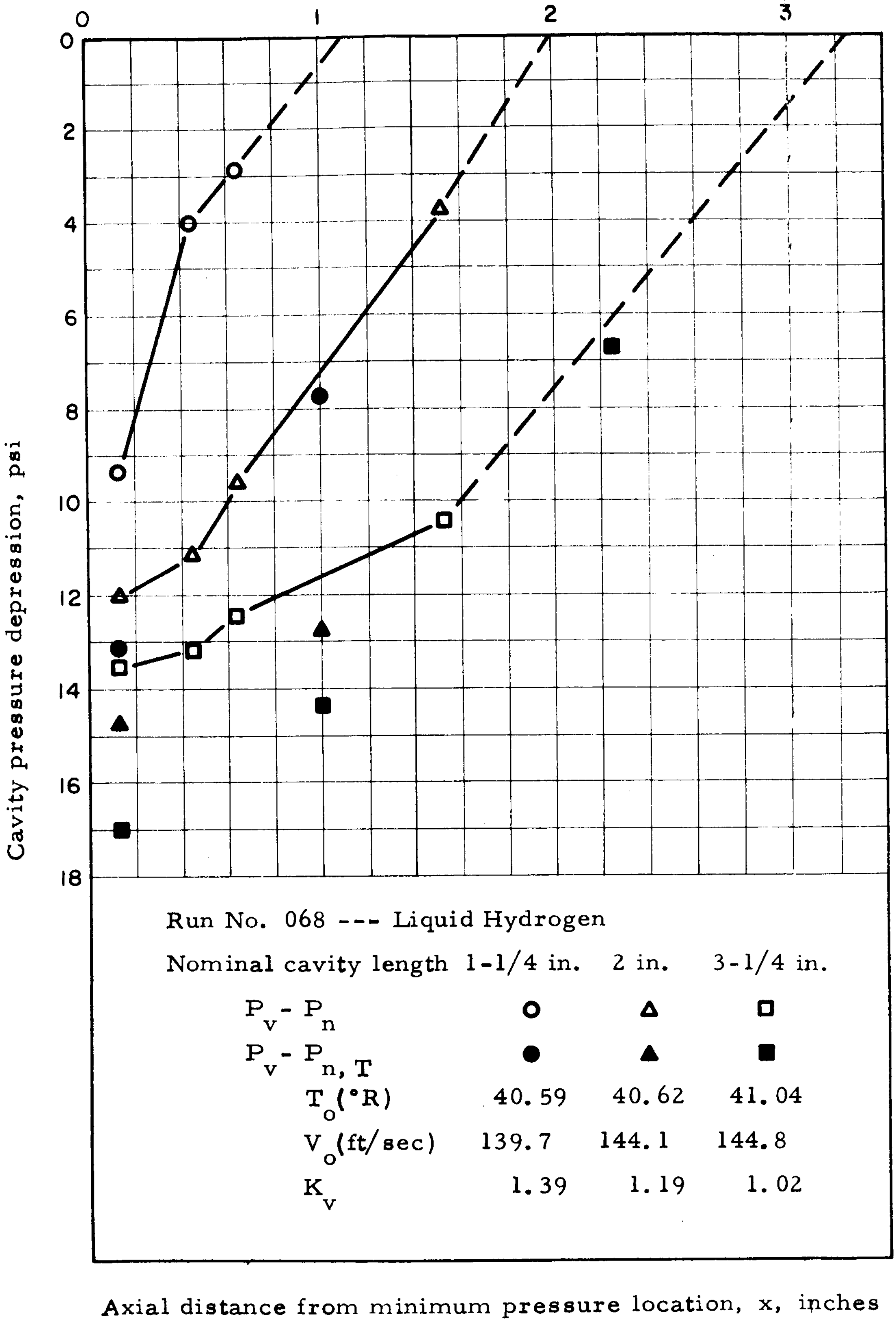

Figure 4.10 Pressure and temperature depressions within cavity in liquid hydrogen.

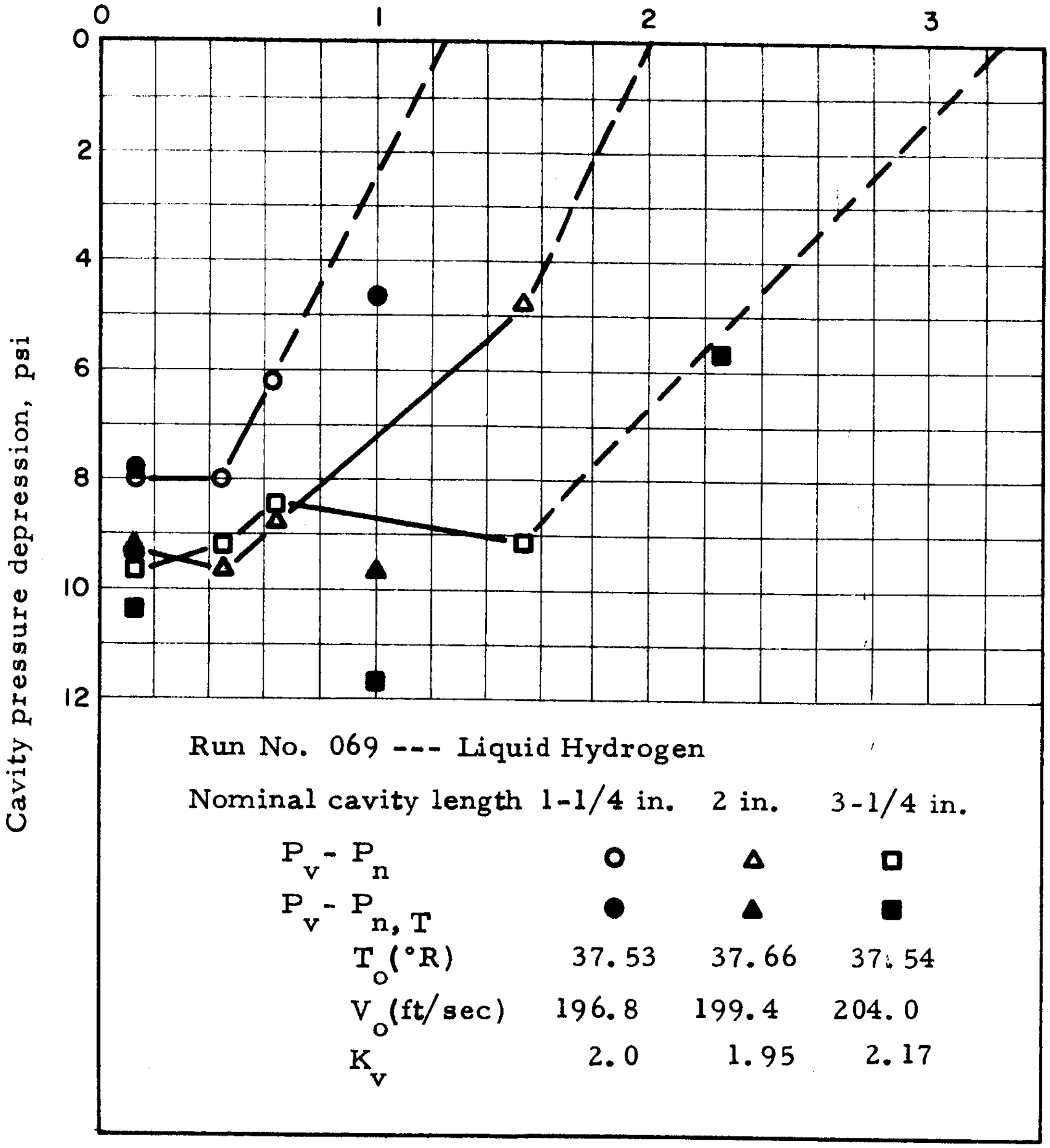

Figure 4.11 Pressure and temperature depressions within cavity in liquid hydrogen.

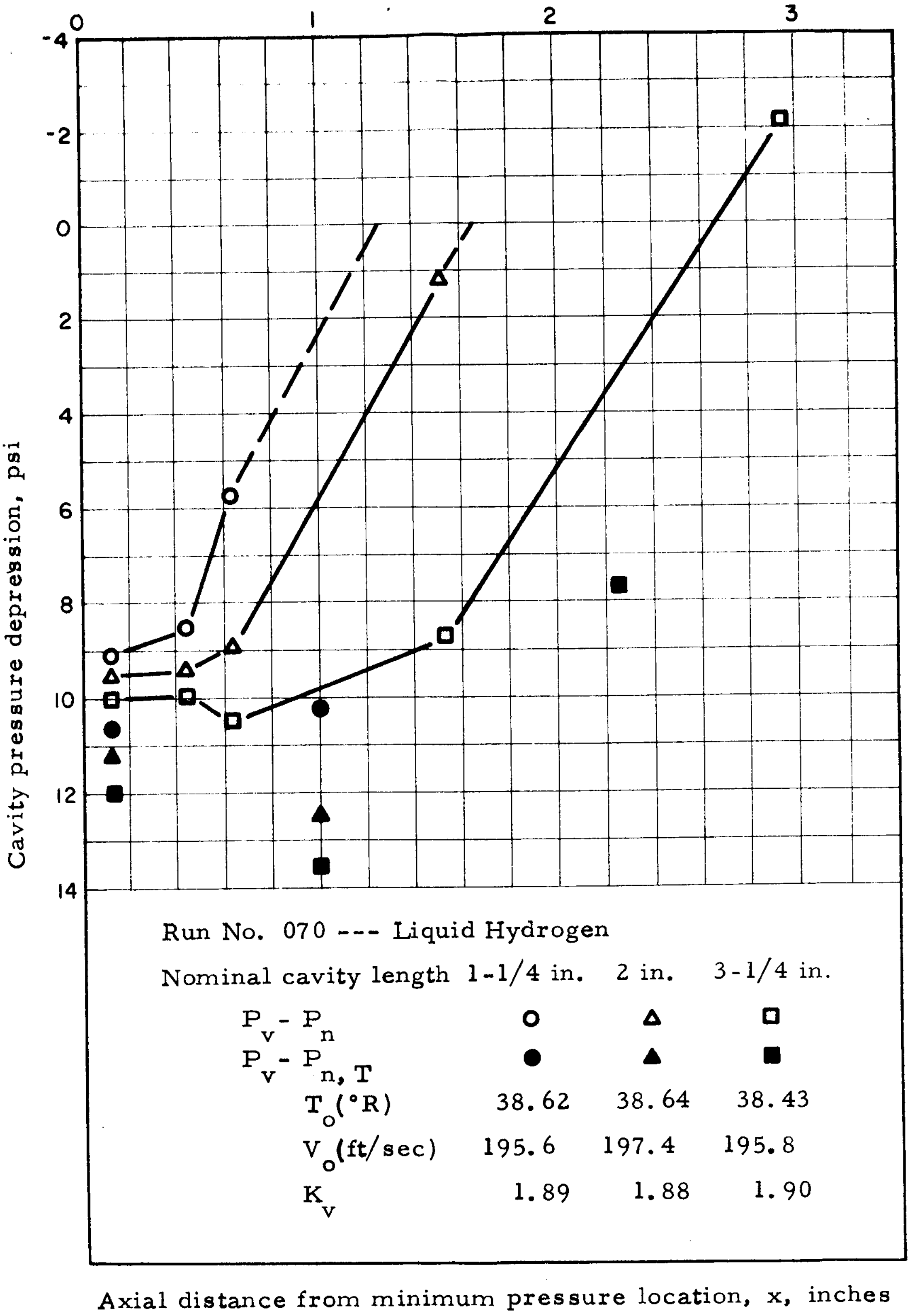

Figure 4.12 Pressure and temperature depressions within cavity in liquid hydrogen.

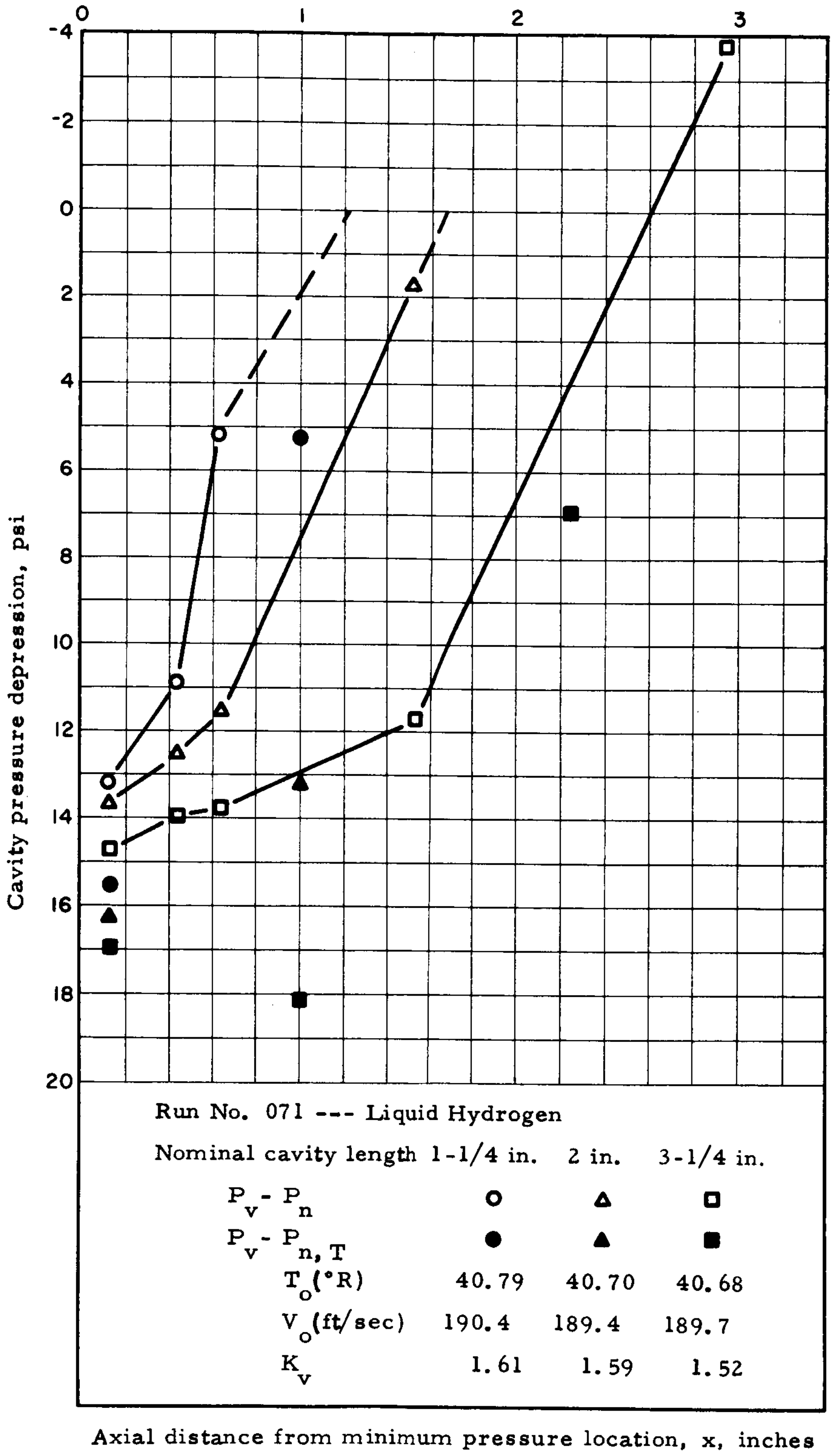

Figure 4.13 Pressure and temperature depressions within cavity in liquid hydrogen.

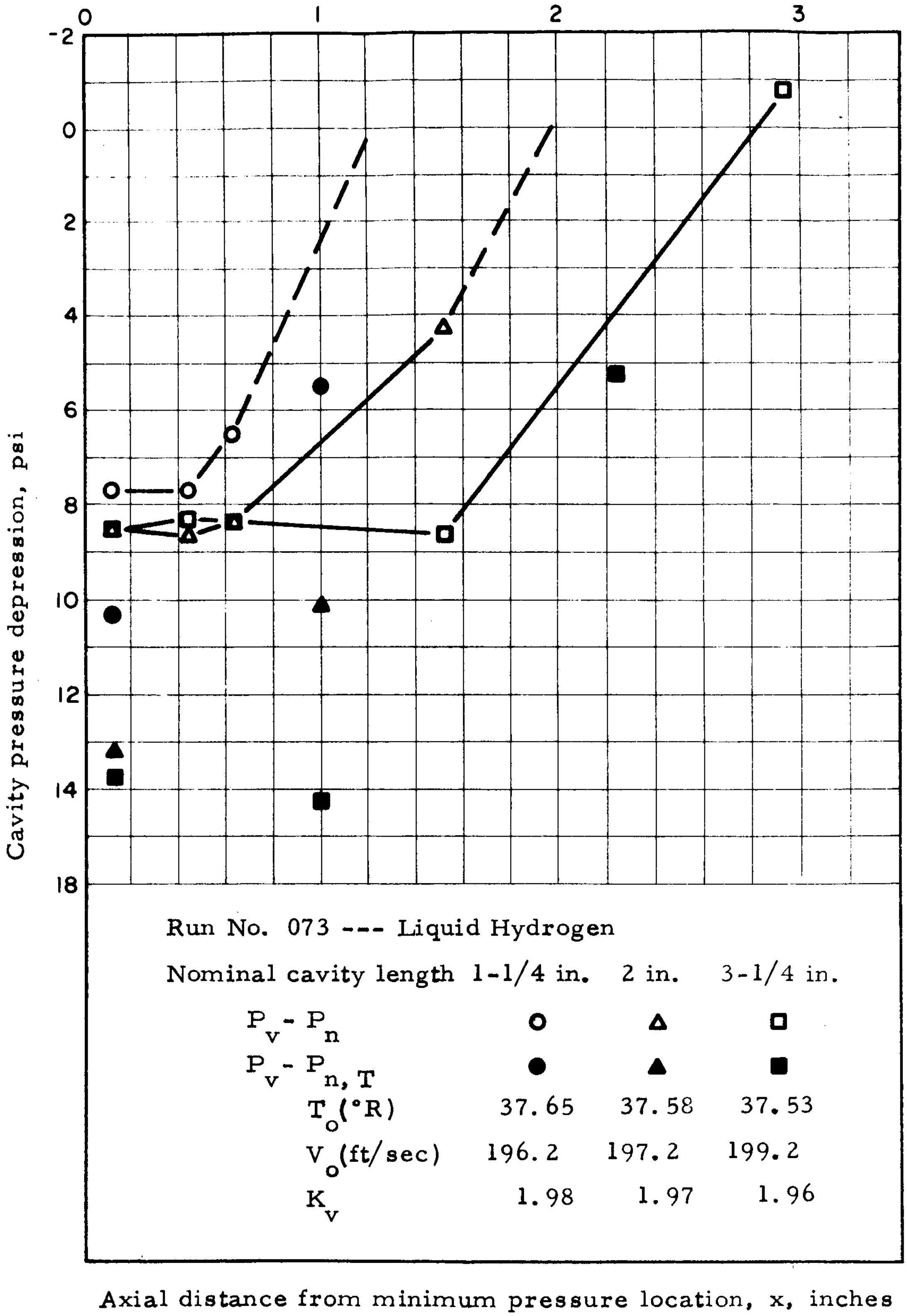

Figure 4. 14 Pressure and temperature depressions within cavity in liquid hydrogen.

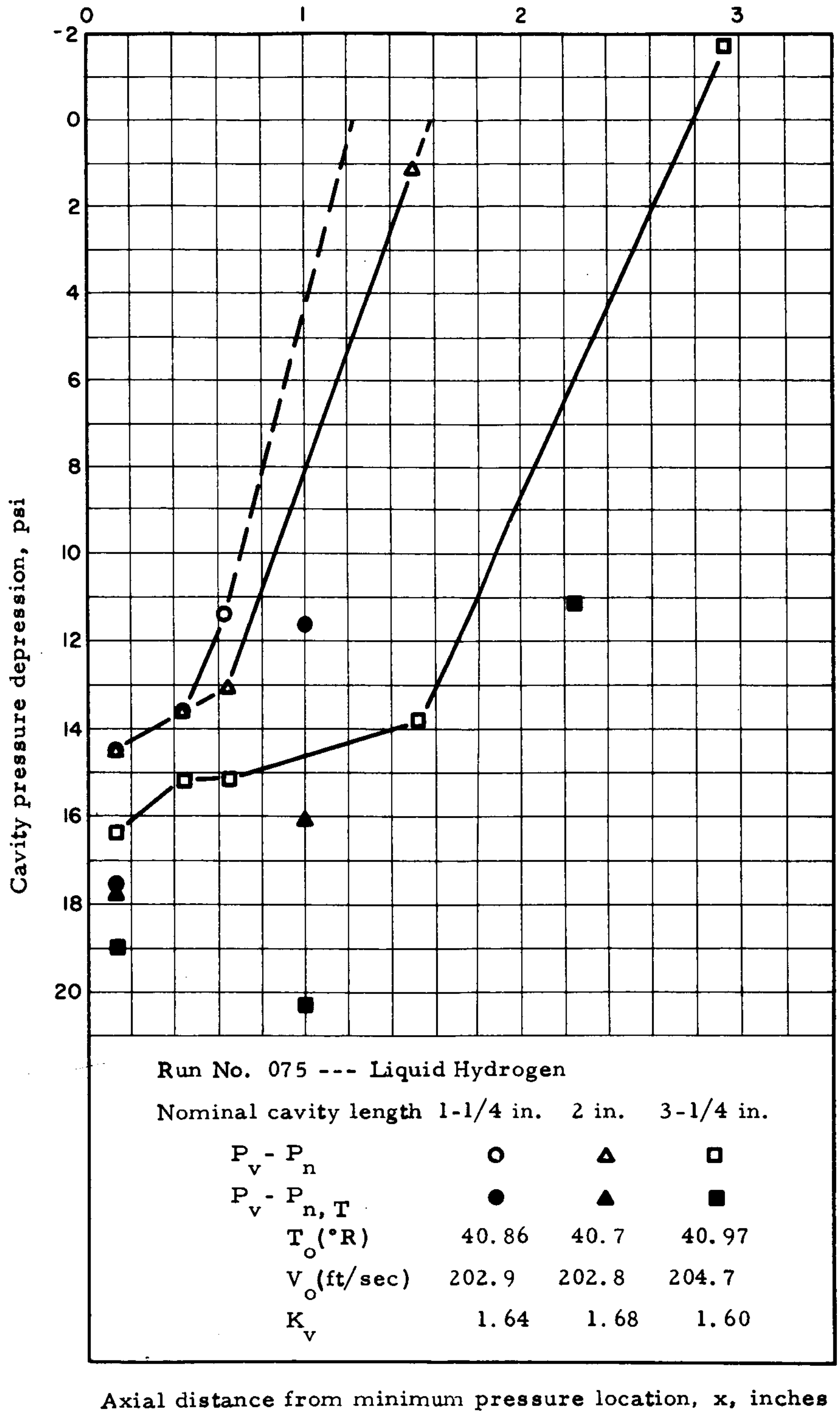

Figure 4.15 Pressure and temperature depressions within cavity in liquid hydrogen.

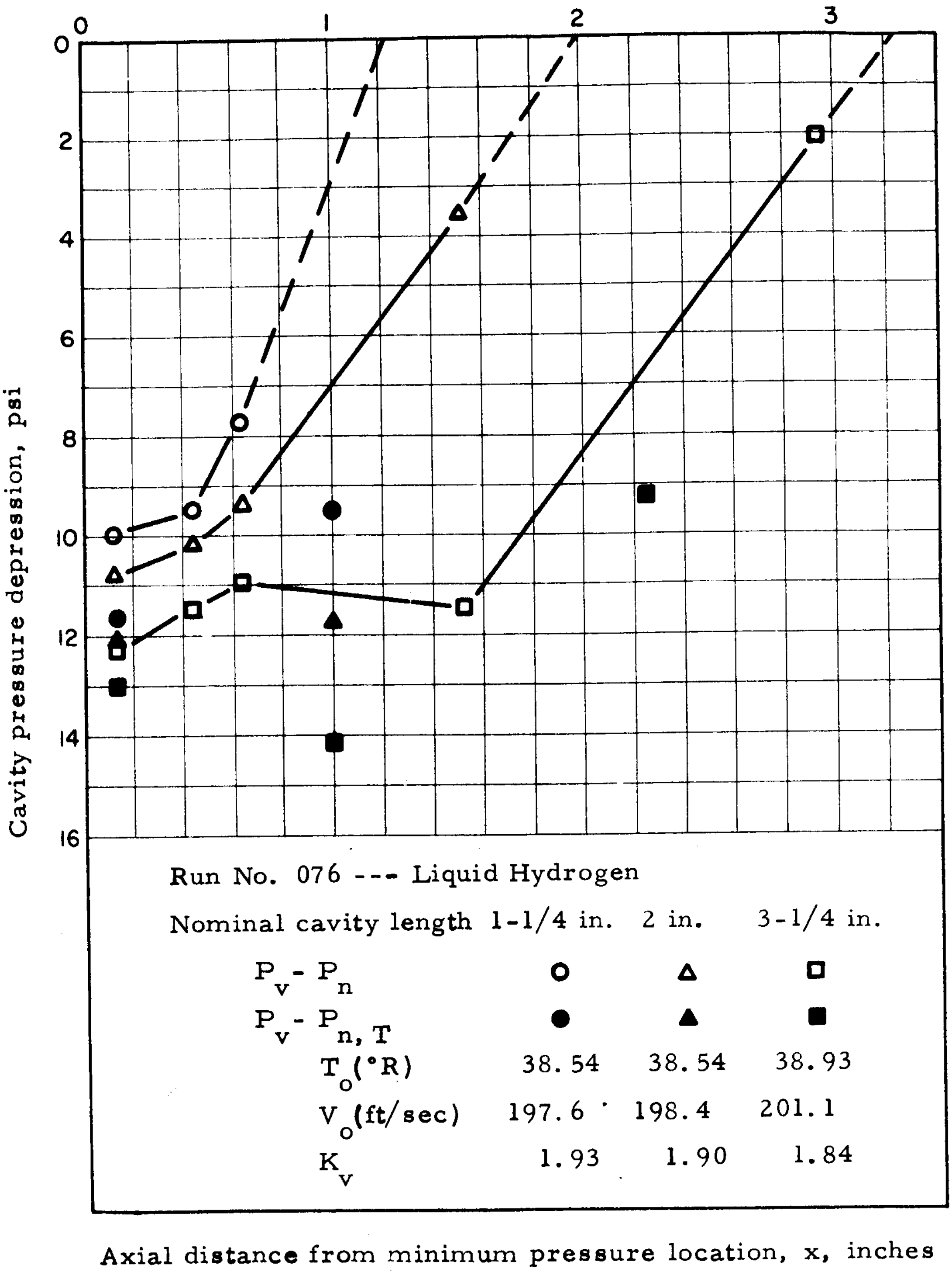

Figure 4.16 Pressure and temperature depressions within cavity in liquid hydrogen.

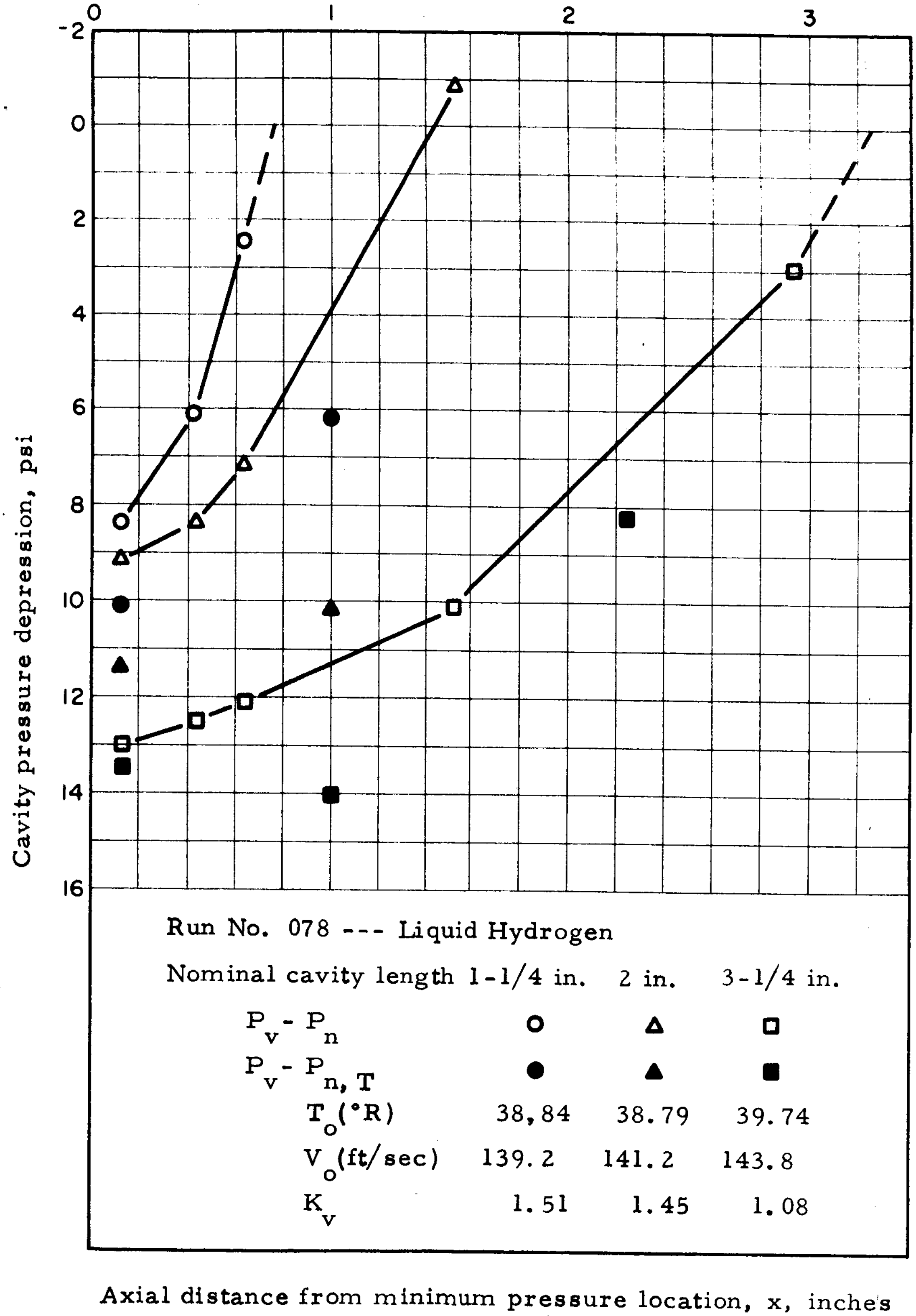

Figure 4.17 Pressure and temperature depressions within cavity in liquid hydrogen.

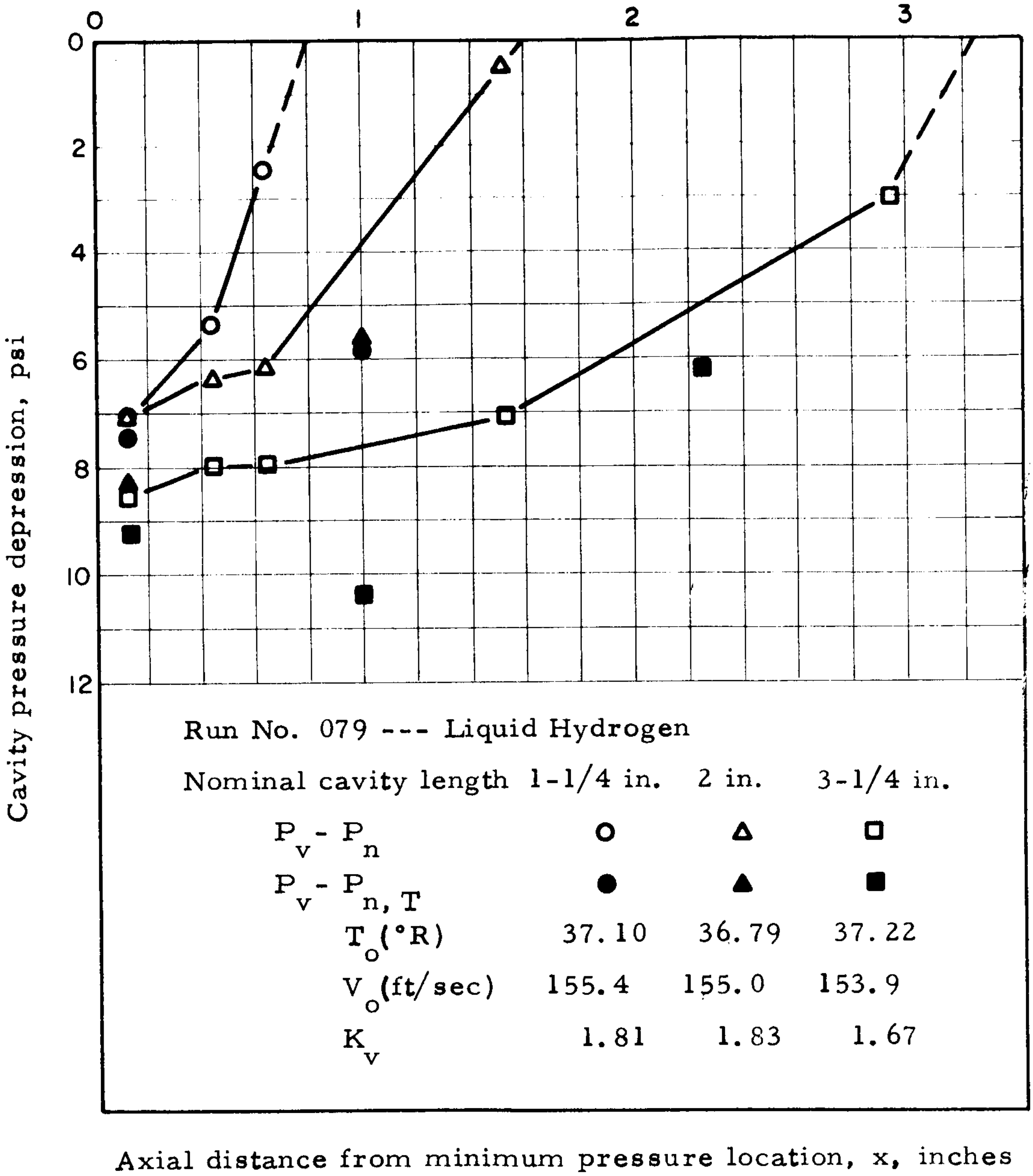

Figure 4.18 Pressure and temperature depressions within cavity in liquid hydrogen.

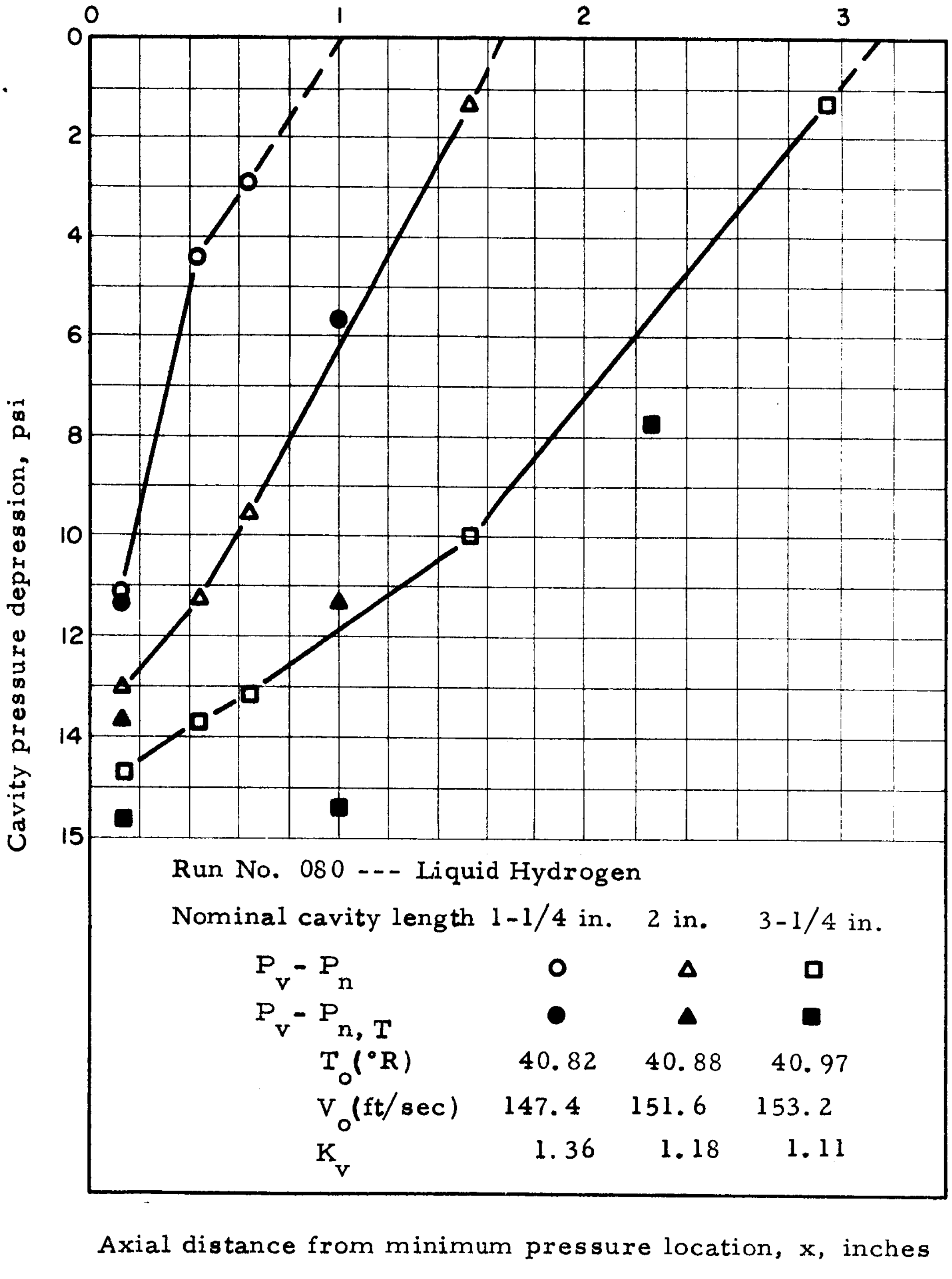

Figure 4.19 Pressure and temperature depressions within cavity in liquid hydrogen.

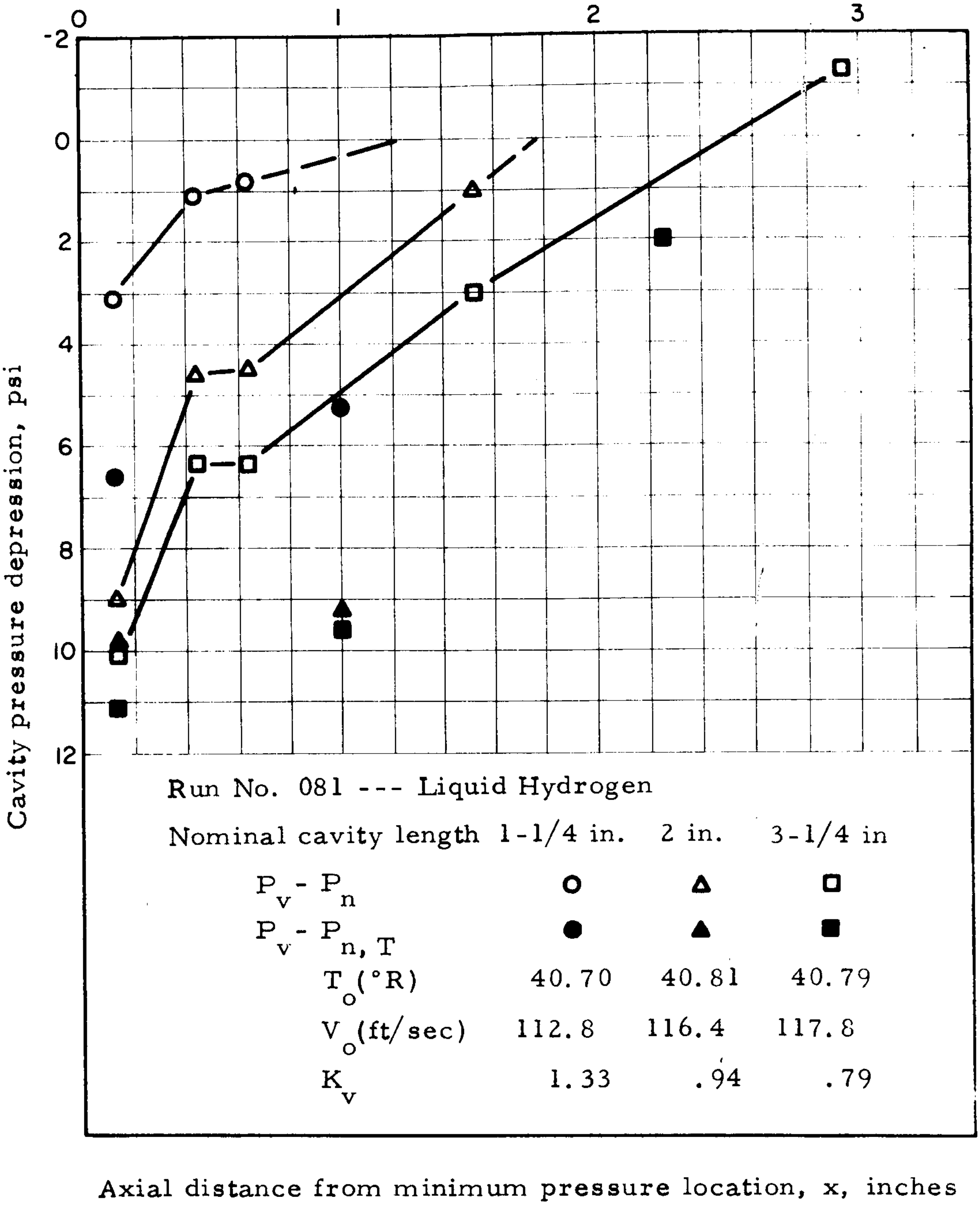

Figure 4.20 Pressure and temperature depressions within cavity in liquid hydrogen.

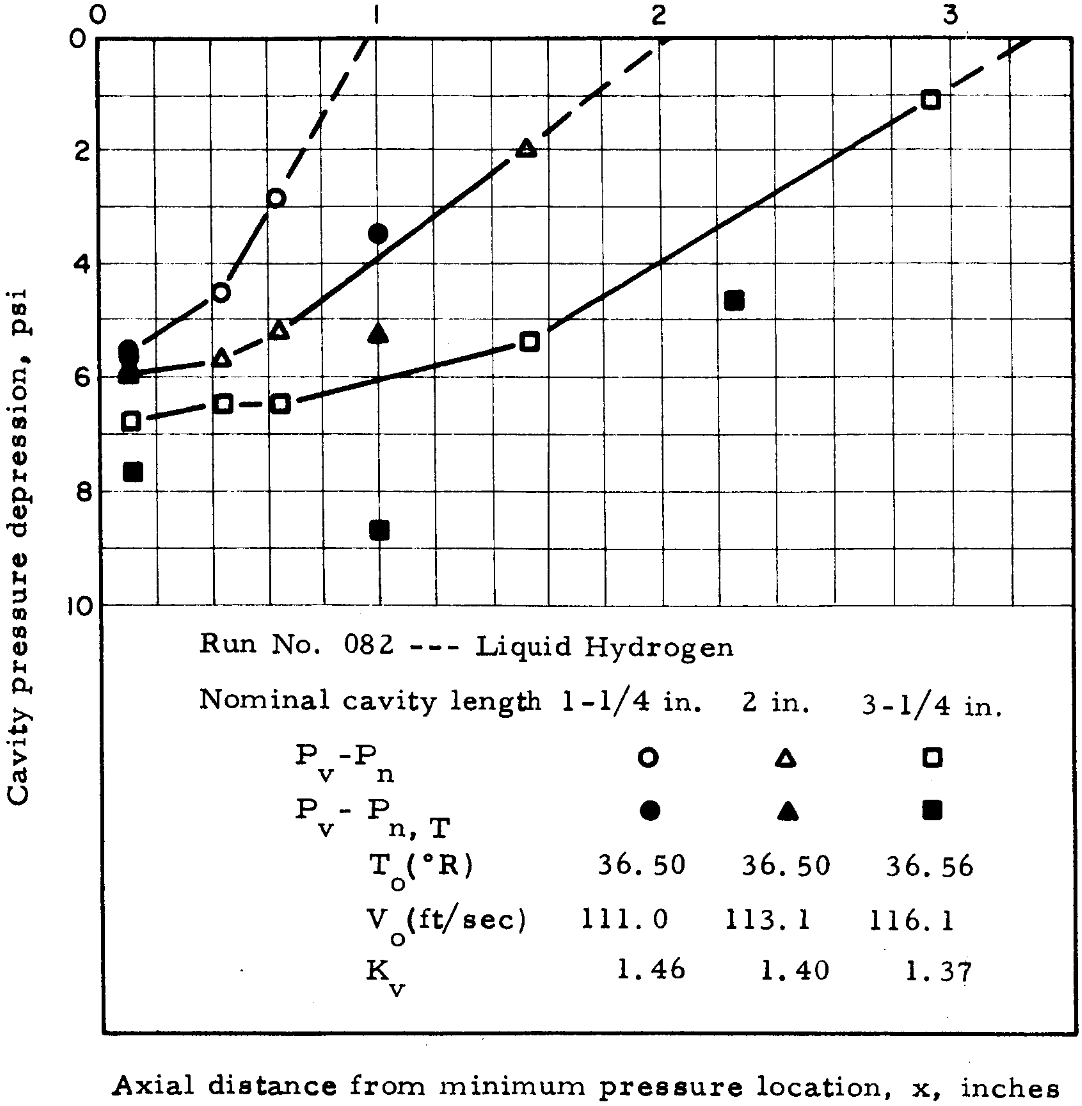

Figure 4.21 Pressure and temperature depressions within cavity in liquid hydrogen.

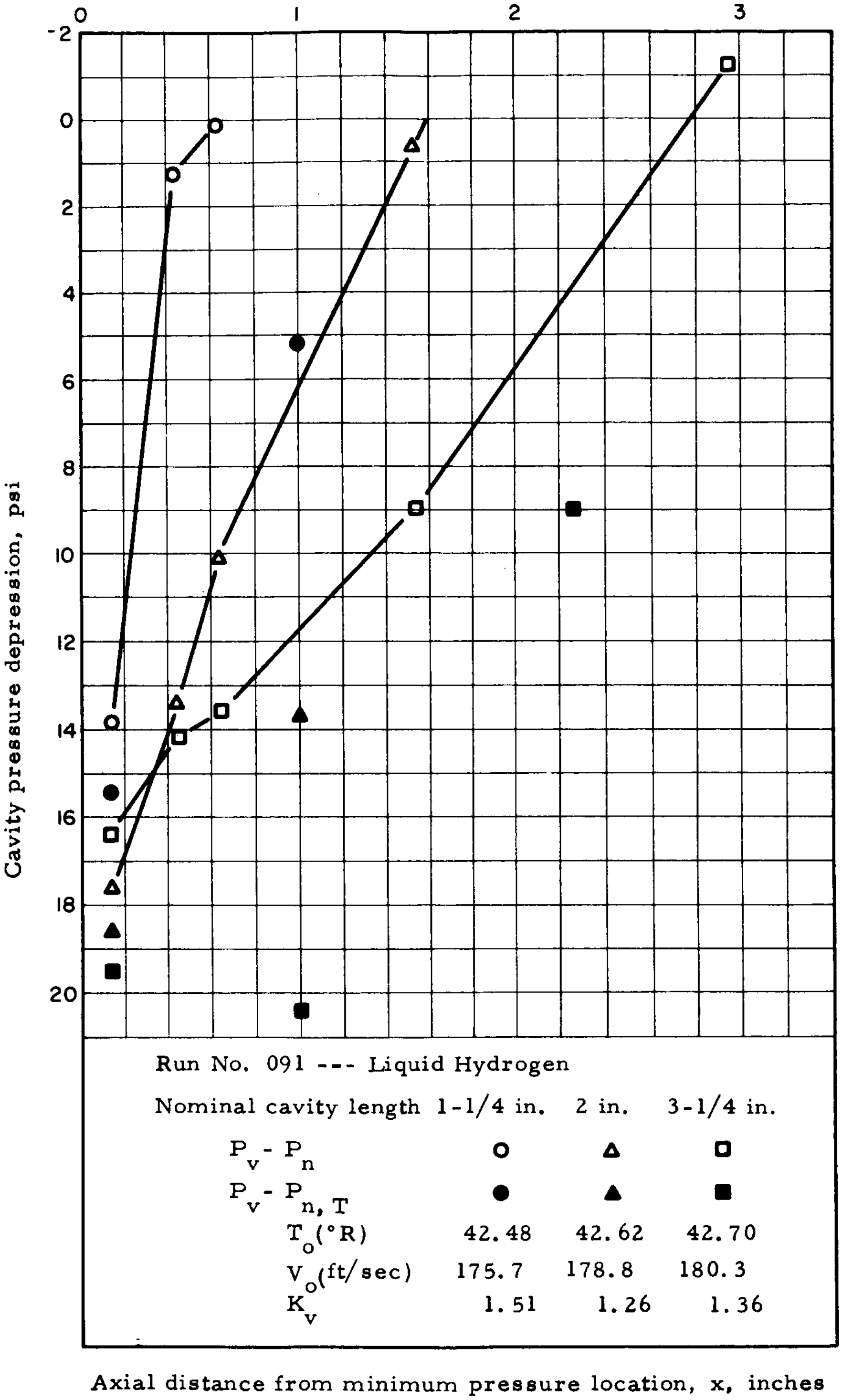

Figure 4.22 Pressure and temperature depressions within cavity in liquid hydrogen.

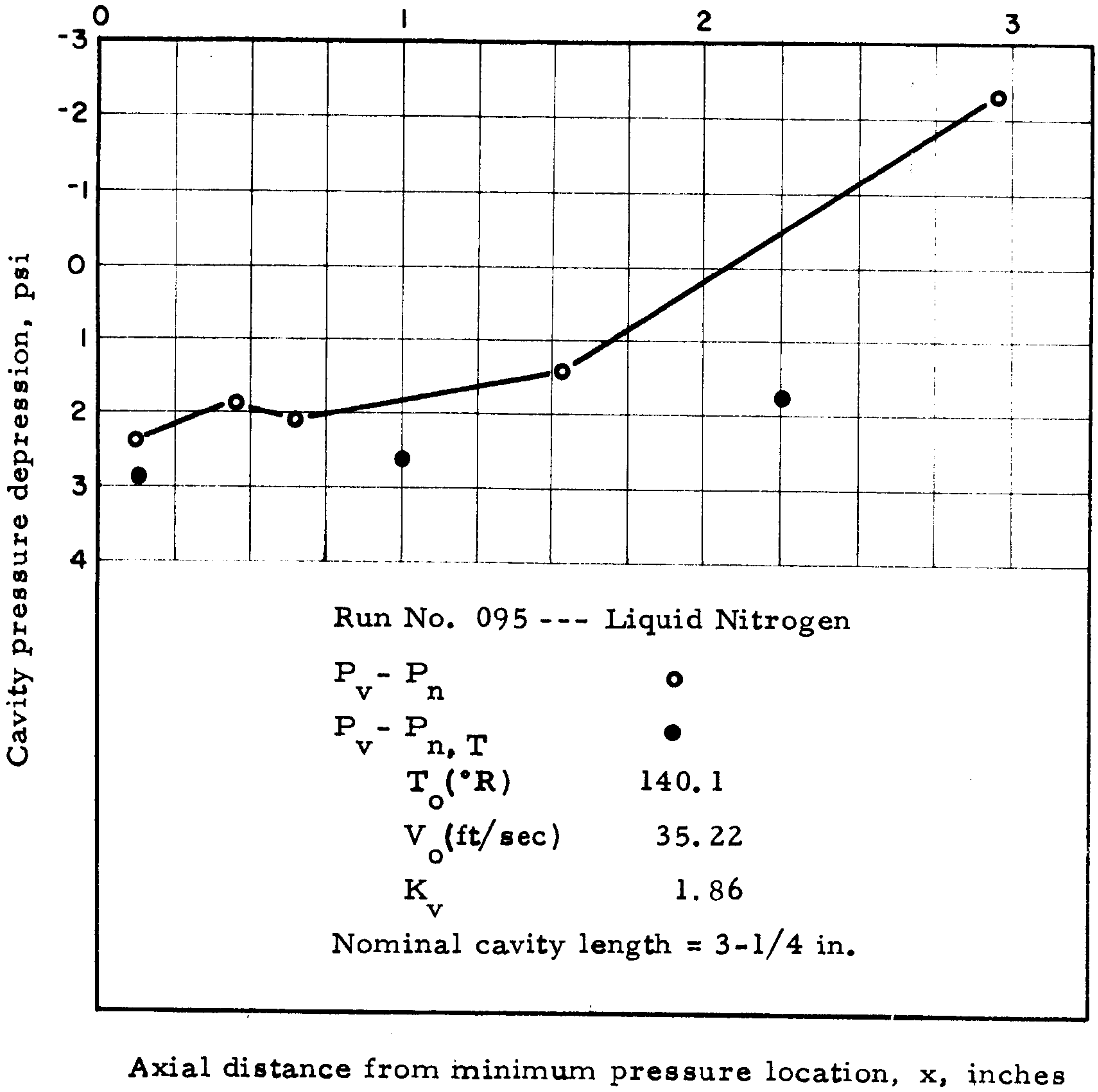

Figure 4.23 Pressure and temperature depressions within cavity in liquid nitrogen.

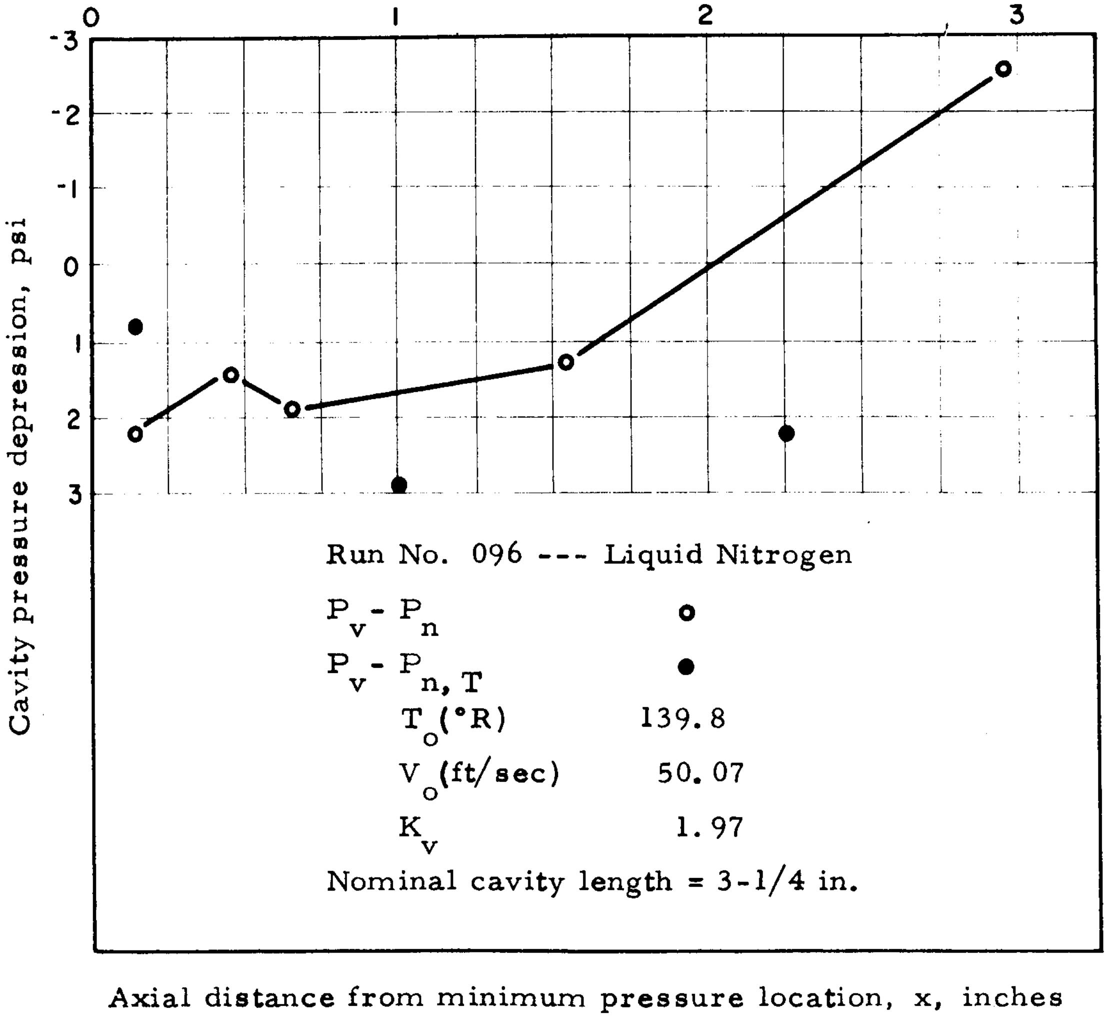

Figure 4.24 Pressure and temperature depressions within cavity in liquid nitrogen.

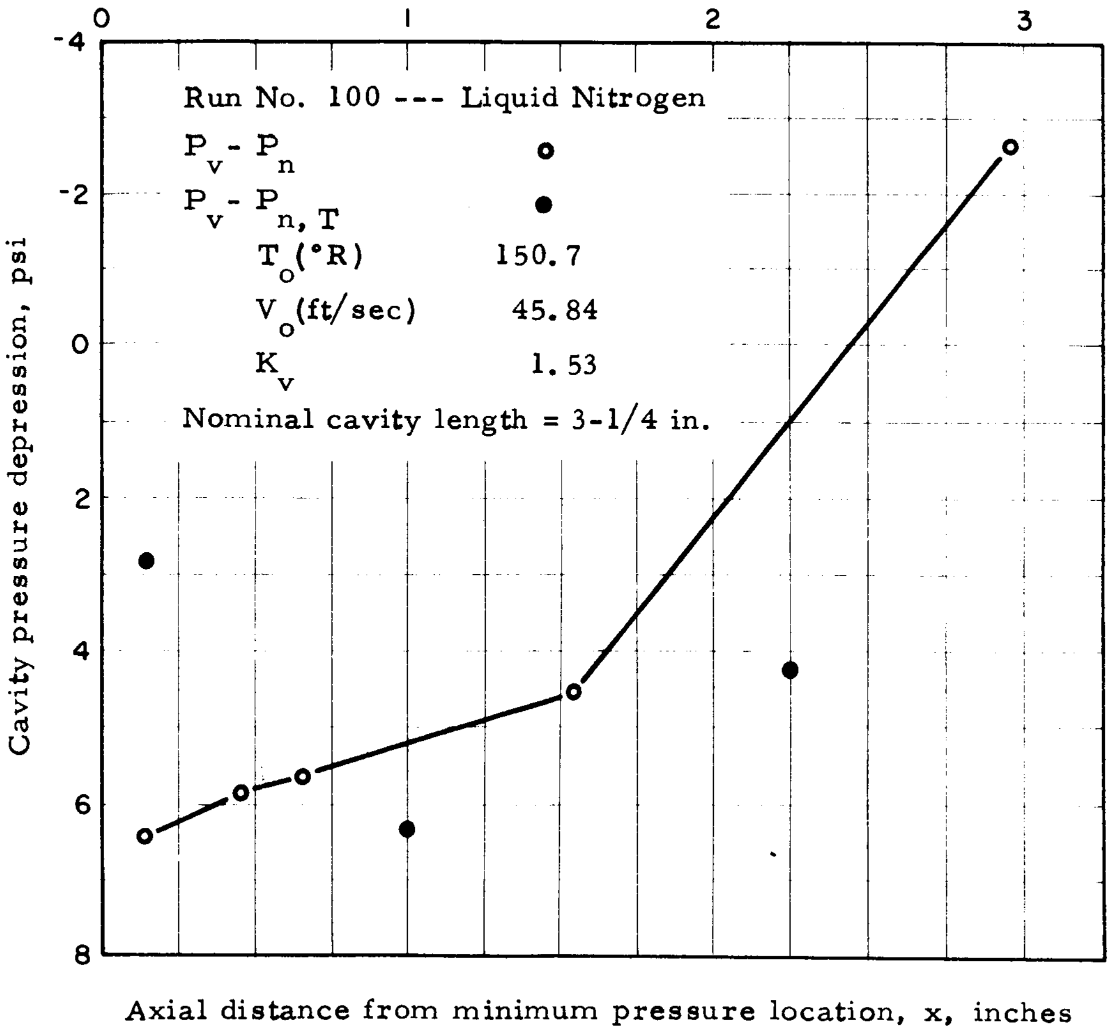

Figure 4.26 Pressure and temperature depressions within cavity in liquid nitrogen.

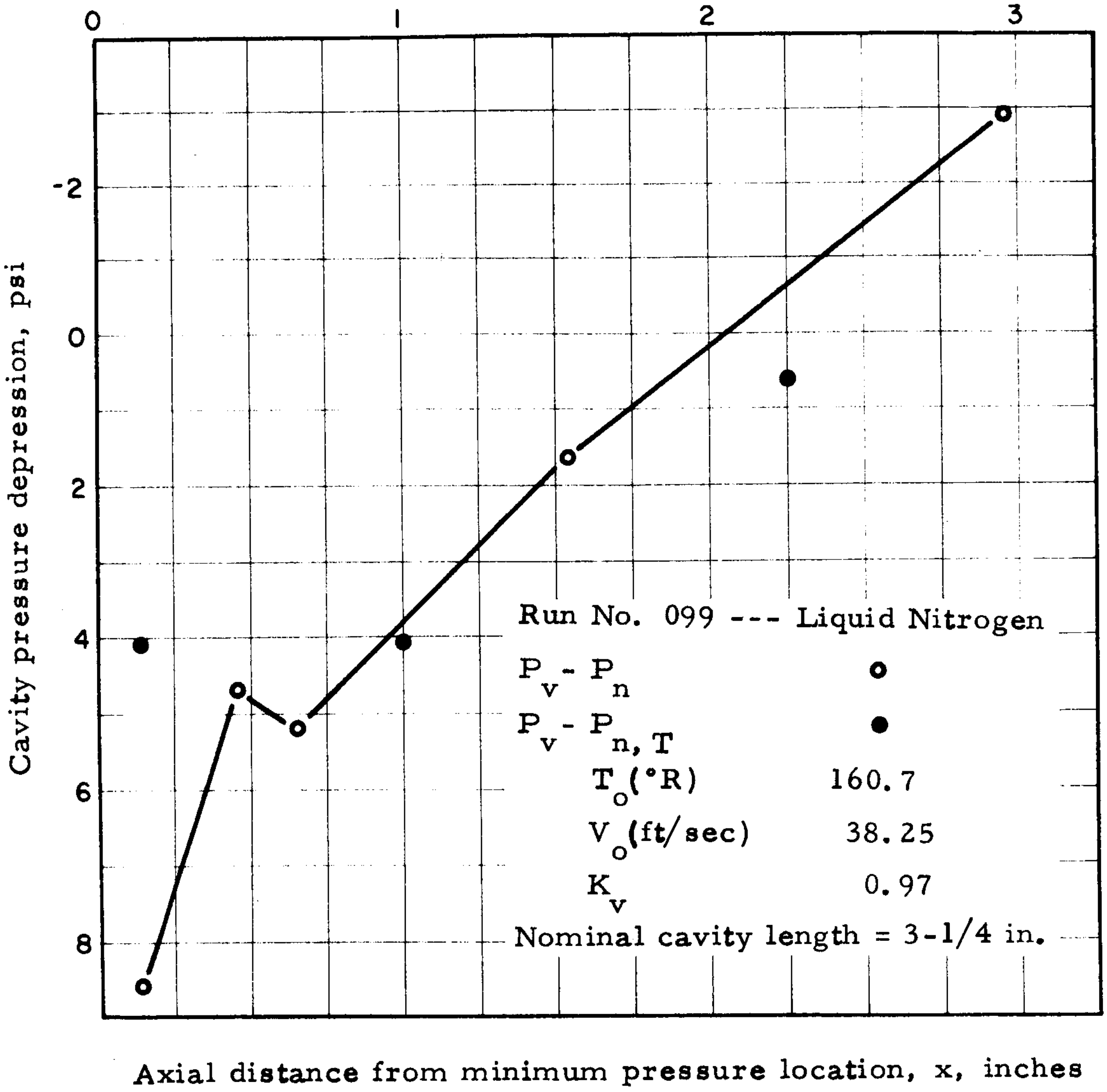

Figure 4.25 Pressure and temperature depressions within cavity in liquid nitrogen.

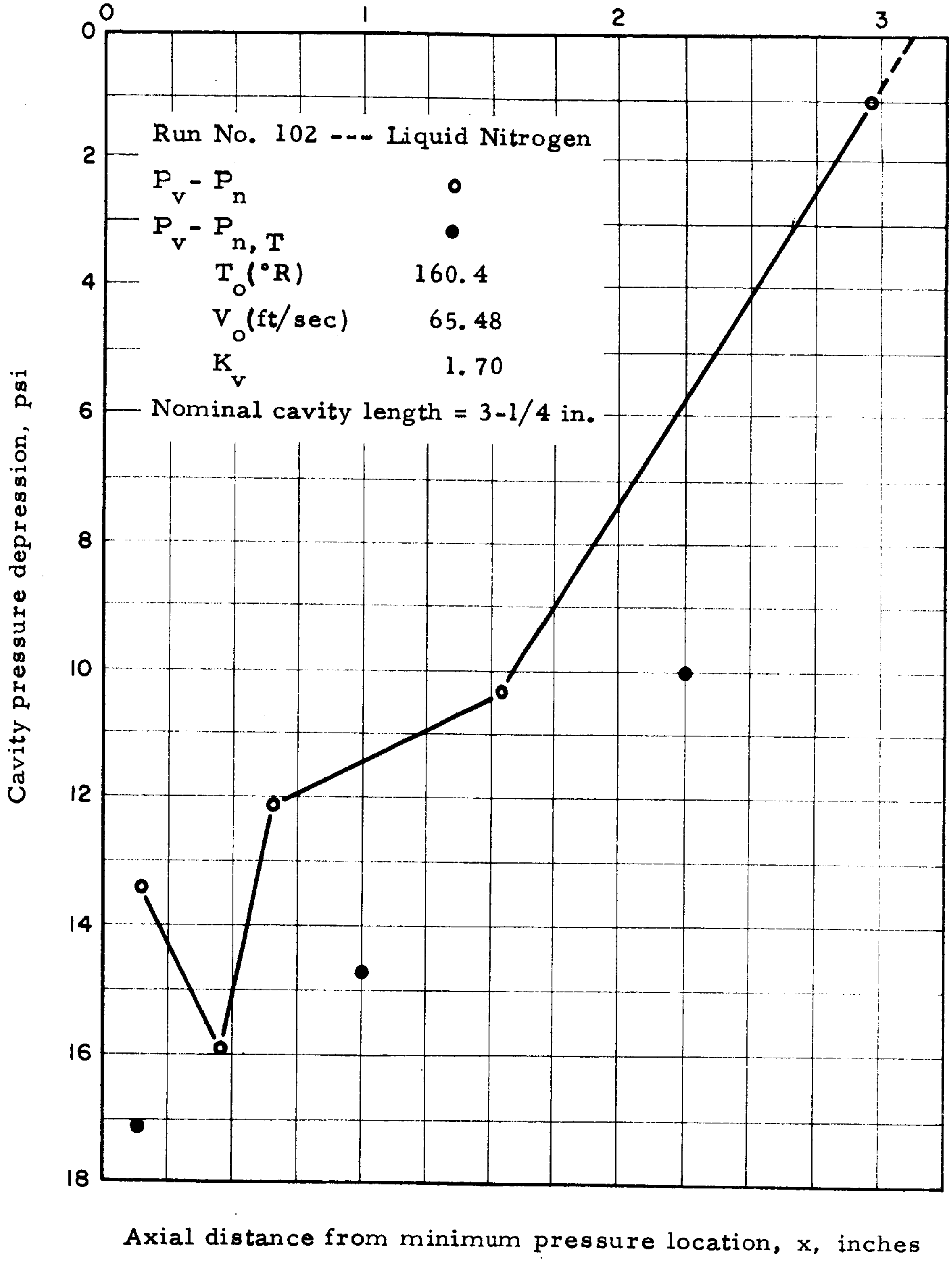

Figure 4.27 Pressure and temperature depressions within cavity in liquid nitrogen.

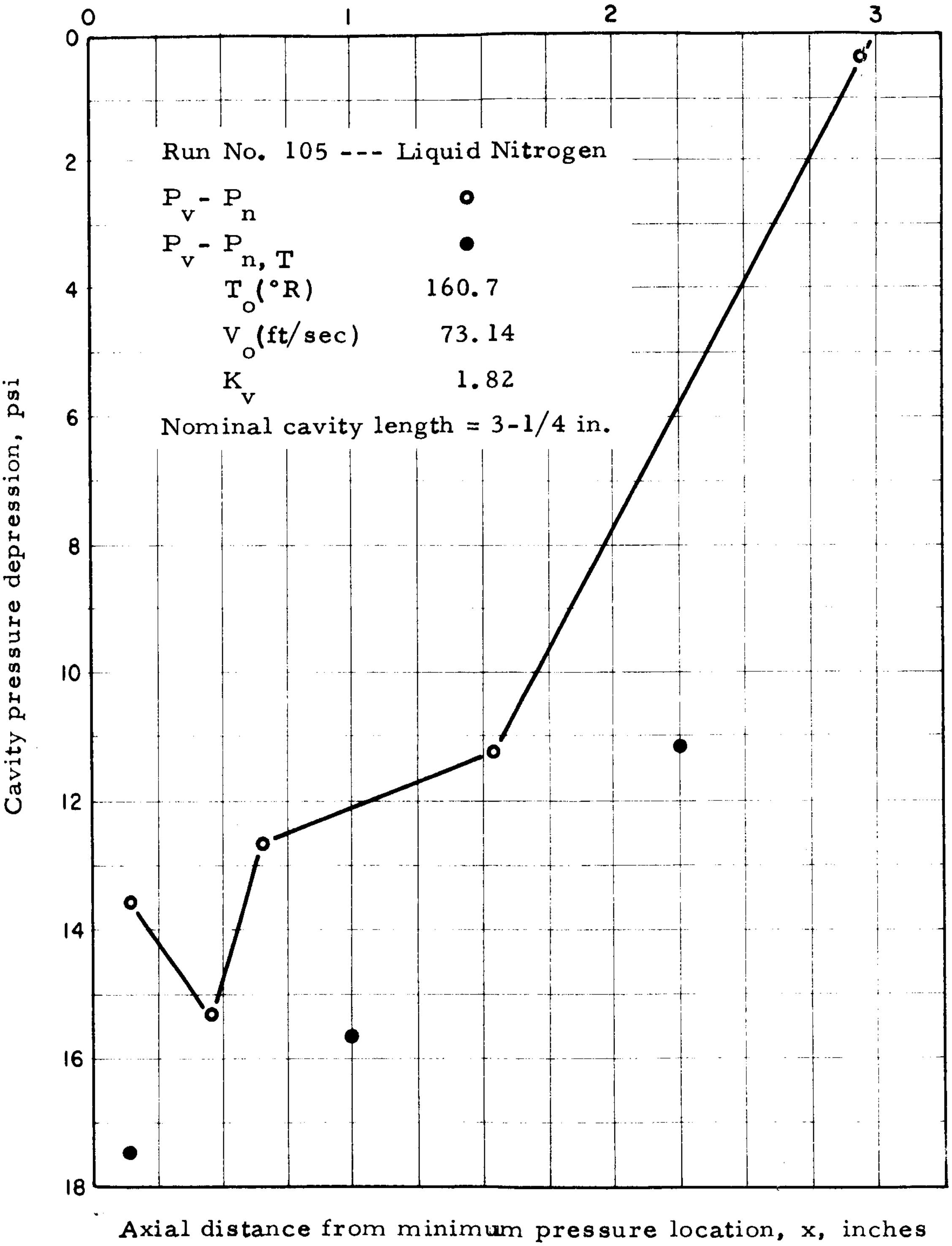

Figure 4.28 Pressure and temperature depressions within cavity in liquid nitrogen.

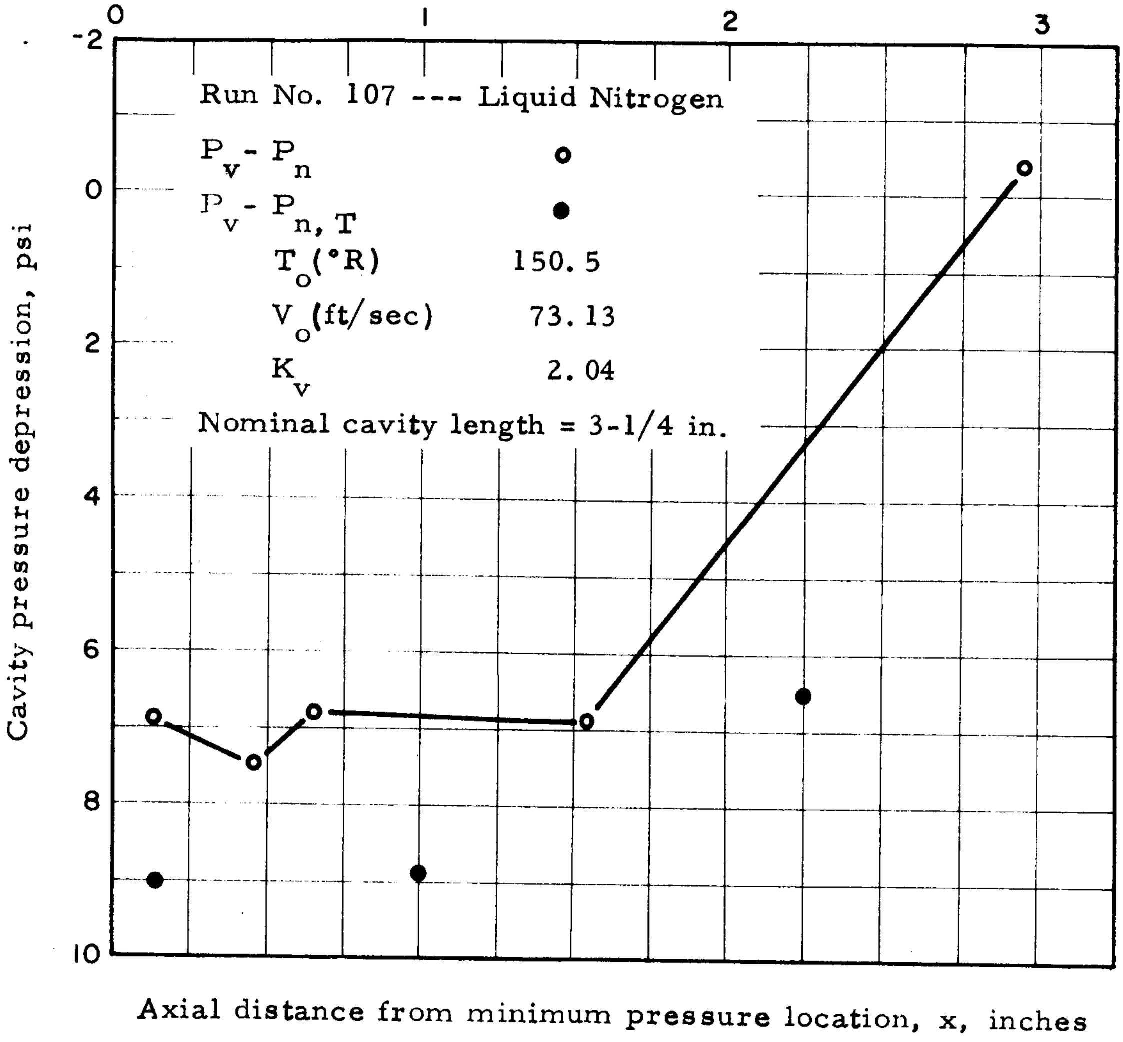

Figure 4.29 Pressure and temperature depressions within cavity in liquid nitrogen.

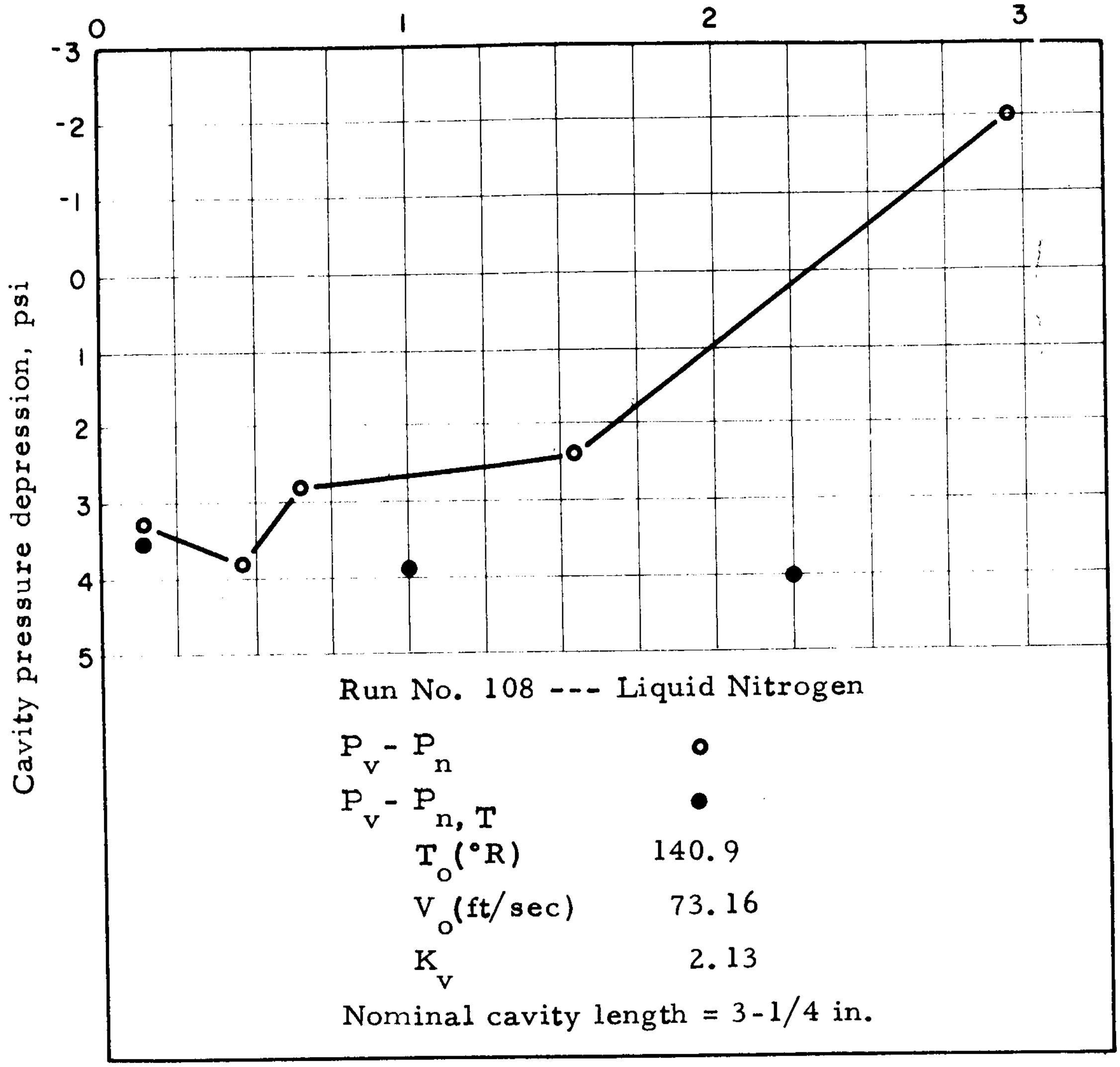

Axial distance from minimum pressure location, x, inches

Figure 4.30 Pressure and temperature depressions within cavity in liquid nitrogen.

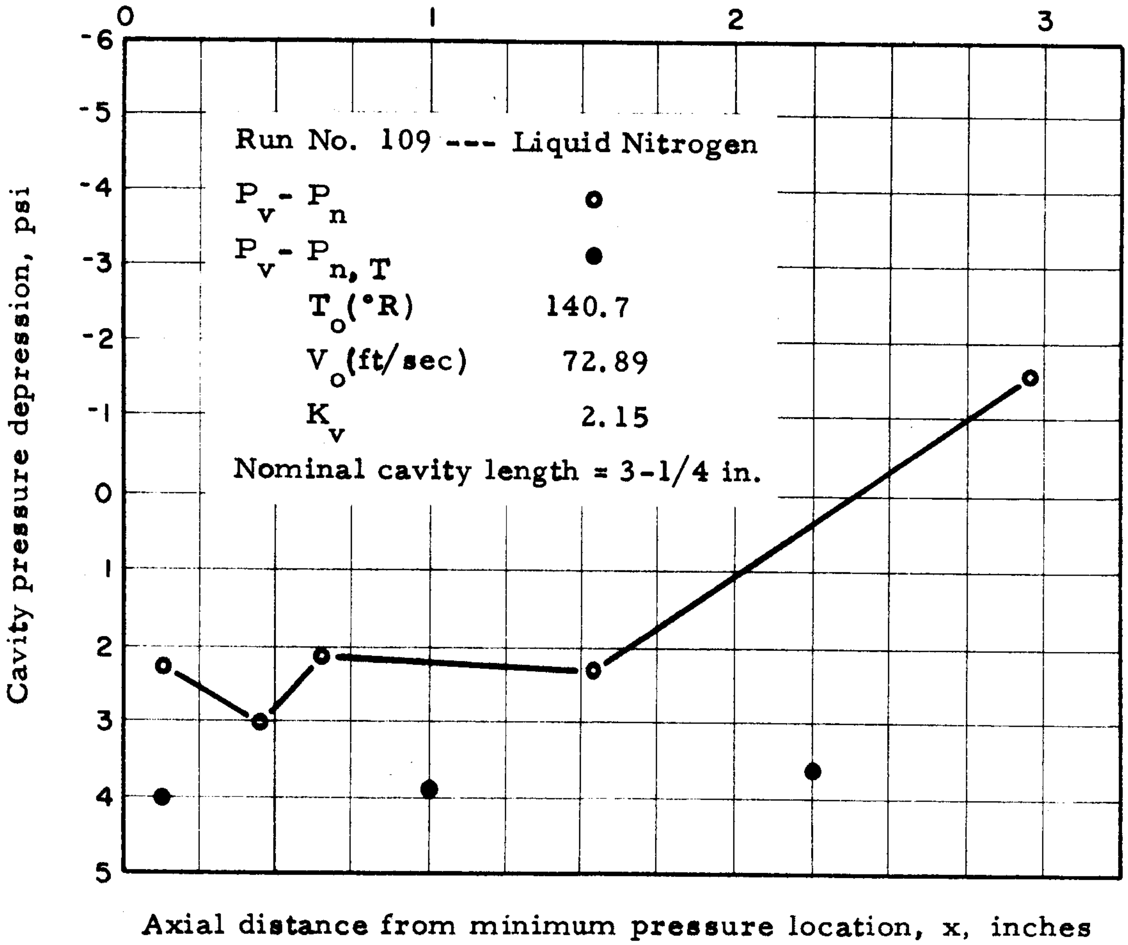

Figure 4.31 Pressure and temperature depressions within cavity in liquid nitrogen.

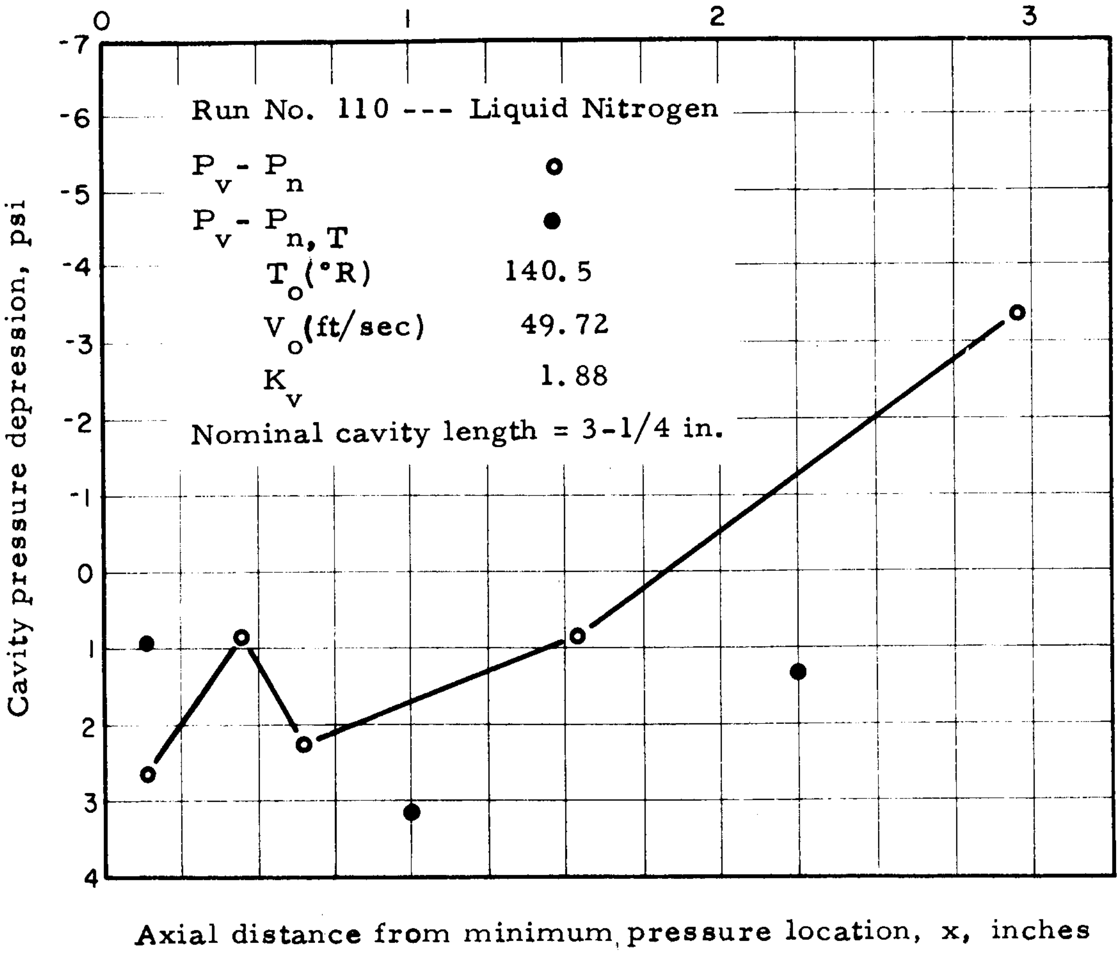

Figure 4.32 Pressure and temperature depressions within cavity in liquid nitrogen.

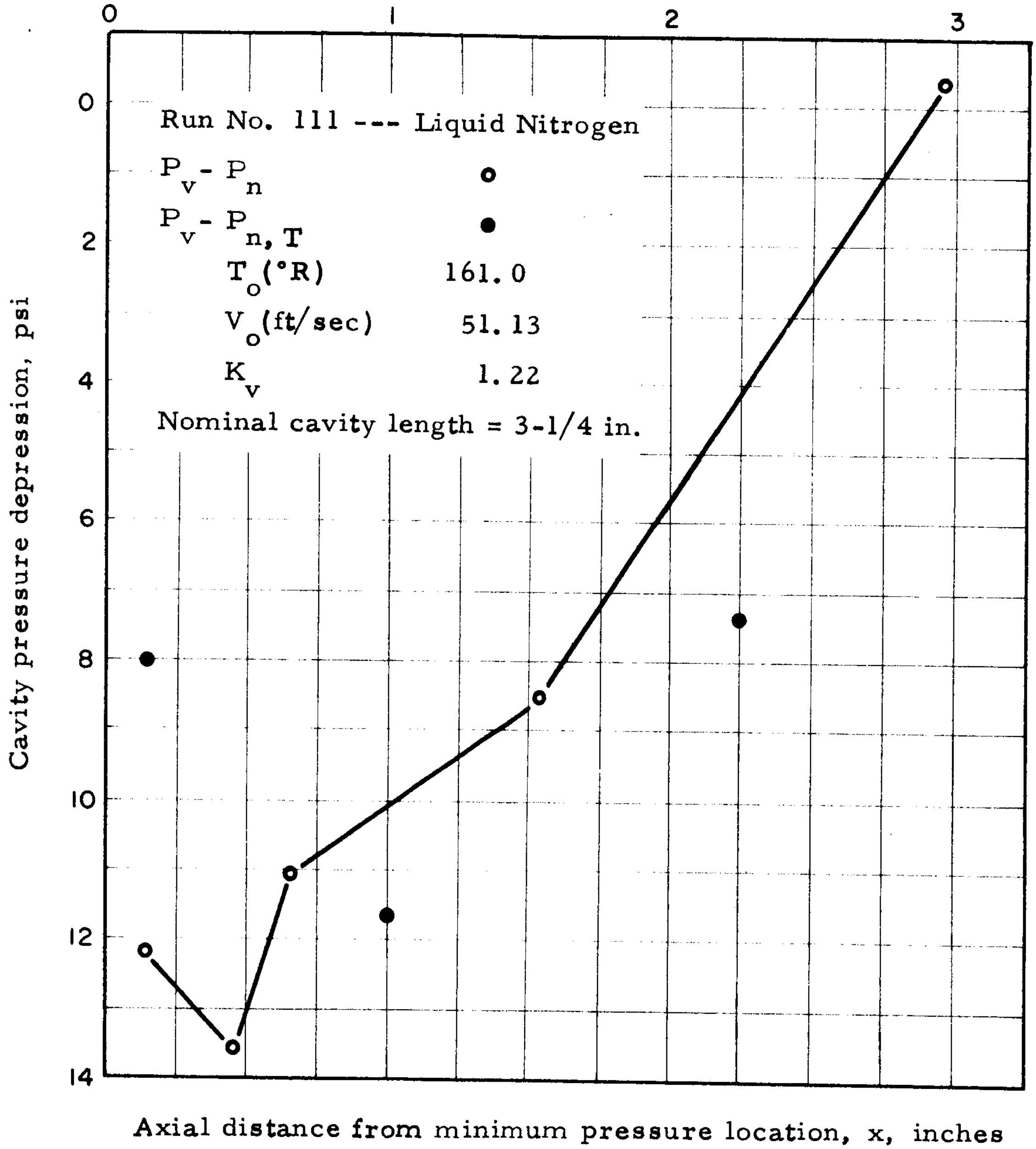

Figure 4.33 Pressure and temperature depressions within cavity in liquid nitrogen.

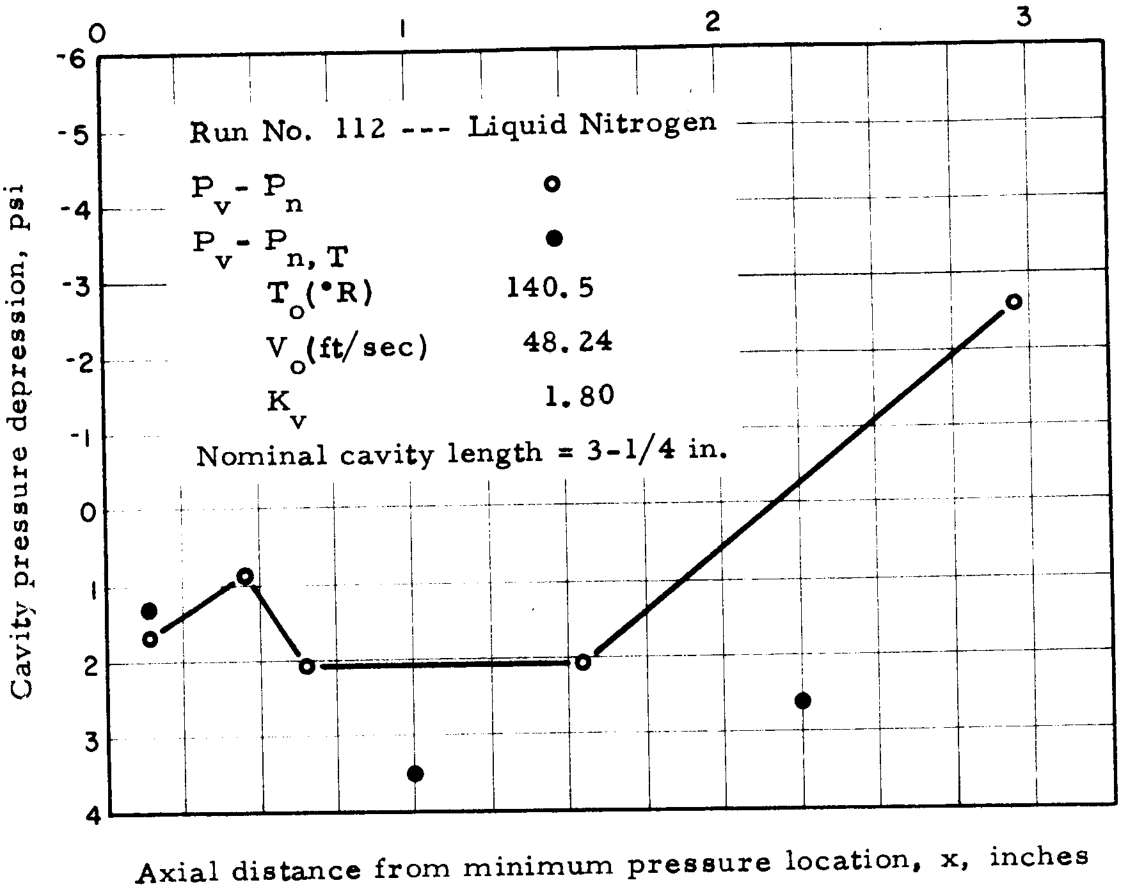

Figure 4.34 Pressure and temperature depressions within cavity in liquid nitrogen.

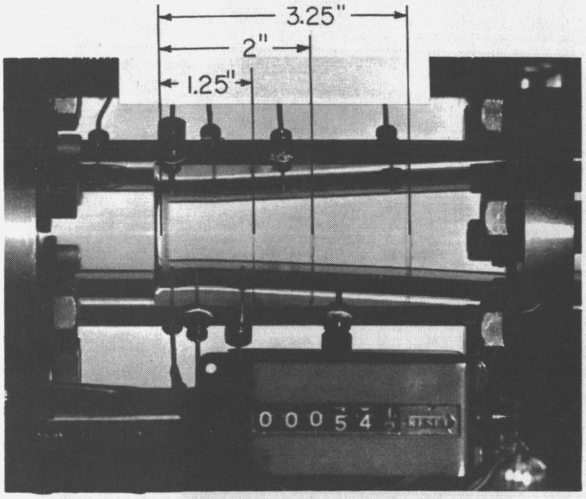

(.1): Typical incipient cavitation. Note scribe marks used to identify nominal cavity length.

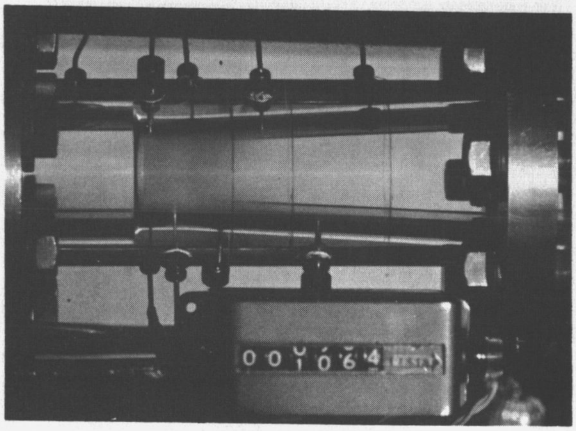

(.2): Nominal cavity length, 1-1/4 inch; V_o = 111 ft/sec, T_o = 36.50°R, P_o = 23.3 psia, K_v = 1.46.

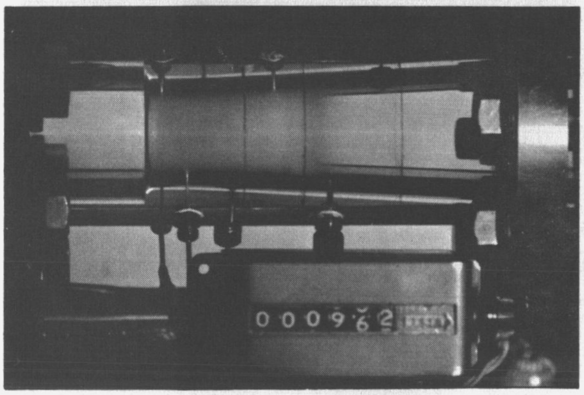

(.3): Nominal cavity length, 2 inch; V_o = 155 ft/sec, T_o = 36.79°R, P_o = 36.3 psia, K_v = 1.83.

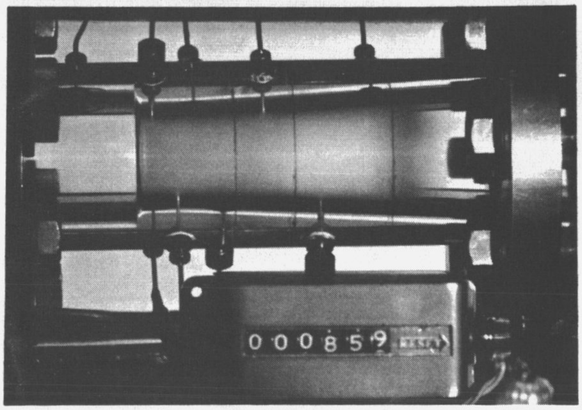

(.4): Nominal cavity length, 3-1/4 inch; V_o = 204.7 ft/sec, T_o = 40.97°R, P_o = 59.3 psia, K_v = 1.60.

Figure 4.35 Photographs showing typical appearance of developed cavities in liquid hydrogen.

B- 70407

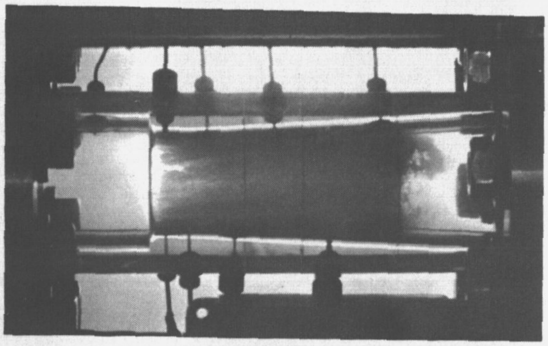

(.1): V_o = 35.22 ft/sec, T_o = 140.1°R, P_o = 15.55 psia, K_v = 1.86.

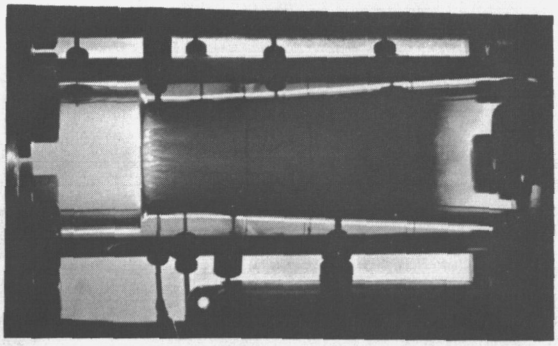

(.2): V_o = 72.89 ft/sec, T_o = 140.7°R, P_o = 16.20 psia, K_v = 2.15.

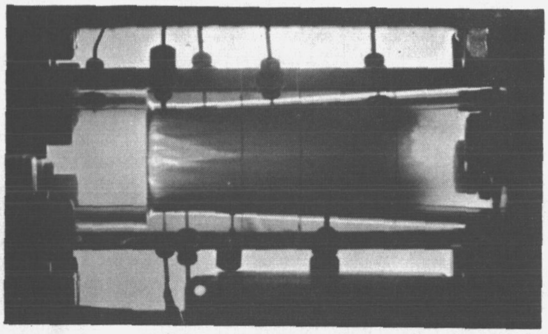

(.3): V_o = 45.84 ft/sec, T_o = 150.7°R, P_o = 29.25 psia, K_v = 1.53.

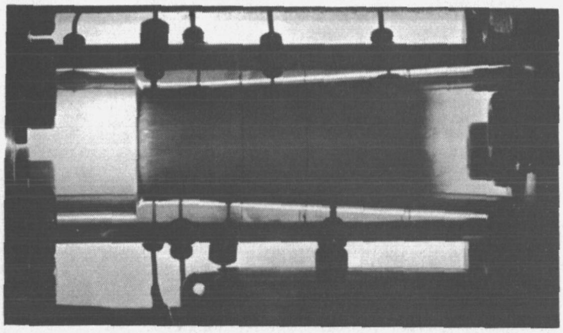

(.4): V_o = 73.13 ft/sec, T_o = 150.5°R, P_o = 28.90 psia, K_v = 2.04.

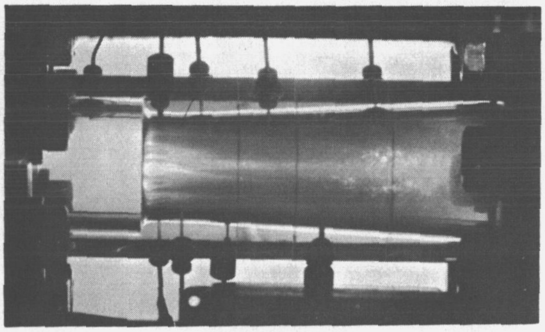

(.5): V_o = 38.25 ft/sec, T_o = 160.7°R, P_o = 49.20 psia, K_v = 0.97.

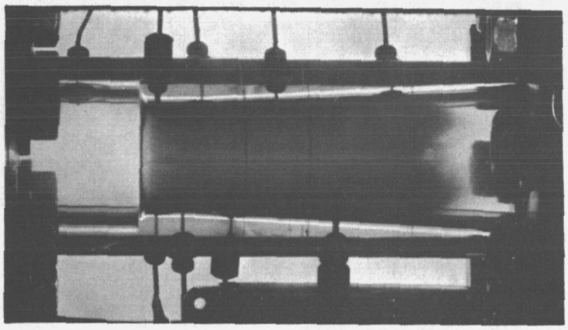

(.6): V_o = 74.14 ft/sec, T_o = 160.7°R, P_o = 48.95 psia, K_v = 1.82.

Figure 4.36 Photographs showing effects of velocity and temperature on the appearance of developed cavities in liquid nitrogen; nominal cavity length, 3-1/4 inch.

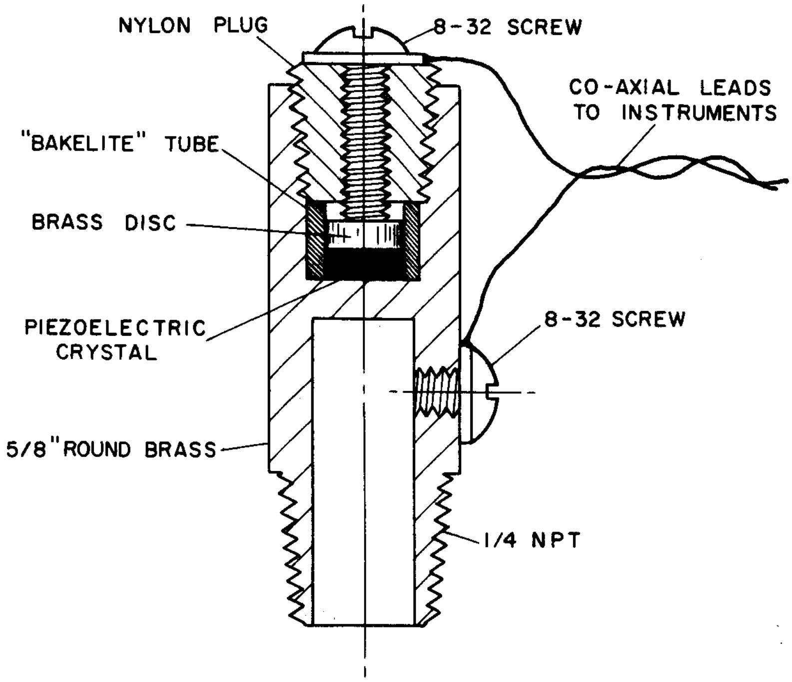

Figure 9. 1 Acoustic Transducer for Detection of Cavitation Inception.

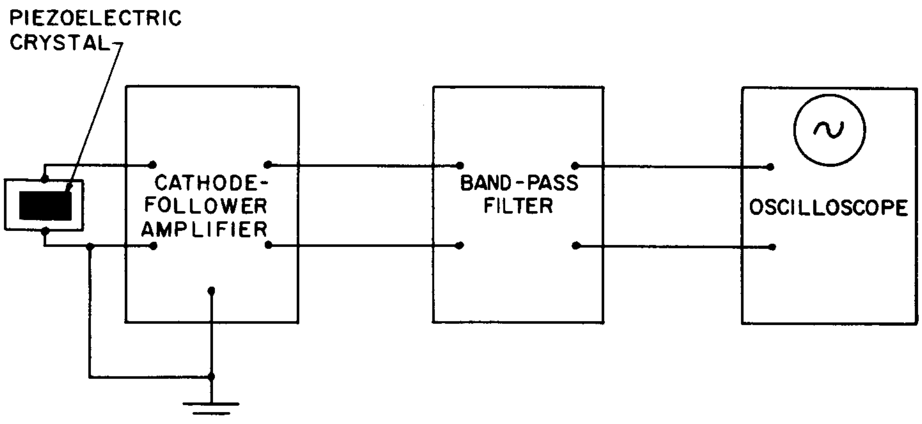

Figure 9. 2 Block Diagram of Signal Conditioning Instruments Used with Acoustic Cavitation Detection Device.

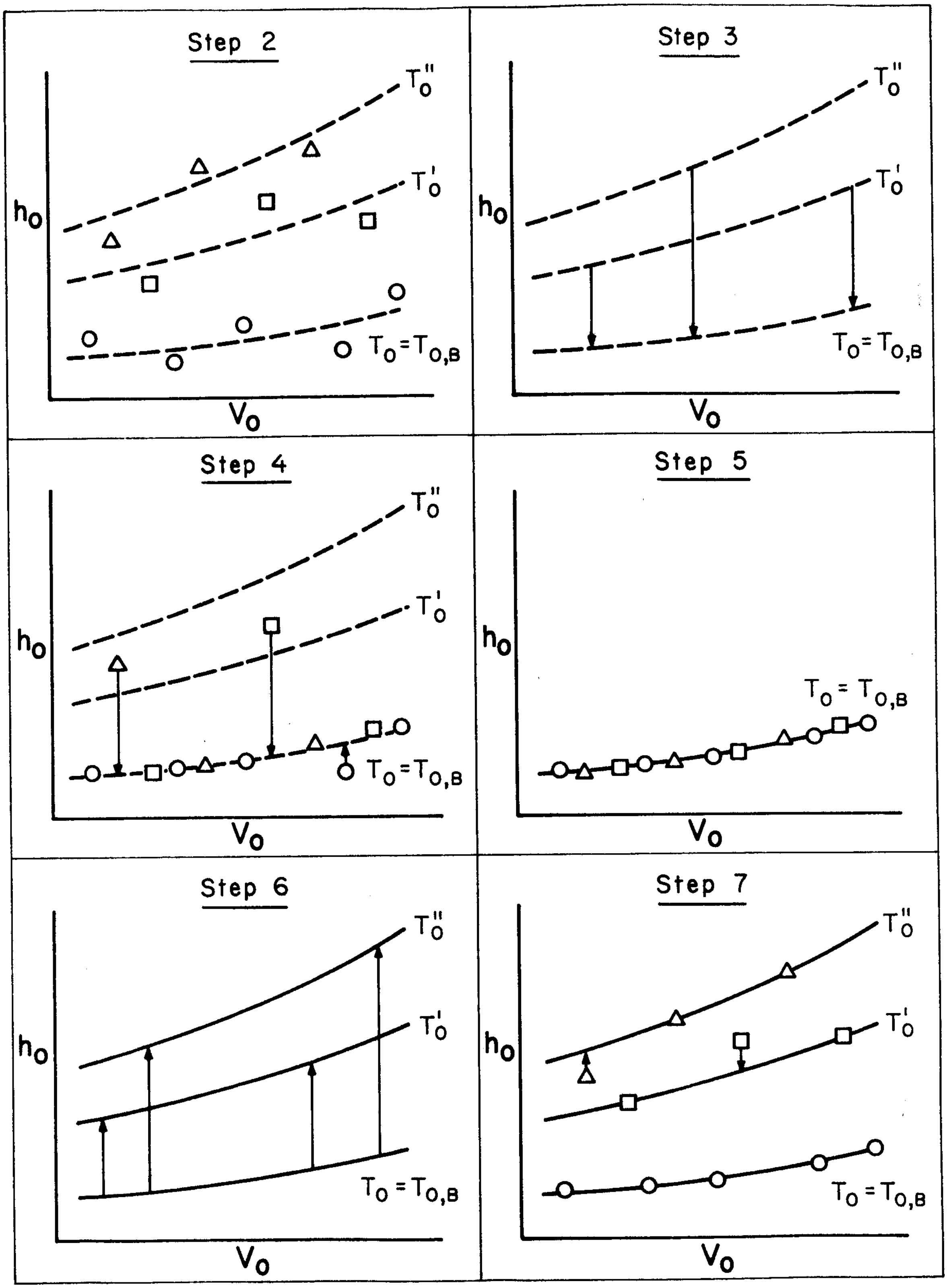

Figure 10.1 Illustration of Method Used to Construct Nominal Isotherms from Experimental Data.

Table 4.1 Cavitation Inception Data for Liquid Hydrogen

Run #	T_o (°R)	V_o (ft/sec)	$\dot{m}$ (lb_m/sec)	h_o (ft, abs)	P_o (psia)	h_v (ft, abs)	P_v (psia)	K_{iv}	$\check{h}$ (ft, abs)
R026A	36.47	73.6	2.623	614.6	18.87	478.9	14.70	1.61	333.8
R026B	36.77	72.4	2.572	606.1	18.56	505.0	15.45	1.24	334.6
R031A	36.63	132.1	4.713	1244.9	38.26	492.6	15.09	2.78	339.9
031C	36.59	133.1	4.750	1228.0	37.76	488.0	14.95	2.69	309.3
R032	37.22	167.1	5.945	1756.2	53.81	548.1	16.70	2.79	308.1
R034	36.50	106.2	3.788	962.0	29.56	481.8	14.78	2.74	377.1
035	37.19	169.7	6.040	1755.0	53.81	538.0	16.40	2.72	261.5
R036	37.67	108.2	3.819	1062.0	32.36	585.0	17.75	2.62	454.9
R037	37.55	134.7	4.769	1362.6	41.56	573.7	17.43	2.80	421.7
R038	38.21	170.5	6.010	1822.0	56.36	638.4	19.27	2.62	309.8
R039	36.99	184.9	6.599	1973.5	60.66	524.0	16.00	2.73	200.5
040	37.40	185.6	6.600	2042.5	62.56	560.8	17.06	2.77	256.1
R040	37.55	183.3	6.511	2051.5	62.76	574.1	17.44	2.83	309.1
043A	37.03	180.6	6.440	1906.0	58.56	524.0	16.00	2.73	214.5
043B	36.97	180.0	6.420	1902.0	58.46	521.0	15.90	2.74	221.7
049	36.63	91.0	3.241	802.7	24.62	492.3	15.08	2.41	373.2
051	36.85	91.2	3.241	825.3	25.27	511.2	15.63	2.43	394.2
052	38.00	92.6	3.257	915.1	27.72	616.5	18.65	2.24	470.4
054	40.64	125.0	4.288	1577.3	46.62	931.6	27.45	2.66	767.6
056	40.79	154.3	5.298	1989.3	58.82	951.5	28.00	2.81	754.1
057	40.91	174.1	5.975	2303.9	68.12	969.0	28.47	2.84	732.9
058	40.88	124.3	4.254	1604.8	47.32	964.3	28.35	2.67	804.2
059	40.70	120.2	4.120	1507.4	44.52	939.1	27.66	2.54	758.8

Table 4.2 Cavitation Inception Data for Liquid Nitrogen

Run #	T_o (°R)	V_o (ft/sec)	$\dot{m}$ (lb_m/sec)	h_o (ft, abs)	P_o (psia)	h_v (ft, abs)	P_v (psia)	K_{iv}	$\check{h}$ (ft, abs)
005B	138.08	19.27	7.86	49.7	17.45	38.71	13.6	1.9	30.44
021RR	169.34	61.68	22.51	374.1	117.6	232.4	72.9	2.4	176.80
022RR	168.2	64.54	23.68	379.7	120.0	219.5	69.2	2.48	163.68
024RR	152.91	66.44	25.83	276.5	92.6	98.4	32.9	2.60	47.58
095	140.3	33.70	13.65	86.3	30.1	45.34	15.81	2.32	27.40
099	161.1	33.90	12.77	184.6	59.9	154.1	50.0	1.71	125.00
100	150.75	43.21	16.91	154.3	52.0	87.05	29.32	2.32	57.47
105	161.0	67.1	25.33	334.6	108.8	153.2	49.7	2.59	101.11
106A	166.45	65.45	24.18	368.6	117.3	201.8	64.08	2.51	164.45
106B	166.4	66.67	24.64	367.9	117.1	201.2	63.9	2.42	137.39
107	150.88	70.62	27.66	298.8	100.8	87.68	29.52	2.73	40.16
108	140.87	65.39	26.47	229.7	80.1	47.08	16.39	2.75	7.95
109	140.76	72.05	29.19	268.3	93.6	46.75	16.28	2.75	-.92
110	140.72	43.64	17.66	111.6	38.9	46.54	16.21	2.20	12.84
111A	161.15	49.92	18.81	240.1	77.9	154.5	50.15	2.21	110.86
111B	161.08	50.76	19.13	240.6	78.1	154.1	50.0	2.16	106.98
112	140.63	47.90	19.39	128.8	44.9	46.27	16.12	2.32	9.81

Table 4.3 Experimental Data Points Which Have Been Temperature Compensated by Means of Equation [10-3] for Hydrogen and Equation [10-4] for Nitrogen

Run #	Nominal Temp (°R)	h_o (ft, abs)	V_o (ft/sec)	Run #	Nominal Temp (°R)	h_o (ft, abs)	V_o (ft/sec)	Run #	Nominal Temp (°R)	h_o (ft, abs)	V_o (ft/sec)
					HYDROGEN						
R026A	36.5	616.3	73.6	R037	37.5	1357.9	134.7	051	36.5	801.9	91.2
R026B	36.5	590.3	72.4	R038	37.5	1742.5	170.5	052	37.5	875.1	92.6
R031A	36.5	1234.2	132.1	R039	36.5	1921.5	184.9	054	41.0	1623.8	125.0
031C	36.5	1220.6	133.1	040	37.5	2054	185.6	056	41.0	2019.2	154.3
R032	37.5	1785.9	167.1	R040	37.5	2045.8	183.3	057	41.0	2317.5	174.1
R034	36.5	962.0	106.2	043A	37.5	1957.9	180.6	058	41.0	1620.4	124.3
035	37.5	1788.1	169.7	043B	36.5	1853.1	180.0	059	41.0	1545.7	120.2
R036	37.5	1047.6	108.2	049	36.5	794.2	91.0				
					NITROGEN						
005B	140	54.84	19.27	100	150	150.73	43.21	109	140	266.06	72.05
021RR	170	380.48	61.68	105	160	327.51	67.10	110	140	109.52	43.64
022RR	170	396.79	64.54	106A	165	356.31	65.45	111A	160	231.88	49.92
024RR	150	262.13	66.44	106B	165	356.00	66.67	111B	160	232.93	50.76
095	140	85.41	33.70	107	150	294.63	70.62	112	140	126.97	47.90
099	160	176.82	33.90	108	140	227.20	65.39				

V_o (ft/sec)	h_o (ft, abs)	h_v (ft, abs)	K_{iv}	h_o (ft, abs)	h_v (ft, abs)	K_{iv}	h_o (ft, abs)	h_v (ft, abs)	K_{iv}
	Nominal Temp = 36.5°R			Nominal Temp = 37.5°R			Nominal Temp = 41.0°R		
70	581	481.77	1.30	643	569.25	0.97	952	981.82	--
80	681		2.00	747		1.79	1071		0.89
90	781		2.38	851		2.24	1189		1.65
100	885		2.59	959		2.51	1311		2.12
110	990		2.70	1068		2.65	1435		2.41
120	1099		2.76	1181		2.74	1562		2.59
130	1209		2.77	1296		2.77	1691		2.70
140	1324		2.77	1415		2.78	1825		2.77
150	1442		2.75	1537		2.77	1961		2.80
160	1564		2.72	1663		2.75	2101		2.82
170	1697		2.71	1800		2.74	2253		2.83
180	1849		2.72	1956		2.76	2423		2.86
185	1935	481.77	2.73	2044	569.25	2.77	2518	981.82	2.89

Table 4.4 Calculated Data Used to Construct Nominal Isotherms for Liquid Hydrogen Inception

Table 4.5 Calculated Data Used to Construct Nominal Isotherms for Liquid Nitrogen Inception

V_o (ft/sec)	h_o (ft, abs)	h_v (ft, abs)	K_{iv} --	h_o (ft, abs)	h_v (ft, abs)	K_{iv} --	h_o (ft, abs)	h_v (ft, abs)	K_{iv} --
	Nominal Temp = 140°R			Nominal Temp = 150°R			Nominal Temp = 160°R		
20	56.0	44.40	1.87	93.0	83.50	1.53	150.5	145.78	0.77
25	63.5		1.97	100.5		1.75	158.0		1.27
30	73.5		2.08	110.5		1.93	168.0		1.59
35	85.0		2.13	122.0		2.02	179.5		1.78
40	99.0		2.20	136.0		2.11	193.5		1.92
45	116.0		2.28	153.0		2.21	210.5		2.06
50	136.5		2.37	173.5		2.32	231.0		2.20
55	161.5		2.49	198.5		2.45	256.0		2.35
60	190.0		2.60	227.0		2.57	284.5		2.48
65	221.5		2.70	258.5		2.67	316.0		2.60
70	254.0	44.40	2.75	291.0	83.50	2.73	348.5	145.78	2.67
	Nominal Temp = 165°R			Nominal Temp = 170°R					
20	188.5	187.87	0.12	233.5	239.50	--			
25	196.0		0.85	241.0		0.18			
30	206.0		1.31	251.0		0.84			
35	217.5		1.56	262.5		1.22			
40	231.5		1.74	276.5		1.50			
45	248.5		1.93	293.5		1.72			
50	269.0		2.09	314.0		1.92			
55	294.0		2.26	339.0		2.12			
60	322.5		2.41	367.5		2.29			
65	354.0		2.53	399.0		2.43			
70	386.5	187.87	2.61	431.5	239.50	2.53			

Table 4.6 Experimental thermodynamic data for liquid hydrogen

Run #	Cavity Length (inches)	T_o (°R)	V_o (ft/sec)	P_o (psia)	P_v (psia)	P_2 (psia)	P_4 (psia)	P_5 (psia)	P_7 (psia)	P_9 (psia)	$P_{2,T}$ (psia)	$P_{6,T}$ (psia)	$P_{8,T}$ (psia)	K_v
	1-1/4	36.91	151.4	35.97	15.80	9.42	9.82	10.57	-	-	10.10	12.26	-	1.85
066	2	37.09	152.9	35.57	16.25	8.67	9.2	9.35	13.52	-	8.78	9.83	-	1.74
	3-1/4	37.11	152.8	35.12	16.30	8.22	8.77	8.57	10.04	-	8.36	7.81	10.38	1.70
	1-1/4	38.66	128.7	30.97	20.62	12.37	13.37	15.32	-	-	11.82	14.07	-	1.34
067	2	38.74	127.1	30.77	20.82	11.97	12.67	13.77	19.37	-	11.42	12.53	-	1.32
	3-1/4	38.84	130.5	30.57	21.20	11.57	11.97	12.52	14.37	21.57	10.68	10.71	15.85	1.18
	1-1/4	40.59	139.7	39.57	27.42	18.02	23.37	24.52	-	-	14.28	19.63	-	1.39
068	2	40.62	144.1	38.67	27.37	15.27	16.17	17.72	23.59	-	12.57	14.50	-	1.19
	3-1/4	41.04	144.8	38.67	28.95	15.37	15.72	16.47	18.49	-	11.97	14.51	22.20	1.02
	1-1/4	37.53	196.8	54.20	17.38	9.40	9.40	11.20	-	-	9.54	12.61	-	2.00
069	2	37.66	199.4	54.40	17.72	8.30	8.20	8.90	12.90	-	8.27	8.13	-	1.95
	3-1/4	37.54	204.0	56.80	17.37	7.80	8.20	8.90	8.30	-	7.08	5.60	11.63	2.17
	1-1/4	38.62	195.6	54.40	20.50	11.40	11.90	14.70	-	-	9.80	10.26	-	1.89
070	2	38.64	197.4	54.90	20.55	11.00	11.10	11.60	19.40	-	9.39	8.10	-	1.88
	3-1/4	38.43	195.8	54.20	19.90	9.90	10.00	9.40	11.10	22.00	7.92	5.33	12.17	1.90
	1-1/4	40.79	190.4	54.80	28.00	14.80	17.10	22.80	-	-	12.53	22.74	-	1.61
071	2	40.70	189.4	53.80	27.65	14.00	15.10	16.00	25.90	-	11.38	14.42	-	1.59
	3-1/4	40.68	189.7	52.70	27.60	12.80	13.60	13.80	15.80	31.40	10.68	9.52	20.83	1.52
	1-1/4	37.65	196.2	53.80	17.72	10.00	10.00	11.20	-	-	7.40	12.20	-	1.98
073	2	37.58	197.2	53.90	17.52	9.00	8.90	9.20	13.20	-	4.30	7.48	-	1.97
	3-1/4	37.53	199.2	54.35	17.37	8.85	9.05	9.05	8.75	18.10	3.50	3.17	7.70	1.96
	1-1/4	40.86	202.9	59.30	28.27	13.80	14.60	16.80	-	-	10.62	16.59	-	1.64
075	2	40.70	202.8	59.30	27.65	13.20	14.00	14.60	26.60	-	9.88	11.57	-	1.68
	3-1/4	40.97	204.7	59.30	28.68	12.30	13.50	13.55	14.85	30.40	9.68	8.33	17.58	1.60

Table 4.6 (Continued)

Run #	Cavity Length (inches)	T_o (°R)	V_o (ft/sec)	P_o (psia)	P_v (psia)	P_2 (psia)	P_4 (psia)	P_5 (psia)	P_7 (psia)	P_9 (psia)	$P_{2,T}$ (psia)	$P_{6,T}$ (psia)	$P_{8,T}$ (psia)	K_v
	1-1/4	38.54	197.6	55.80	20.27	10.30	10.70	12.55	-	-	8.56	10.86	-	1.93
076	2	38.54	198.4	55.40	20.22	9.40	10.00	10.80	16.65	-	8.13	8.40	-	1.90
	3-1/4	38.93	201.1	56.30	21.50	9.20	10.00	10.50	10.00	19.45	8.55	7.40	12.28	1.84
	1-1/4	38.84	139.2	34.80	21.20	12.80	15.10	18.70	-	-	11.09	15.04	-	1.51
078	2	38.79	141.2	34.60	21.00	11.80	12.60	13.80	21.85	-	9.58	10.86	-	1.45
	3-1/4	39.74	143.8	34.50	24.22	11.20	11.70	12.10	14.10	21.25	10.73	10.20	16.00	1.08
	1-1/4	37.10	155.4	37.10	16.26	9.10	10.85	13.80	-	-	8.80	10.35	-	1.81
079	2	36.79	155.0	36.30	15.50	8.30	9.10	9.30	14.55	-	7.08	9.82	-	1.83
	3-1/4	37.22	153.9	35.30	16.60	8.00	8.60	8.55	9.50	13.60	7.38	6.18	10.42	1.67
	1-1/4	40.82	147.4	41.50	28.15	17.00	23.70	25.20	-	-	16.76	22.42	-	1.36
080	2	40.88	151.6	40.70	28.30	15.20	16.95	18.70	26.95	-	14.58	16.90	-	1.18
	3-1/4	40.97	153.2	40.40	28.68	13.90	14.90	15.50	18.60	27.35	12.93	13.15	20.94	1.11
	1-1/4	40.70	112.8	35.30	27.65	24.55	26.50	26.80	-	-	21.00	22.37	-	1.33
081	2	40.81	116.4	33.80	28.15	19.10	23.55	23.60	27.10	-	18.18	18.93	-	.94
	3-1/4	40.79	117.8	32.80	28.00	17.90	21.55	21.60	25.05	29.30	16.77	18.42	25.95	.79
	1-1/4	36.50	111.0	23.30	14.77	9.20	10.20	11.90	-	-	9.05	21.26	-	1.46
082	2	36.50	113.1	23.30	14.77	8.80	9.05	9.50	12.80	-	8.77	9.48	-	1.40
	3-1/4	36.56	116.1	23.60	14.90	8.10	8.30	8.30	9.40	13.75	7.18	6.17	10.17	1.37
	1-1/4	42.48	175.7	56.06	34.95	21.06	33.66	34.86	-	-	19.47	29.71	-	1.51
091	2	42.62	178.8	53.96	35.60	17.96	22.16	25.46	36.26	-	16.91	21.83	-	1.26
	3-1/4	42.70	180.3	55.99	35.95	19.49	21.80	22.30	26.89	37.16	16.35	15.53	26.93	1.36

Table 4.6 (Continued)

Run #	Cavity length (inches)	h_o (ft, abs)	h_v (ft, abs)	h_2 (ft, abs)	h_4 (ft, abs)	h_5 (ft, abs)	h_7 (ft, abs)	h_9 (ft, abs)	$h_{2,T}$ (ft, abs)	$h_{6,T}$ (ft, abs)	$h_{8,T}$ (ft, abs)	T_2 (°R)	T_6 (°R)	T_8 (°R)
	1-1/4	1173.8	514	300.5	314	337	-	-	322	398	-	34.33	35.42	-
066	2	1162.8	532	276	293	298	438	-	282	316	-	33.55	34.20	-
	3-1/4	1148.3	531	261	278	272	321	-	269	253	333	33.30	32.94	34.49
	1-1/4	1028.8	684	399	433	501	-	-	380	457	-	35.23	36.22	-
067	2	1022.6	692	386	410	447	642	-	368	407	-	35.03	35.55	-
	3-1/4	1017.1	705	369	386	406	467	719	344	345	517	34.65	34.67	36.94
	1-1/4	1339.7	920	593	784	826	-	-	464	652	-	36.31	38.34	-
068	2	1310.1	925	494	530	584	792	-	408	472	-	35.57	36.40	-
	3-1/4	1315.9	985	497	514	540	611	-	387	472	742	35.30	36.40	39.15
	1-1/4	1773.7	570	300	300	360	-	-	314	409	-	34.00	35.59	-
069	2	1782.1	581	264	260	284	418	-	266	262	-	33.25	33.16	-
	3-1/4	1858.4	570	247	261	284	264	-	226	176	376	32.44	31.30	35.14
	1-1/4	1798.8	677	367	384	479	-	-	312	328	-	34.15	34.42	-
070	2	1816.9	682	351	357	373	642	-	300	261	-	33.91	33.14	-
	3-1/4	1789.9	657	317	320	300	357	735	255	205	395	33.01	31.99	35.39
	1-1/4	1854.6	946	477	562	763	-	-	402	761	-	35.55	39.31	-
071	2	1819.1	932	451	493	523	875	-	368	470	-	35.01	36.36	-
	3-1/4	1782.0	932	410	441	450	517		344	304	693	34.65	33.98	38.74
	1-1/4	1762.6	582	321	320	360	-	-	235	396	-	32.67	35.41	-
073	2	1765.1	576	287	284	294	427	-	133	241	-	30.15	32.72	-
	3-1/4	1779.0	570	282	289	289	279	597	108	97	395	29.29	28.84	32.87
	1-1/4	2006.9	958	437	475	552	-	-	341	544	-	34.61	37.22	-
075	2	2003.4	932	424	455	475	900	-	315	374	-	34.18	35.10	-
	3-1/4	2009.7	970	392	438	440	484	1039	309	268	580	34.07	33.28	37.60

Table 4.6 (Continued)

Run #	Cavity Length (inches)	h_o (ft, abs)	h_v (ft, abs)	h_2 (ft, abs)	h_4 (ft, abs)	h_5 (ft, abs)	h_7 (ft, abs)	h_9 (ft, abs)	$h_{2,T}$ (ft, abs)	$h_{6,T}$ (ft, abs)	$h_{8,T}$ (ft, abs)	T_2 (°R)	T_6 (°R)	T_8 (°R)
	1-1/4	1843.2	670	330	344	406	-	-	272	350	-	33.43	34.74	-
076	2	1830.2	671	300	321	347	546	-	262	270	-	33.16	33.32	-
	3-1/4	1867.5	715	294	321	337	321	644	275	238	400	33.43	32.67	35.44
	1-1/4	1157.0	703	411	492	618	-	-	357	317	-	34.87	36.61	-
078	2	1149.8	700	376	407	448	728	-	365	350	-	34.02	34.74	-
	3-1/4	1158.2	810	357	377	390	458	708	345	327	522	34.67	34.38	36.99
	1-1/4	1212.4	532	290	348	448	-	-	286	333	-	33.57	34.49	-
079	2	1183.1	502	267	290	297	474	-	226	314	-	32.44	34.16	-
	3-1/4	1155.3	540	253	274	272	304	442	237	196	335	32.65	31.77	34.51
	1-1/4	1408.5	950	555	796	849	-	-	548	750	-	37.30	39.22	-
080	2	1381.9	961	491	557	618	912	-	476	556	-	36.43	37.35	-
	3-1/4	1373.3	970	446	486	507	615	927	421	428	698	35.73	35.84	38.77
	1-1/4	1197.0	935	828	897	907	-	-	700	748	-	38.79	39.20	-
081	2	1147.8	950	632	791	792	918	-	602	627	-	37.84	38.11	-
	3-1/4	1113.9	943	587	719	720	844	998	550	610	880	37.30	37.93	40.23
	1-1/4	757.6	479	293	327	384	-	-	288	364	-	33.71	34.96	-
082	2	757.6	479	280	289	304	414	-	282	303	-	33.55	33.97	-
	3-1/4	768.9	482	255	264	264	300	447	230	195	325	32.51	31.75	34.34
	1-1/4	1933.9	1210	701	1159	1205	-	-	645	1017	-	38.29	41.24	-
091	2	1866.0	1240	589	740	858	1258	-	556	728	-	37.35	39.04	-
	3-1/4	1936.2	1250	644	727	746	909	1293	536	507	916	37.13	36.81	40.50

Table 4.7 Experimental thermodynamic data for liquid nitrogen

Run #	Cavity Length (inches)	T_o (°R)	V_o (ft/sec)	P_o (psia)	P_v (psia)	P_2 (psia)	P_4 (psia)	P_5 (psia)	P_7 (psia)	P_9 (psia)	$P_{2,T}$ (psia)	$P_{6,T}$ (psia)	$P_{8,T}$ (psia)	K_v
095	3-1/4	140.1	35.22	28.00	15.55	13.20	13.70	13.50	14.15	17.90	12.70	12.95	13.85	1.86
096	"	139.8	50.07	42.10	15.30	13.10	13.90	13.40	14.00	17.85	14.50	12.40	13.10	1.97
099	"	160.7	38.25	56.30	49.20	40.60	44.50	44.00	47.55	52.10	45.10	45.10	48.60	0.97
100	"	150.7	45.84	46.10	29.25	22.80	23.40	23.60	24.70	31.90	26.40	22.90	25.00	1.53
102	"	160.4	65.48	85.10	48.05	34.60	32.10	35.90	37.70	47.00	30.90	33.30	38.00	1.70
105	"	160.7	74.14	98.10	48.95	35.40	33.60	36.30	37.70	49.60	31.50	33.30	37.80	1.82
107	"	150.5	73.13	86.10	28.90	22.00	21.40	22.10	22.00	29.30	19.90	20.00	22.40	2.04
108	"	140.9	73.16	78.10	16.40	13.10	12.60	13.60	14.00	18.40	12.90	12.50	12.40	2.13
109	"	140.7	72.89	78.00	16.20	14.00	13.20	14.10	13.90	17.80	12.20	12.30	12.60	2.15
110	"	140.5	49.72	41.20	16.05	13.40	15.20	13.80	15.20	19.40	15.10	12.90	14.70	1.88
111	"	161.0	51.13	65.85	49.95	37.75	36.35	38.85	41.40	50.30	41.90	38.30	42.60	1.22
112	"	140.5	48.24	38.60	16.00	14.30	15.10	13.30	13.90	18.60	14.70	12.50	13.40	1.80

Table 4.7 (Continued)

Run #	Cavity Length (inches)	h_o (ft, abs)	h_v (ft, abs)	h_2 (ft, abs)	h_4 (ft, abs)	h_5 (ft, abs)	h_7 (ft, abs)	h_9 (ft, abs)	$h_{2,T}$ (ft, abs)	$h_{6,T}$ (ft, abs)	$h_{8,T}$ (ft, abs)	T_2 (°R)	T_6 (°R)	T_8 (°R)
095	3-1/4	80.18	44.35	37.35	38.90	38.25	40.20	51.60	36.05	36.60	39.45	137.1	137.3	138.4
096	"	120.44	43.72	37.05	39.45	37.95	39.75	51.40	41.22	35.12	37.35	139.0	136.7	137.6
099	"	173.20	151.10	123.10	136.80	135.30	146.20	161.05	138.12	138.12	149.32	159.0	159.0	160.5
100	"	136.76	86.70	66.75	68.60	69.25	72.60	95.30	77.58	66.93	73.50	148.8	146.4	147.9
102	"	260.92	147.55	103.90	95.90	108.00	113.75	144.50	92.25	99.82	114.50	151.7	153.1	155.6
105	"	301.50	150.45	106.45	107.00	109.25	113.75	152.80	94.20	99.68	113.95	152.1	153.1	155.5
107	"	254.98	85.75	64.25	62.45	64.60	64.25	87.05	57.65	60.02	65.27	144.0	144.7	146.0
108	"	224.05	46.85	37.05	35.55	38.55	39.65	53.15	36.62	35.55	35.12	137.3	136.9	136.7
109	"	223.62	46.38	39.70	37.15	40.00	39.45	51.20	34.42	34.82	35.78	136.4	136.6	137.0
110	"	118.15	45.90	37.95	43.35	39.15	43.35	56.20	43.15	36.42	41.97	139.6	137.2	139.2
111	"	202.85	153.45	114.00	109.45	117.40	125.70	155.10	127.25	115.45	129.50	157.5	155.7	157.8
112	"	110.69	45.75	40.65	43.00	37.70	39.45	53.75	43.90	35.55	37.85	139.2	136.9	137.7

Table 4.8 Results of Computer Solutions of Equation [4.2-2] Using Hydrogen Thermodynamic Data.

Cavity length used	m	n	p	S.D.† $= \sqrt{(1/N)\sum(B - B_t)^2}$
Nominal[1]	.5*	.5*	.5*	2.223
Nominal	.5*	-.278	.5*	.583
Nominal	.5**	-.16**	.57	.628
Nominal	.5**	-.16**	.85**	.665
Nominal	.5**	-.326	.85**	.568
Nominal	.5*	-.308	.732	.562
Nominal	-3.52	-.348	.554	.379
Estimated[2]	.5**	-.16**	.85**	.604
Estimated	.5**	-.306	.85**	.498
Estimated	.5*	-.288	.71	.489
Estimated	-2.938	-.306	.54	.346

1 - Nominal cavity length obtained from movie films.

2 - Cavity length obtained by extrapolation of cavity pressure measurement data.

* - Denotes exponents held constant in computer fit program.

** - Denotes exponents obtained from reference [13].

† - Standard deviation, where N = number of data points, B_t = B obtained from theory [13], and B is computed from equation [4.2-2].

Equation [4.2-2]: $$B = (B)_{ref}\left(\frac{\alpha_{ref}}{\alpha}\right)^m \left(\frac{x_{ref}}{x}\right)^n \left(\frac{V_o}{V_{o,ref}}\right)^p .$$

Table 4.9 Results of Computer Solutions of Equation [4.2-2] Using Nitrogen Thermodynamic Data.

Cavity length used	m	p	S.D.† $=\sqrt{(1/N)\sum(B - B_t)^2}$
Nominal[1]	.5*	.5*	.545
Nominal	.5**	.85**	.671
Nominal	.5*	.384	.533
Nominal	-1.22	.492	.498
Nominal	0*	.85**	.644
Nominal	0*	.414	.517

1 - Nominal cavity length obtained from movie films. The exponent n does not appear in these data, as only one cavity length (3-1/4 inches) was used in the nitrogen tests.

* - Denotes exponents held constant in computer fit program.

** - Denotes exponents obtained from reference [13].

† - Standard deviation, where N = number of data points, B_t = B obtained from theory [13], and B is computed from equation [4.2-2].

Equation [4.2-2]: $$B = (B)_{ref}\left(\frac{\alpha_{ref}}{\alpha}\right)^m \left(\frac{x_{ref}}{x}\right)^n \left(\frac{V_o}{V_{o,ref}}\right)^p.$$

Distribution List for Final Report NASA CR-72286

Contract C-35560A

		Copies
National Aeronautics and Space Administration Lewis Research Center 21000 Brookpark Road Cleveland, Ohio 44135		
Attention:	Contracting Officer, MS 500-313	1
	Liquid Rocket Technology Branch, MS 500-209	10
	Technical Report Control Office, MS 5-5	1
	Technology Utilization Office, MS 3-16	1
	AFSC Liaison Office, MS 4-1	2
	Library	2
	D. L. Nored, MS 500-209	1
	Office of Reliability & Quality Assurance, MS 500-203	1
	W. E. Roberts, MS 3-17	1
	E. W. Conrad, MS 100-1	1
	Fluid Systems Components Division, MS 5-3	3
	W. A. Rostafinski, MS 500-305	1
National Aeronautics and Space Administration Washington, D. C. 20546		
Attention:	Code MT	1
	RPX	2
	RPL	2
	SV	1
	Jack Suddreth, RPL	1
Scientific and Technical Information Facility P. O. Box 33 College Park, Maryland 20740		
Attention:	NASA Representative Code CRT	6
National Aeronautics and Space Administration Ames Research Center Moffett Field, California 94035		
Attention:	Library	1
	C. A. Syvertson	1

	Copies
National Aeronautics and Space Administration Flight Research Center P. O. Box 273 Edwards, California 93523	
Attention: Library	1
National Aeronautics and Space Administration Goddard Space Flight Center Greenbelt, Maryland 20771	
Attention: Library	1
National Aeronautics and Space Administration John F. Kennedy Space Center Cocoa Beach, Florida 32931	
Attention: Library	1
National Aeronautics and Space Administration Langley Research Center Langley Station Hampton, Virginia 23365	
Attention: Library	1
National Aeronautics and Space Administration Manned Spacecraft Center Houston, Texas 77001	
Attention: Library	1
National Aeronautics and Space Administration George C. Marshall Space Flight Center Huntsville, Alabama 35812	
Attention: Library	1
Keith Chandler, R-P & VE-PA	1
Leren Gross, R-P & VE-PAC	1
Hugh Campbell, R-P & VE-PEC	1
J. L. Vaniman, R-P & VE-PTP	1

	Copies
Jet Propulsion Laboratory 4800 Oak Grove Drive Pasadena, California 91103	
Attention: Library	1
Henry Burlage	1
Office of the Director of Defense Research & Engineering Washington, D. C. 20301	
Attention: Dr. H. W. Schulz, Office of Asst. Dir. (Chem. Technology)	1
Defense Documentation Center Cameron Station Alexandria, Virginia 22314	1
RTD(RTNP) Bolling Air Force Base Washington, D. C. 20332	1
Arnold Engineering Development Center Air Force Systems Command Tullahoma, Tennessee 37389	
Attention: AEOIM	1
Advanced Research Projects Agency Washington, D. C. 20525	
Attention: D. E. Mock	1
Aeronautical Systems Division Air Force Systems Command Wright-Patterson Air Force Base, Dayton, Ohio 45433	
Attention: D. L. Schmidt, Code ASRCNC-2	1
Air Force Missile Test Center Patrick Air Force Base, Florida 32925	
Attention: L. J. Ullian	1

	Copies
Air Force Systems Command (SCLT/Capt. S. W. Bowen) Andrews Air Force Base Washington, D. C. 20332	1
Air Force Rocket Propulsion Laboratory (RPR) Edwards, California 93523	1
Air Force Rocket Propulsion Laboratory (RPM) Edwards, California 93523	1
Air Force FTC (FTAT-2) Edwards Air Force Base, California 93523 Attention: Col. J. M. Silk	1
Air Force Office of Scientific Research Washington, D. C. 20333 Attention: SREP, Dr. J. F. Masi	1
Office of Research Analyses (OAR) Holloman Air Force Base, New Mexico 88330 Attention: RRRT	1
Maj. R. E. Brocken, Code MDGRT	1
U. S. Air Force Washington, D. C. 20330 Attention: Col. C. K. Stambaugh, Code AFRST	1
Commanding Officer U. S. Army Research Office (Durham) Box CM, Duke Station Durham, North Carolina 27706	1
U. S. Army Missile Command Redstone Scientific Information Center Redstone Arsenal, Alabama 35808 Attention: Chief, Document Section	1
Dr. W. Wharton	1

	Copies
Bureau of Naval Weapons Department of the Navy Washington, D. C. 20360	
Attention: J. Kay, Code RTMS-41	1
Commander U. S. Naval Missile Center Point Mugu, California 93041	
Attention: Technical Library	1
Commander U. S. Naval Ordnance Test Station China Lake, California 93557	
Attention: Code 45	1
Code 753	1
Commanding Officer Office of Naval Research 1030 E. Green Street Pasadena, California 91101	1
Director (Code 6180) U. S. Naval Research Laboratory Washington, D. C. 20390	
Attention: H. W. Carhart	1
Picatinny Arsenal Dover, New Jersey 07801	
Attention: I. Forsten, Chief Liquid Propulsion Laboratory	1
Union Carbide - Nuclear Division Oak Ridge Gaseous Diffusion Plant P. O. Box P Oak Ridge, Tennessee 37830	
Attention: W. J. Wilcox	1

	Copies
Air Force Aero Propulsion Laboratory Research & Technology Division Air Force Systems Command United States Air Force Wright-Patterson AFB, Ohio 45433 Attention: APRP (C. M. Donaldson)	1
Aeroject-General Corporation P. O. Box 296 Azusa, California 91703 Attention: Librarian	1
Aerojet-General Corporation 11711 South Woodruff Avenue Downey, California 90241 Attention: F. M. West, Chief Librarian	1
Aerojet-General Corporation P. O. Box 1947 Sacramento, California 95809 Attention: Technical Library 2484-2015A	1
Aeronutronic Division of Philco Corporation Ford Road Newport Beach, California 92600 Attention: Dr. L. H. Linder, Manager Technical Information Department	1 1
Aerospace Corporation P. O. Box 95085 Los Angeles, California 90045 Attention: Library-Documents	1
Arthur D. Little, Inc. Acorn Park Cambridge, Massachusetts 02140 Attention: A. C. Tobey	1

Copies

ARO, Incorporated
Arnold Engineering Development Center
Arnold AF Station, Tennessee 37389

Attention: Dr. B. H. Goethert 1
Chief Scientist

Atlantic Research Corporation
Shirley Highway & Edsall Road
Alexandria, Virginia 22314

Attention: Security Office for Library 1

Battelle Memorial Institute
505 King Avenue
Columbus, Ohio 43201

Attention: Report Library, Room 6A 1

Beech Aircraft Corporation
Boulder Facility
Box 631
Boulder, Colorado 80302

Attention: Library 1

Bell Aerosystems, Inc.
Box 1
Buffalo, New York 14205

Attention: Library 1

Bendix Systems Division
Bendix Corporation
Ann Arbor, Michigan 48106

Attention: Library 1

The Boeing Company
Aero Space Division
P. O. Box 3707
Seattle, Washington 98124

Attention: Ruth E. Peerenboom (1190) 1

Copies

Chemical Propulsion Information Agency
Applied Physics Laboratory
8621 Georgia Avenue
Silver Spring, Maryland 20910 1

Chrysler Corporation
Space Division
New Orleans, Louisiana 70150

Attention: Librarian 1

Curtiss-Wright Corporation
Wright Aeronautical Division
Woodridge, New Jersey 07075

Attention: G. Kelley 1

University of Denver
Denver Research Institute
P. O. Box 10127
Denver, Colorado 80210

Attention: Security Office 1

Douglas Aircraft Company, Inc.
Santa Monica Division
3000 Ocean Park Blvd.,
Santa Monica, California 90405

Attention: Library 1

Fairchild Stratos Corporation
Aircraft Missiles Division
Hagerstown, Maryland 20740

Attention: J. S. Kerr 1

General Dynamics/Astronautics
P. O. Box 1128
San Diego, California 92112

Attention: Library & Information Services (128-00) 1

Copies

Convair Division
General Dynamics Corporation
P. O. Box 1128
San Diego, California 92112

Attention: Mr. W. Fenning 1
Centaur Resident Project Office

General Electric Company
Flight Propulsion Lab. Department
Cincinnati, Ohio 45215

Attention: D. Suichu 1

Grumman Aircraft Engineering Corporation
Bethpage, Long Island,
New York 11714

Attention: Joseph Gavin 1

IIT Research Institute
Technology Center
Chicago, Illinois 60616

Attention: Library 1

Kidde Aero-Space Division
Walter Kidde & Company, Inc.
675 Main Street
Belleville, New Jersey 07109

Attention: R. J. Hanville, 1
Director of Research Engineering

Lockheed Missiles & Space Company
P. O. Box 504
Sunnyvale, California 94088

Attention: Technical Information Center 1

Lockheed Propulsion Company
P. O. Box 111
Redlands, California 92374

Attention: Miss Belle Berlad, Librarian 1

	Copies
Lockheed Missiles & Space Company Propulsion Engineering Division (D. 55-11) 1111 Lockheed Way Sunnyvale, California 94087	1
Marquardt Corporation 16555 Saticoy Street Box 2013 - South Annex Van Nuys, California 91404	
Attention: Librarian	1
Purdue University Lafayette, Indiana 47907	
Attention: Technical Librarian	1
Rocketdyne, A Division of North American Rockwell Corporation 6633 Canoga Avenue Canoga Park, California 91304	
Attention: Library, Department 596-306	1
Stanford Research Institute 333 Ravenswood Avenue Menlo Park, California 94025	
Attention: Thor Smith	1
TRW Systems, Incorporated One Space Park Redondo Beach, California 90200	
Attention: G. W. Elverum	1
STL Tech. Lib. Doc. Acquisitions	1
TRW, Incorporated TAPCO Division 23555 Euclid Avenue Cleveland, Ohio 44117	
Attention: P. T. Angell	1

Copies

United Aircraft Corporation
Corporation Library
400 Main Street
East Hartford, Connecticut 06118

Attention:	Library	1
	Frank Owen	1
	W. E. Taylor	1

United Aircraft Corporation
Pratt and Whitney Division
Florida Research and Development Center
P. O. Box 2691
West Palm Beach, Florida 33402

Attention:	Library	1

California Institute of Technology
Pasadena, California 91109

Attention:	Dr. A. Acosta	1
	Prof. M. S. Plesset	1

The Pennsylvania State University
Ordnance Research Laboratory
P. O. Box 30
State College, Pennsylvania 16801

Attention:	Prof. G. F. Wislicenus	1
	Dr. J. W. Holl	1

Hydronautics, Incorporated
Pendell School Road
Howard County
Laurel, Maryland 20810

Attention:	Dr. Philip Eisenberg	1

St. Anthony Falls Hydraulic Laboratory
Mississippi River at Third Avenue, S. E.
Minneapolis, Minnesota 55414

Attention:	Prof. J. F. Ripkin	1

	Copies
State University of New York - Buffalo Mechanical Engineering Department Buffalo, New York 14214 Attention: Dr. Virgil J. Lunardini	1
Weapons Research Establishment Department of Supply Box 1424H G. P. O. Adelaide Salisbury, South Australia Attention: Peter Pemberton	1
NUMEC P. O. Box 306 Lewiston, New York 14092 Attention: Thomas T. Nagamoto	1
Aerojet-General Corporation P. O. Box 1947 Sacramento, California 95809 Attention: Dale R. Nielsen	1
Wyle Laboratories 128 Maryland Street El Segundo, California 92246 Attention: W. Harry Probert	1
TRW Systems, Incorporated Bldg. 01, Room 1070F One Space Park Redondo Beach, California 90278 Attention: Lincoln B. Dumont	1
Aerojet-General Corporation Liquid Rocket Operations Dept. 9680, Bldg. 2025-2 Sacramento, California 95809 Attention: Ralph L. Sabiers	1